

Résumé

Ce manuscrit rapporte l'étude de l'anisotropie magnétique au sein de complexes à base de dysprosium. Ces travaux font appel à différentes techniques de mesures magnétiques sur monocristal en mode statique et dynamique. L'interprétation des données magnétiques est réalisée en se basant sur des calculs *ab initio* pour certains composés. L'ensemble du travail permet de comprendre le comportement magnétique de complexes anisotropes qui pourraient servir pour le stockage moléculaire de l'information. La perspective d'assembler ces molécules sur des surfaces pour étudier leurs propriétés individuelles est évoquée en proposant d'utiliser la propriété d'échange magnétique entre la pointe d'un microscope à force magnétique et les molécules individuelles.

L'introduction décrit le contexte général qui situe le travail de thèse au sein du domaine du magnétisme moléculaire. Une rapide présentation des aimants moléculaires est précédée par la description du principal mécanisme de relaxation observé pour ce type de composés. Si l'on considère un ensemble de spins, qui peut être assimilé à un unique spin équivalent et que celui-ci démontre une anisotropie de type Ising (à savoir une anisotropie uniaxiale), l'énergie de ce système peut être décrite par un modèle de double puits de potentiel (voir figure A). La relaxation de ce système se fera alors par échange phononique permettant ainsi de franchir la barrière énergétique ΔE , aussi appelée température de blocage. Ce processus de relaxation est caractérisé par un temps de relaxation τ qui s'exprime selon une loi de type Arrhénius :

$$\tau = \tau_0 \exp(\Delta E / k_B T)$$

Dans cette formule apparaît la barrière d'énergie qui peut également s'écrire DS^2 , où D représente l'anisotropie magnétique et S est la valeur de l'état fondamental de spin.

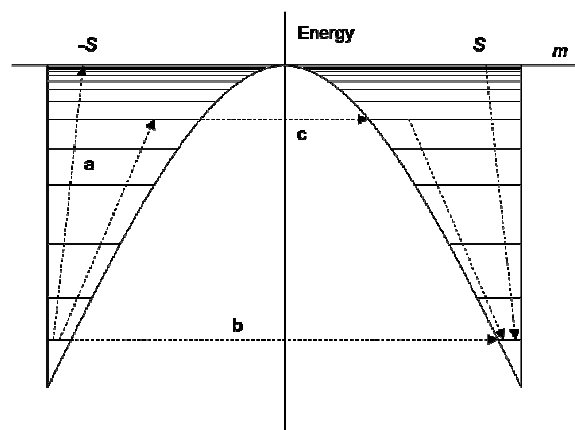


Figure A: Possible processus de relaxation

Un des objectifs de la recherche sur les aimants moléculaires est d'obtenir des composés possédant une haute barrière en énergie. Pour cela on recherche des éléments présentant une forte anisotropie magnétique ainsi qu'une valeur de spin élevée. Les lanthanides représentent une famille d'éléments appropriée pour ces études. Tout d'abord, l'écrantage des orbitales 4f par les orbitales 5p et 6s confère aux terres rares des propriétés chimiques voisines ce qui facilite l'obtention de familles isostructurales. Une diminution du rayon ionique en fonction du numéro atomique croissant, appelée contraction lanthanidique, est le principal paramètre pouvant induire des différences structurales pour un même composé synthétisé à partir de différentes terres rares. En parallèle, les lanthanides offrent de diverses propriétés physiques (catalyse, luminescence, magnétisme, ...). Concernant le magnétisme, le Gd est isotropique, alors que le Dy possède lui une forte anisotropie associée à un fort moment angulaire ce qui fait du Dy un potentiel candidat à l'obtention d'aimants moléculaires. On notera également l'yttrium, considéré comme terre rare, pour son caractère diamagnétique, pouvant s'avérer utile lors d'études par substitution.

Chapitre 1

Le premier chapitre est consacré à l'étude d'une famille de chaînes aimants à base de lanthanides et de radicaux nitronyl nitroxides, avec une attention particulière sur le composé à base de Dy. Afin de pouvoir étudier l'anisotropie de l'ion Dy au sein du composé tout en supprimant l'interaction d'échange le long de la chaîne, un analogue monomérique conservant la première sphère de coordination du Dy a été synthétisé (voir figure B).

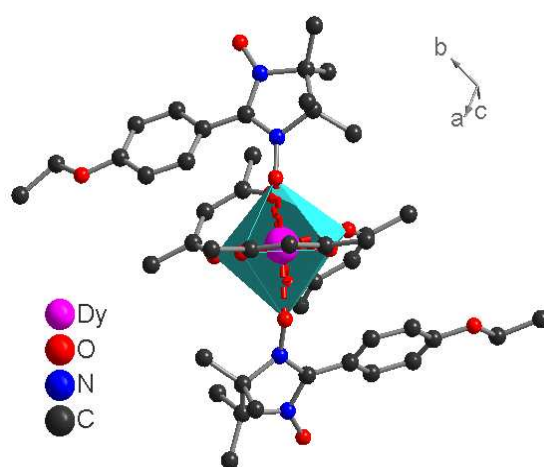


Figure B: *Représentation de l'analogue monomérique $[Dy(hfac)_3(NITC_6H_4-OEt)_2]$*

Pour pouvoir étudier l'anisotropie du Dy dans ce composé, la technique de mesure de l'aimantation en fonction de l'angle a été utilisée. La mise en place et l'optimisation d'un mode opératoire permettant d'utiliser cette technique de mesure a fait l'objet d'une importance particulière lors de cette thèse. Pour pouvoir utiliser cette technique, l'analogue doit cristalliser dans un système triclinique afin d'éviter la non équivalence magnétique des molécules dans la structure cristallographique. En modifiant le radical, un analogue cristallisant dans un système triclinique à finalement été obtenu. Les composés à base de Dy ne donnant généralement pas de signal en RPE, une autre technique de mesure a du être employée : la mesure de l'aimantation en fonction de l'angle (voir figure C).

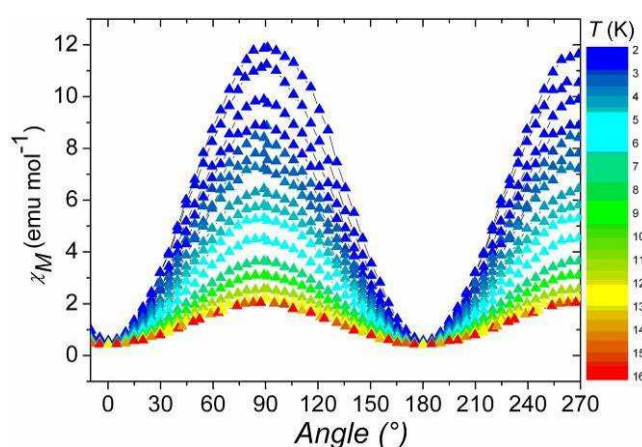


Figure C: variation angulaire de la susceptibilité du monomère de Dy en fonction de la température.

Le couplage entre des calculs *ab initio* et l'utilisation de mesures expérimentales, et en particulier la mesure de l'aimantation en fonction de l'angle, a permis de déterminer les axes principaux de l'aimantation de ce système à base de Dy et de radicaux organiques (voir figure D). Ces informations ont permis une analyse claire de la dépendance en température et en champ de l'aimantation, et ce même en présence d'une forte contribution orbitale. Une interaction ferromagnétique entre Dy et radicale, ainsi qu'une interaction antiferromagnétique aux plus proches voisins entre radicaux (par intermédiaire de l'ion Dy^{III}) ont pu être mises en évidence. Ces informations ont ainsi permis l'étude du comportement complexe de cette famille de chaînes aimants à base de terre rare.

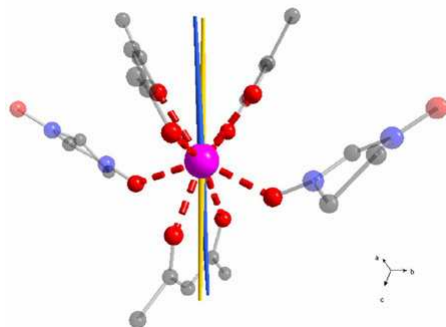


Figure D: Représentation de l'axe de facile aimantation sur le monomère
(en jaune: experimental / en bleu: ab-Initio)

Ce travail a donc démontré qu'il était possible d'étudier l'anisotropie du dysprosium dans un environnement de basse symétrie. Il est donc intéressant d'essayer de transposer cette étude sur d'autres systèmes.

Chapitre 2

Le chapitre 2 est une partie introductive à l'étude de l'anisotropie d'un complexe de Dy(III), un hexanucléaire obtenu en couplant deux entités trinucéaires grâce à un ligand organique. Ce chapitre traite donc de l'étude magnétique de l'entité trinucéaire, pour ensuite étudier l'héxanucléaire au chapitre 3.

Ce cluster triangulaire de dysprosium, synthétisé par le groupe du professeur Annie Powell à Karlsruhe, en Allemagne, a la particularité de montrer un caractère d'aimant moléculaire alors que son état fondamental de spin est nul. Ceci s'explique par le fait que les trois spins se trouvent dans un même plan et sont orientés à 120° l'un de l'autre, leur résultante est ainsi nulle (voir figure E). Cette configuration donne également au composé la propriété de chiralité de spins : les spins pouvant être orientés dans un sens ou dans l'autre. Finalement, l'étude de l'aimantation a pu déterminer que l'anisotropie de ce composé résulte comme étant de type plan.

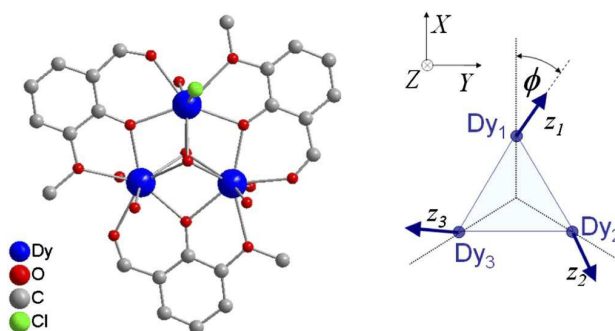


Figure E: Représentation du cluster triangulaire de Dy, ainsi que l'orientation des spins.

Si l'on s'intéresse à l'évolution des niveaux d'énergie en fonction du champ magnétique externe, on notera la présence d'un croisement de niveau aux alentours de 0.9 Tesla. Si l'on mesure l'aimantation pour un champ magnétique parallèle au plan du triangle, on observe pour cette valeur de champ, un saut de l'aimantation qui va subitement à saturation, alors que la mesure effectuée avec le champ magnétique perpendiculaire au plan du triangle dénote une aimantation qui croît difficilement en fonction du champ.

Chapitre 3

Le chapitre 3 est donc consacré à l'étude d'un hexanucléaire de Dy(III) obtenu par la condensation de deux triangles de dysprosium (voir figure F). La comparaison des mesures de susceptibilité en dynamique entre le cluster de Dy_3 et le cluster de Dy_6 se caractérise par l'apparition d'un deuxième pic aux alentours de 22K. Afin d'essayer de comprendre la nature de ce second pic, l'anisotropie du composé a été étudiée en utilisant la technique présentée au cours du chapitre 1.

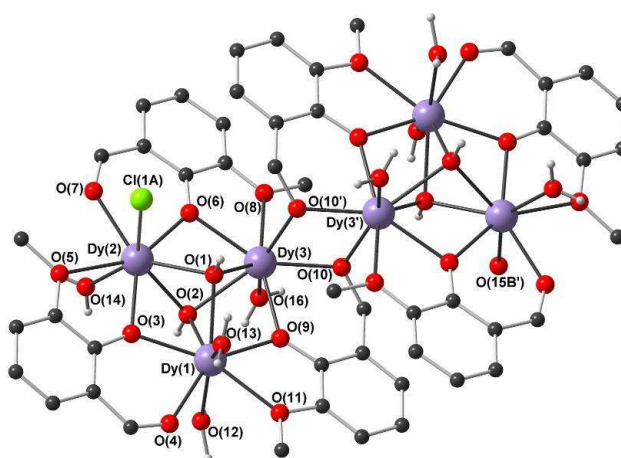


Figure F: Représentation du cluster de Dy_6

De la même manière, l'aimantation a été mesurée en fonction de l'angle et en fonction de la température. Contrairement au cas du monomère de Dy étudié au chapitre 1, les minima et maxima d'aimantation se déplacent en angle en fonction de la température. Deux cas limites se dégagent, les mesures à 2K (plus basse température disponible) et 10K (absence de déplacement pour des températures supérieures). Après extraction et diagonalisation des tenseurs de susceptibilité respectifs à ces deux cas limites, on obtient comme résultat qu'à 2K, deux des composantes de la

susceptibilité sont sensiblement égales quand la troisième est nulle (anisotropie de type *plan*), alors qu'à 10K on observe trois composantes différentes, dont une majoritaire (anisotropie de type *Ising*) (voir figure G). L'anisotropie de type plan observée à 2K n'est pas sans rappeler celle du triangle de dysprosium et pourrait donc être interprétée comme l'anisotropie moyenne des deux triangles. A 10K, une direction préférentielle se dégage et l'anisotropie tend à devenir axiale. Une modification au niveau de l'interaction entre Dy des deux triangles pourrait être une explication.

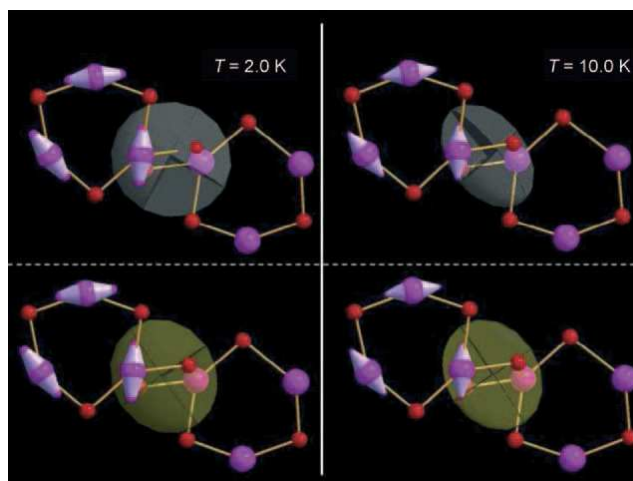


Figure G: Représentation des ellipsoïdes de susceptibilité pour 2K et 10K
(en blanc : expérimental / en jaune : Ab-Initio)

Cette variation de la nature de l'anisotropie du composé en fonction de la température pourrait être une explication de la seconde relaxation lente de l'aimantation observée dans le cas de cet hétérodimère.

Chapitre 4

Toujours à la recherche de composés moléculaires démontrant une température de blocage élevée, une autre stratégie est la combinaison de centre métallique de nature diverse du moment qu'une des espèces possède une anisotropie axiale forte. Le chapitre 4 est dédié à l'exploration de complexes comprenant des terres rares et des métaux de transition de la première série dans la perspective d'obtenir de nouveaux aimants moléculaires. Deux composés associant le dysprosium au nickel sont l'objet de ce chapitre, ils ont été synthétisés par le laboratoire du professeur Andruh de l'université de Bucharest (Roumanie), groupe qui a déjà présenté de nombreux composés hétérométalliques combinés à des ligands tels que l'*o*-vaniline ou les diamines.

Le premier composé est un complexe tétranucléaire qui résulte de la coordination de deux groupements NiDy par un oxygène appartenant au groupe carboxylate d'une des deux parties (voir figure H). Le second est un polymère de coordination ayant une topologie de type échelle (voir figure H). Les unités Ni-Dy sont cette fois connectées par des groupements téréphtalates. Les téréphtalates connecte les Dy entre eux pour constitués les barreaux de l'échelle, un second groupement téréphtalate connecte ce même Dy au Dy et au Ni de l'unité voisine.

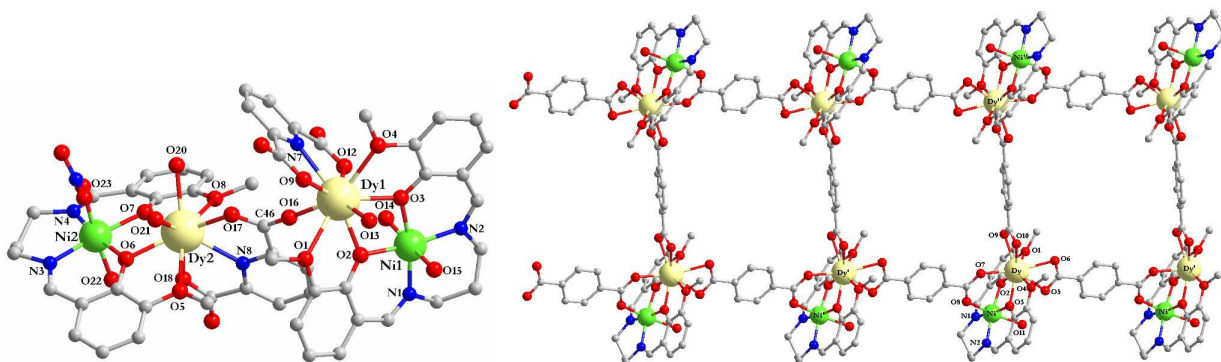


Figure H: Représentation des deux composés à base de Dy et Ni
(à gauche : le tétranucléaire / à droite : la chaîne)

Concernant l'étude des propriétés statiques de l'aimantation, les fits réalisés à basses températures indiquent que dans le cas de la chaîne, en appliquant un modèle de type Ising pour caractérisé l'anisotropie du Dy, l'augmentation de XT peut se traduire par une interaction ferromagnétique entre le Dy et le Ni au sein d'un même motif, comportement déjà observé dans le passé sur d'autre composé de Ni et terre rare. En revanche, pour ce qui est du tétramère si l'on applique la même interaction entre Ni et Dy, il en ressort une interaction antiferromagnétique entre Dy (via la pince carboxylate), ce qui pourrait dénoter une non colinéarité des axes d'anisotropie des Dy, mais sans études expérimentales, il est difficile d'en dire plus.

Concernant la dynamique, pour le tétranucléaire, en l'absence de champ extérieur, on observe très peu de dépendance en fréquence de la susceptibilité, ceci peut se traduire par la présence d'un effet tunnel de l'aimantation important. Les mesures effectuées sur la chaîne, les conditions d'obtention de maxima sur la χ'' sont observées, même si l'effet tunnel de l'aimantation est toujours présent. Des mesures sous champ magnétique extérieur ont donc été effectuées pour chacun des composés, un scan en champs ayant permis de déterminer pour quelle valeur la levée de l'effet tunnel était la plus importante. Des maxima sont désormais définissables pour le tétramère quand les maxima relatifs à la chaîne se déplacent vers de plus basses fréquences. L'étude et le fit de ces courbes permettent l'extraction du temps de relaxation pour chaque température. Dans le cas

du tétramère, on observe des valeurs caractéristiques des aimants moléculaires. Pour la chaîne, la valeur de la barrière d'énergie passe de 2K à 17K, τ_0 perd par contre plus d'un ordre de grandeur, ce comportement est typique de l'application d'un champ extérieur. Ces deux composés présentent donc des caractéristiques d'aimants moléculaires, mais malheureusement, l'absence de matériel ne nous permet pas d'effectuer l'étude de l'anisotropie afin de mieux comprendre le comportement du Dy au sein de ces composés et ainsi comprendre comment potentiellement améliorer les propriétés de composés de la même famille.

Chapitre 5

Le chapitre 5 introduit un axe de recherche particulier, celui de la nanostructuration d'aimants moléculaires. En effet, la possibilité de pouvoir, à l'aide de technique de microscopie de type STM, venir écrire ou lire l'état magnétique d'une molécule aimant déposée sur une surface conductrice, ou bien la possibilité de réaliser des nanotransistors, sont des axes de développement de grand intérêt. Pour cela, il est nécessaire de pouvoir déposer sur surfaces des couches uniques de molécules(voir figure I).

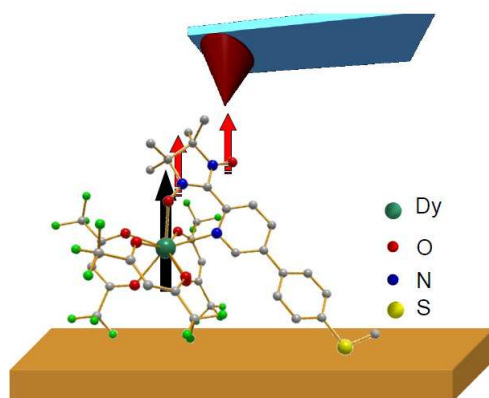


Figure I: Lecture de l'état magnétique d'un complexe de Dy sur surface d'or

Ce chapitre traite de la synthèse d'un nouveau composé comprenant un ion Dy(III) et deux radicaux organiques dérivés du nitronyl nitroxyde. L'objectif est d'obtenir un complexe mononucléaire anisotrope robuste dans la perspective de le greffer sur surface et d'étudier le comportement magnétique d'une molécule individuelle. Effectivement, un des problèmes rencontrés dans ce domaine est le manque de complexes possédant une relaxation lente de l'aimantation qui soient suffisamment robustes pour envisager de les déposer sur surface par

sublimation sous ultra-vide ou à partir d'une solution. La technique ici utilisée est dite d'auto-assemblage. Dans ce cas, on introduit un substrat d'or dans une solution contenant les molécules, ces dernières vont venir se chimisorber sur la surface et ce en plusieurs cycles. Un nettoyage permet alors d'éliminer l'ensemble du matériel physisorber, pour au final obtenir une couche mono moléculaire. Plusieurs essais ont été effectués sur des complexes à base de Dy et de radicaux Nitronyl Nitroxides fonctionnalisés, mais le manque de stabilité de ces complexes en solution, passage obligatoire pour l'auto-assemblage, n'a pas permis de fixer ces molécules sur surface.

Un moyen de renforcer la stabilité des complexes, et d'essayer de modifier le radical. Il a donc été synthétisé ce complexe contenant un biradical. L'effet chelatant des deux nitronyl nitroxide augmentant la stabilité du complexe. Cette stabilité en solution a donc été étudiée par spectroscopie RPE (voir figure J). Ces mesures confirment que le complexe est majoritairement stable dans une solution de dichloromethane, et dans le temps. Ce qui en fait donc un bon candidat pour une fonctionnalisation.

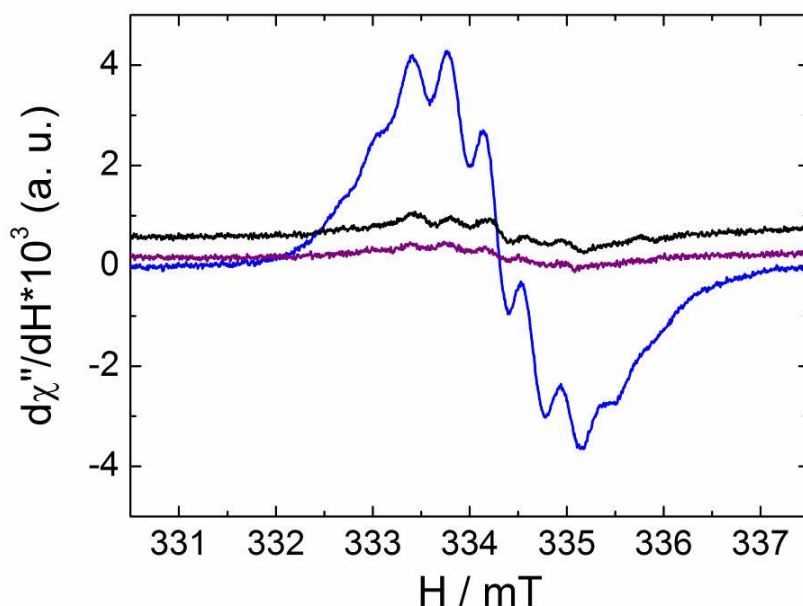


Figure J: Spectres RPE du biradical (bleu), du complexe de Dy (mauve) et du même complexe après deux jours (noir)

De plus ce composé montre une dépendance en fréquence au niveau de la partie imaginaire de la susceptibilité dynamique et ce sans champ appliqué, les valeurs sont une fois de plus caractéristiques des aimants moléculaires (voir figure K). On a donc un potentiel candidat parmi les complexe Dy-rad pour l'étude d'aimant moléculaire sur surface. Les étapes suivantes sont donc la fonctionnalisation puis le dépôt sur surface, avant de pouvoir essayer de mesurer les propriétés de la mono-couche sur surface.

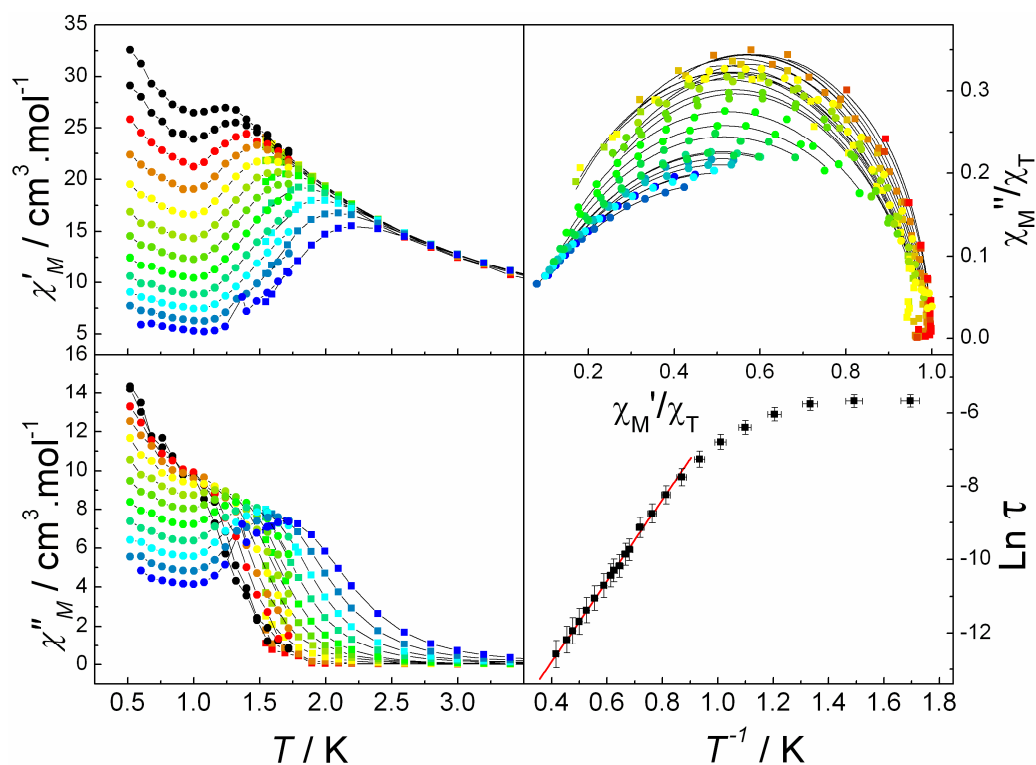


Figure K: Mesures de la susceptibilité dynamique du complexe de Dy et du bi-radical nitronil nitroxyde

Conclusion

Les travaux présentés, utilisant des techniques sophistiquées, et réalisés grâce à plusieurs collaborations fructueuses, démontrent que l'étude de l'anisotropie de composés à base de lanthanides en environnement de basse symétrie est désormais accessible, et ce grâce au puissant outil que constitue l'usage de la mesure de l'aimantation en fonction de l'angle, combinée au calcul ab-initio. A travers la diversité des composés présentés au cours de cette thèse, il a été mis en évidence que les lanthanides, et en particuliers le Dy, constituent des éléments de choix pour la recherche d'aimants moléculaires possédant une haute barrière d'énergie. Finalement, la fonctionnalisation de ce type de composés pour un futur dépôt sur surface conductrice est une possibilité qui s'avère possible et ouvre des perspectives encourageantes dans ce secteur de recherche.

Riassunto

Questo lavoro di tesi è incentrato sullo studio dell'anisotropia magnetica di una serie di complessi a base di disprosio. Questo studio si basa su misure magnetiche su monocristalli, effettuate con diverse tecniche sia statiche che dinamiche. Per alcuni dei composti studiati l'interpretazione dei dati magnetici è stata effettuata basandosi su calcoli ab initio. L'insieme del lavoro permette di capire il comportamento magnetico di complessi anisotropi, i quali potrebbero servire per l'immagazzinamento molecolare dell'informazione. La prospettiva di assemblare queste molecole su superficie per studiarne le proprietà è stata menzionata, proponendo di utilizzare la proprietà di scambio magnetico tra la punta di un microscopio a forza magnetica e le molecole.

L'introduzione descrive il contesto generale che colloca questo lavoro di tesi nel ambito del magnetismo molecolare. Una rapida presentazione dei magneti molecolari è preceduta dalla descrizione del meccanismo principale di rilassamento osservato per questo tipo di composti. Se consideriamo un insieme di spins assimilabile ad un unico spin equivalente, dimostrando un'anisotropia di tipo Ising (un'anisotropia uni-assiale), l'energia di questo sistema può essere descritta con un modello di doppio pozzo di potenziale (vedi figura A). Il rilassamento di questo sistema avverrà tramite scambi fononici permettendo di superare la barriera di energia ΔE , chiamata anche temperatura di bloccaggio. Questo processo è caratterizzato da un tempo di rilassamento τ espresso secondo una legge di tipo Arrhenius:

$$\tau = \tau_0 \exp(\Delta E / k_B T)$$

In questa formula compare la barriera d'energia che può essere ugualmente scritta come DS^2 : D rappresenta l'anisotropia magnetica e S il valore dello stato fondamentale di spin.

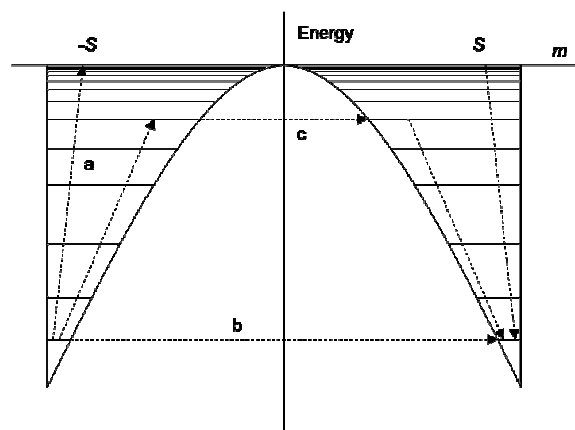


Figura A: Possibile processo di rilassamento.

Uno degli obiettivi della ricerca sui magneti molecolari è quello di ottenere composti che possiedono un' alta barriera energetica. Per questo motivo, si ricercano elementi che presentano una forte anisotropia magnetica insieme ad un valore elevato di spin. I lantanidi sono una famiglia di elementi appropriata per questo tipo di studi. In primo luogo, poiché gli orbitali 4f sono schermati dagli orbitali 5p e 6s, le terre rare hanno proprietà chimiche molto simili tra loro e questo facilita l'ottenimento di famiglie isostrutturali. La diminuzione del raggio ionico all'aumentare del numero atomico, fenomeno chiamato contrazione lantanidica, è il principale parametro che può indurre differenze strutturali. Parallelamente, i lantanidi offrono diverse proprietà fisiche interessanti, quali catalisi, luminescenza e magnetismo. Riguardo alle proprietà magnetiche, il gadolinio è isotropico mentre il disprosio dimostra una forte anisotropia associata ad un elevato momento angolare: questo fa del Dy un potenziale candidato per la realizzazione di magneti molecolari. Infine, è importante sottolineare come l'ittrio, considerato come una terra rara, risulta di grande utilità quando si tratta di effettuare studi per sostituzione grazie al suo carattere diamagnetico.

Capitolo 1

Il primo capitolo tratta dello studio di una famiglia di magneti a singola catena a base di lantanidi e di radicali nitronil nitrossidi, con un' attenzione particolare per i composti a base di Dy. Per potere studiare l'anisotropia dello ione Dy sopprimendo l'interazione di scambio lungo la catena, è stato sintetizzato un analogo monomero, conservando la prima sfera di coordinazione del Dy (vedi figura B).

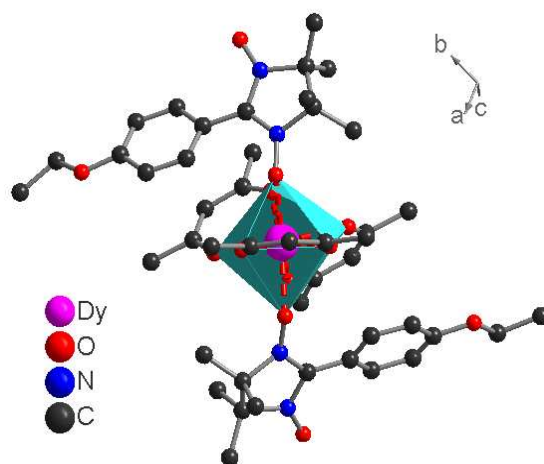


Figura B: Rappresentazione del analogo monomero $[Dy(hfac)_3(NITC_6H_4-OEt)_2]$.

Il composto è stato studiato misurando la magnetizzazione rispetto all' angolo. Lo sviluppo e l'ottimizzazione di un protocollo di misura per questa tecnica ha riguardato una parte importante di questo dottorato. Per evitare la non equivalenza magnetica delle molecole nella struttura cristallografica, risulta necessaria la cristallizzazione del monomero in un sistema a bassa simetria. Modificando il radicale, un analogo cristallizzando in un sistema triclino è finalmente stato ottenuto. Generalmente, poiché i composti a base di Dy non danno segnale in spettroscopia EPR, è stata utilizzata un'altra tecnica di misura quale la misura della magnetizzazione rispetto all' angolo (vedi figura C).

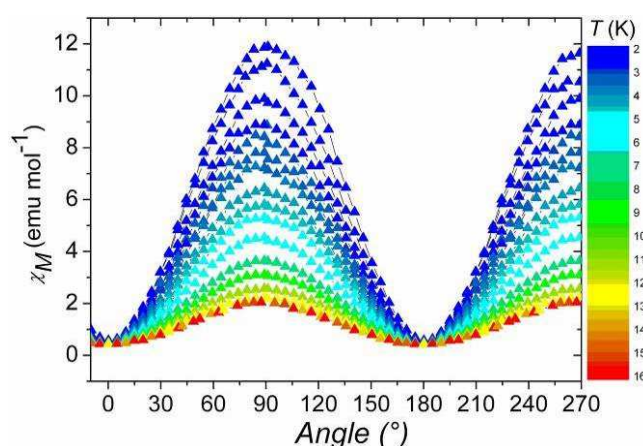


Figura C: *Variazione angolare della suscettività del monomero di Dy rispetto alla temperatura.*

Il confronto dei risultati ottenuti dai calcoli ab-initio e dalle misure sperimentali, in particolare la misura della magnetizzazione rispetto all' angolo, ha permesso di determinare gli assi principali della magnetizzazione di questo sistema a base di Dy e di radicali organici (vedi figura D). Queste informazioni hanno permesso di effettuare un'analisi chiara della dipendenza della magnetizzazione dalla temperatura e dal campo, anche in presenza di un forte contributo orbitale. Sono state evidenziate un' interazione ferromagnetica fra lo ione Dy e i radicali, insieme ad un' interazione antiferromagnetica tra radicali primi vicini tramite gli ioni DyIII. Queste informazioni hanno permesso lo studio del comportamento complessivo di questa famiglia di magneti a singola catena a base di terre rare.

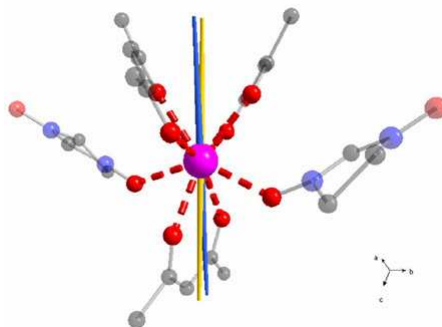


Figura D: Rappresentazione dell'asse di facile magnetizzazione
(in giallo: sperimentale / in blu: ab-initio)

Questo lavoro ha dimostrato la possibilità di studiare l'anisotropia del disprosio in un intorno a bassa simmetria, problematica di interesse anche per altri sistemi.

Capitolo 2

Il capitolo 2 introduce allo studio dell'anisotropia di un complesso di Dy(III) esanucleare ottenuto accoppiando due complessi trinucleari mediante un legante organico. Questo capitolo presenta lo studio magnetico del complesso trinucleare, mentre quello esanucleare è soggetto del capitolo 3.

Questo cluster triangolare di disprosio, sintetizzato dal gruppo della professoressa Annie Powell di Karlsruhe, in Germania, ha la particolarità di mostrare un comportamento di magnete a singola molecola quando il suo stato fondamentale di spin è nullo. Questo fenomeno si spiega con il fatto che i tre spins si trovano in un stesso piano, orientati a 120° l'uno dall'altro: di conseguenza, la loro risultante è nulla (vedi figura E). Questa configurazione dà al composto la proprietà di chiralità di spin; gli spins possono essere orientati in un senso o nell'altro. Infine, lo studio della magnetizzazione ha determinato che l'anisotropia di questo composto è di tipo planare.

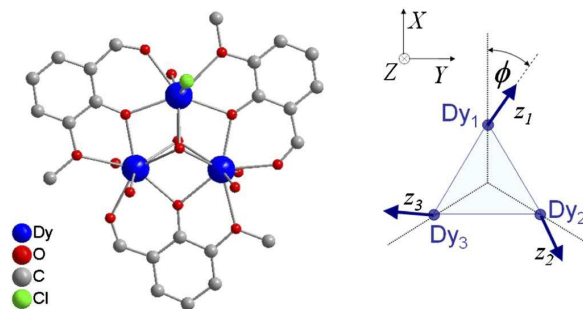


Figura E: Rappresentazione del cluster triangolare di Dy e l'orientazione dei spins nel piano.

Osservando l'evoluzione dei livelli energetici rispetto al campo magnetico, si nota la presenza di un incrocio fra i livelli per un valore di campo intorno a 0.9 Tesla. Se si misura la magnetizzazione per un campo parallelo al piano del triangolo, si osserva, per questo valore di campo (0.9 Tesla), un salto fino alla saturazione. Per un campo perpendicolare al piano del triangolo, la magnetizzazione aumenta con difficoltà.

Capitolo 3

Il capitolo 3 è dedicato allo studio di un complesso esanucleare di Dy(III) ottenuto dalla condensazione di due triangoli di disprosio (vedi figura F). Il confronto delle misure di suscettività dinamica fra il cluster di Dy₃ e il cluster di Dy₆ è caratterizzato dalla comparsa di un secondo picco vicino a 22K. Allo scopo di capire la natura di questo secondo picco, l'anisotropia di questo complesso esanucleare è stata studiata usando la tecnica presentata nel capitolo 1.

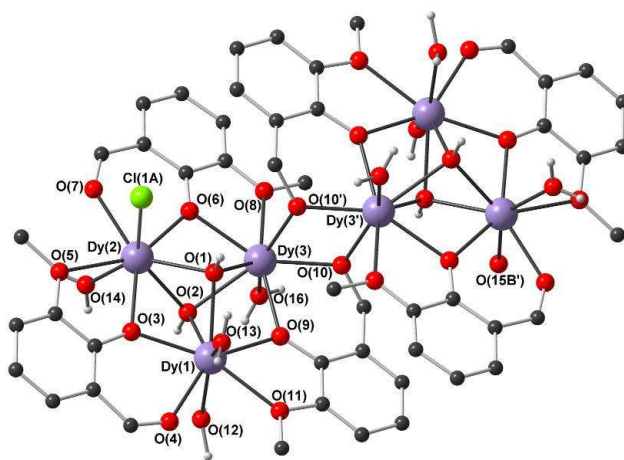


Figura F: Rappresentazione del cluster di Dy₆.

Nello stesso modo, la magnetizzazione è stata misurata rispetto all'angolo e rispetto alla temperatura. Contrariamente al caso del monomero studiato nel capitolo 1, i minimi e i massimi della magnetizzazione si spostano in angolo rispetto alla temperatura. Sono stati individuati due casi limite: a 2K (più bassa temperatura di misura) e a 10K (assenza di spostamento per temperatura maggiore). Dopo l'estrazione e la diagonalizzazione dei tensori di suscettività corrispondenti ai due casi limite, si osserva che a 2K due delle componenti della suscettività sono sensibilmente uguali e la terza è nulla (anisotropia di tipo planare), mentre a 10K si osservano tre componenti diverse di cui una maggiore (anisotropia di tipo Ising) (vedi figura G). L'anisotropia di tipo planare osservata a 2K è analoga a quella del triangolo di disprosio e potrebbe essere interpretata come l'anisotropia media dei due triangoli. A 10K l'anisotropia diventa uniassiale: una possibile spiegazione potrebbe essere la modifica dell'interazione fra disprosi dei due triangoli .

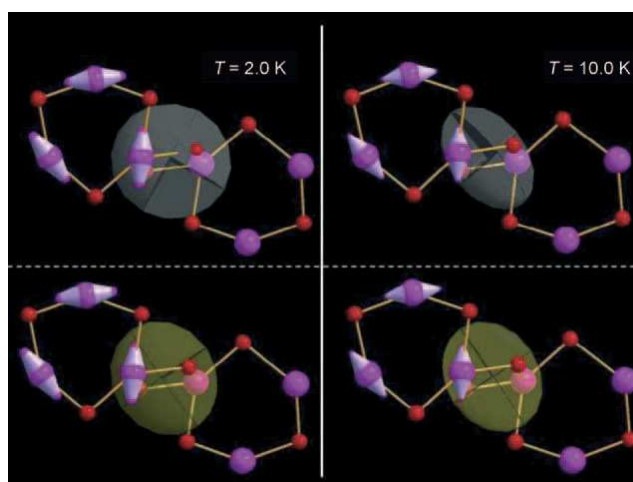


Figura G: Rappresentazione degli ellissoidi di suscettività a 2K e 10K
(in bianco : sperimentale / in giallo :ab-initio)

Questa variazione della natura dell'anisotropia del composto rispetto alla temperatura potrebbe giustificare il secondo rilassamento lento della magnetizzazione osservato nel caso del complesso esanucleare.

Capitolo 4

Ricercando composti molecolari che dimostrano una temperatura di bloccaggio elevata, un'altra strategia è la combinazione di centri metallici di diversa natura, con almeno una specie caratterizzata da una forte anisotropia assiale . Il capitolo 4 è dedicato all'esplorazione di complessi

di terre rare e metalli di transizione della prima serie, nella prospettiva di ottenere nuovi magneti a singola molecola. Soggetto di questo capitolo sono due composti combinanti disprosio e nickel, sintetizzati dal laboratorio del professore Andruh dell'Università di Bucarest (Romania).

Il primo composto è un complesso tetranucleare che risulta dalla coordinazione di due gruppi Ni-Dy tramite un ossigeno appartenente a un gruppo carbossilato di una delle due parti (vedi figura H). Il secondo composto è un polimero di coordinazione di tipologia di tipo “scala”. I gruppi Ni-Dy sono connessi tramite gruppi tereftalati (vedi figura H). Un primo tipo di tereftalato connette i Dy fra di loro per costituire le pioli della scala, mentre il secondo tipo connette un Dy con un altro gruppo Dy-Ni dell'unità vicina.

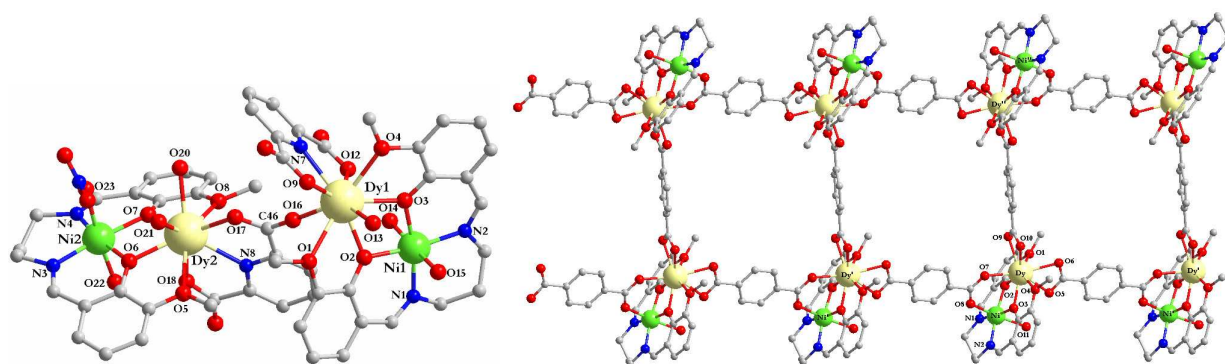


Figura H: Rappresentazione dei due composti a base di Dy-Ni
(a sinistra :il tetranucleare / a destra : la catena)

Dallo studio delle proprietà statiche della magnetizzazione, i *fits* realizzati a bassa temperatura indicano che nel caso della catena, applicando un modello di tipo Ising per caratterizzare l'anisotropia del Dy, l'aumento della χT può essere spiegato dall'interazione ferromagnetica tra Dy e Ni all'interno di un unico gruppo, comportamento già osservato in passato per altri composti di Ni e terre rare. Invece, nel caso del tetranucleare, considerando la stessa interazione fra Ni e Dy, risulta un'interazione antiferromagnetica fra i Dy tramite la connessione carbossilica. Questo comportamento potrebbe indicare una non collinearità degli assi di anisotropia dei Dy, ma non lo si può confermare senza studi sperimentali.

Riguardo la dinamica, per il complesso tetranucleare in assenza di campo esterno si osserva una ridotta dipendenza in frequenza della suscettività. Questo può significare la presenza di un importante effetto tunnel della magnetizzazione. Le misure effettuate sulla catena mostrano che le condizioni necessarie per l'ottenimento di massimi per la χ'' sono soddisfatte, anche se l'effetto tunnel della magnetizzazione è sempre presente. Sono state effettuate per entrambi i composti

misure in presenza di campo magnetico esterno. Il valore del campo applicato é tale da avere un effetto tunnel minimo ed é stato determinato per ogni campione mediante una scansione in campo.. In queste condizioni, il tetranucleare presenta dei massimi, mentre nel caso della catena i massimi già presenti si spostano verso frequenze inferiori. Lo studio e il *fit* di queste curve permettono l'estrazione del valore del tempo di rilassamento per ogni temperatura. Nel caso del tetranucleare, si osservano valori caratteristici tipici dei magneti molecolari. Per la catena, il valore della barriera di energia passa da 2K a 17K, mentre τ_0 perde più di un ordine di grandezza. Questo comportamento a seguito dell'applicazione di un campo esterno è tipico. Questi due composti presentano caratteristiche di magneti a singola molecola, ma sfortunatamente, la mancanza di materiale non permette di effettuare lo studio dell'anisotropia.

Capitolo 5

Il capitolo 5 introduce un asse di ricerca particolare, quello della nanostrutturazione di magneti molecolari. Con l'aiuto di tecniche di microscopia di tipo STM, sono assai di interesse la possibilità di andare a scrivere o a leggere lo stato magnetico di un magnete a singola molecola depositato su una superficie conduttrice. Un punto chiave in questo ambito di ricerca è la necessità di depositare mono-strati e strutturati di molecole su superficie (vedi figura I).

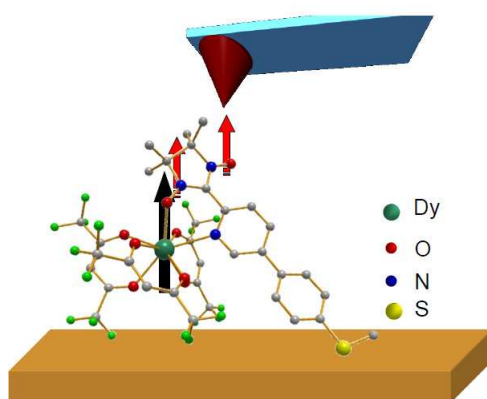


Figura I: Lettura dello stato magnetico di un complesso di Dy su superficie di oro.

Questo capitolo tratta della sintesi di un nuovo composto contenente uno ione Dy(III) e un radicale organico derivato dal nitronil nitrossido. L'obiettivo è di ottenere un complesso mononucleare anisotropo robusto, nella prospettiva di ancorarlo su superficie e studiarne le proprietà magnetiche a livello molecolare. In effetti, uno dei problemi più diffusi in questo ambito è

la mancanza di complessi con un rilassamento lento della magnetizzazione che siano abbastanza robusti per potere essere depositati su superficie, per sublimazione sotto alto vuoto oppure dal passaggio in soluzione, tappa necessaria per la tecnica di “Self Assembling” usata in questo studio. Questa tecnica consiste nell'immersione di un substrato di oro in una soluzione contenente le molecole. Queste verranno a chemisorbirsi sulla superficie a seguito di vari cicli. Una pulizia della superficie permette, in un secondo momento, di eliminare l'eccesso del materiale fisisorbito, per finalmente ottenere un mono-strato molecolare. Sono state effettuate varie prove con complessi di Dy e radicali nitronil nitrossidi funzionalizzati, ma la mancanza di stabilità di questi complessi in soluzione non ha permesso di ancorare queste molecole su superficie.

Un modo di rinforzare la stabilità dei complessi è di modificare il radicale. In questa ottica, è stato sintetizzato un biradicale. L'effetto chelante dei due nitronil nitrossidi aumenta la stabilità del complesso di Dy. Questa stabilità in soluzione è quindi stata studiata tramite spettroscopia EPR (vedi figura J). Queste misure confermano che il complesso è maggiormente stabile nel tempo in una soluzione di diclorometano. Questo risultato fa sì che questo complesso sia un potenziale candidato per una funzionalizzazione.

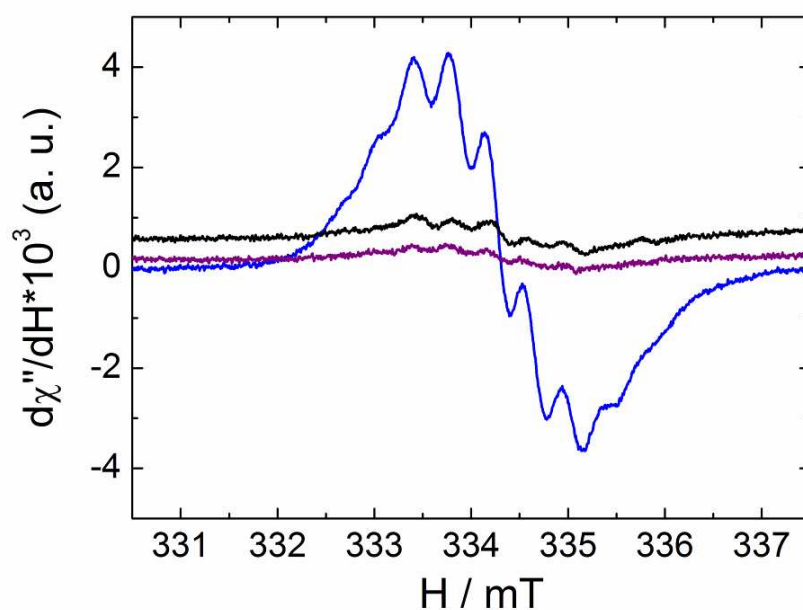


Figura J: Spettri EPR del biradicale (blu), del complesso di Dy (viola) e dello stesso complesso dopo due giorni (nero).

Da un punto di vista magnetico, il composto mostra una dipendenza in frequenza della suscettività dinamica anche in assenza di campo applicato. I valori estratti sono caratteristiche dei magneti a singola molecola (vedi figura K). Questo studio identifica un candidato ideale nei complessi Dy-radicali per lo studio di magneti molecolari su superficie. Le tappe successive sono la

funzionalizzazione del radicale, seguite dalla deposizione su superficie, per finalmente misurare le proprietà magnetiche del monostrato su superficie di oro.

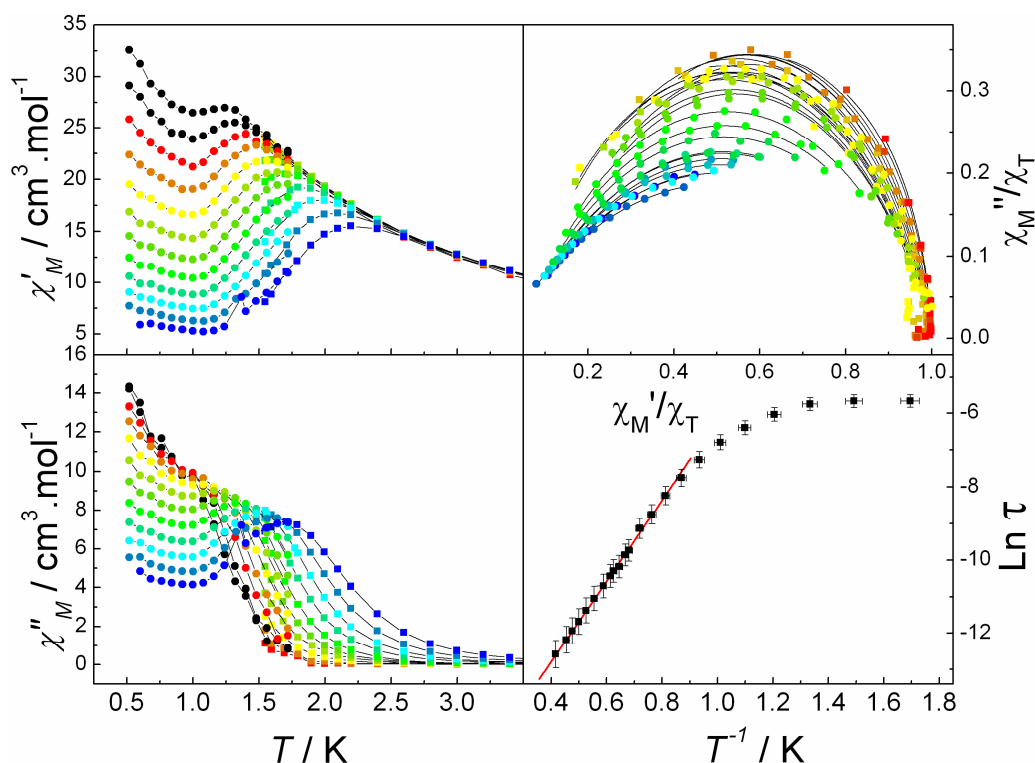


Figura K: Misure della suscettività dinamica del complesso di Dy e biradiale nitronil nitrossido.

Conclusion

Il lavoro presentato, ottenuto utilizzando tecniche sofisticate e realizzato grazie a varie collaborazioni fruttuose, dimostrano che lo studio dell'anisotropia di composti a base di lantanidi in bassa simmetria è ormai accessibile, grazie al potentissimo strumento costituito dalla combinazione della misura della magnetizzazione rispetto all'angolo con il calcolo ab-initio. Attraverso la diversità dei composti presentati in questa tesi, è stato evidenziato che i lantanidi, in particolare il disprosio, costituiscono elementi di scelta per la ricerca di magneti a singola molecola con alta barriera di energia. Infine, la funzionalizzazione di questo tipo di composti finalizzata alla deposizione su superficie conduttrice apre prospettive incoraggianti in questo ambito di ricerca.

Contents

INTRODUCTION.....	3
CHAPTER 1: MAGNETIC ANISOTROPY OF DYSPROSIUM(III) IN A LOW SYMMETRY ENVIRONMENT: A THEORETICAL AND EXPERIMENTAL INVESTIGATION.....	7
1.1 INTRODUCTION.....	9
1.2 SYNTHESIS AND CRYSTAL STRUCTURE	11
1.3 MAGNETIC MEASUREMENTS.....	15
1.4 AB INITIO CALCULATIONS.....	20
1.5 QUANTITATIVE ANALYSIS OF THE MAGNETIC DATA	22
1.6 CONCLUSION	25
CHAPTER 2: PRELIMINARY STUDY FOR CHAPTER 3.....	29
CHAPTER 3: COUPLING DY_3 TRIANGLES TO ENHANCE THEIR SLOW MAGNETIC RELAXATION.....	39
3.1 INTRODUCTION.....	41
3.2 SYNTHESIS AND CRYSTAL STRUCTURE	41
3.3 MAGNETIC MEASUREMENTS	43
3.4 AB INITIO CALCULATIONS.....	46
3.5 ANGLE RESOLVED MAGNETOMETRY	48
3.6 ENERGY SPECTRUM FOR DY_6	52
3.7 CONCLUSION	54
CHAPTER 4: DIMERS AND CHAINS OF {3D-4F} SINGLE MOLECULE MAGNETS CONSTRUCTED FROM HETEROBIMETALLIC TECTONS	57
4.1 INTRODUCTION.....	59
4.2 CRYSTAL STRUCTURES.....	60
4.3 MAGNETIC MEASUREMENTS	65
4.4 CONCLUSION	72
CHAPTER 5: SINGLE MOLECULE MAGNET BEHAVIOUR IN ROBUST DYSPROSIUM-BIRADICAL COMPLEXES.....	75
5.1 INTRODUCTION.....	77
5.2 SYNTHESIS AND CRYSTAL STRUCTURE ANALYSIS.....	77
5.3 SOLUBILITY STUDY	81
5.4 MAGNETIC MEASUREMENTS.....	83
5.5 CONCLUSION	88
CONCLUSIONS AND PERSPECTIVE.....	91
APPENDIX.....	99
A.1 DC-MAGNETOMETER.....	101
A.2 VSM MAGNETOMETER	103
A.3 AC-MAGNETOMETER	104
A.4 HORIZONTAL ROTATOR.....	111

Introduction

In 1983, in a NATO school titled “Structural-magnetic correlations in exchanged coupled systems” was introduced for the first time the Molecular Magnetism¹, in particular the idea to control the magnetic properties of a system synthesizing designed molecules, instead of using the magnetism strictly as an investigation technique. This laid the foundation of a new branch of molecular sciences, able to link chemistry and physics, with the aim to create magnetic objects with tunable properties thank to a bottom-up approach, which exploit the structural and functional flexibility of molecules, as well as their tendency to organize themselves in supramolecular assemblies that can be finely tuned through a chemical approach.

Molecular magnetism initially focused on the realization of molecular networks exhibiting long range magnetic order and mimicking the behavior of bulk magnets.

The observation that the most typical feature of magnets, the presence of a remnant magnetization, could also be observed in discrete molecules, nowadays known by the evocative name of Single Molecule Magnet (SMM), boosted the interest on molecular magnetism. In SMM the opening of the hysteresis cycle is not associated to long range order but rather to the slowing down of the magnetic relaxation. This is an intrinsic property of the molecule and is associated to its magnetic anisotropy, similarly to what occurs in magnetic nanoparticles.

The mechanism of relaxation in SMM has been investigated in detail and is now commonly accepted that it is associated to the presence of a double well energy potential, as sketched in Figure I.1, where crystal field effects remove the $2S+1$ degeneracy in zero magnetic field of the ground S state of a magnetic molecule. In a SMM the $M = \pm S$ levels, eigenstates of the leading term of the magnetic anisotropy $H_{an} = DS_z^2$, are the lowest in energy, being D negative. This corresponds to easy axis magnetic anisotropy.

This picture is the quantum analogue of that encountered in single-domain magnetic nanoparticles. The reversal of the magnetization occurs through coupling with phonons, and obeys the Arrhenius law:

$$\tau = \tau_0 \exp(\Delta E/k_B T)$$

typical of thermally activated processes. The height of the barrier is therefore associated to energy separation between the lowest and highest states in the barrier, *i. e.* $|D|S^2$ or $|D|(S^2-1/4)$ for integer and half-integer spin, respectively but at low temperatures also under-barrier processes are possible.

However, in contrast to nanoparticles, no size and shape distribution is observed when investigating a crystal of SMM.

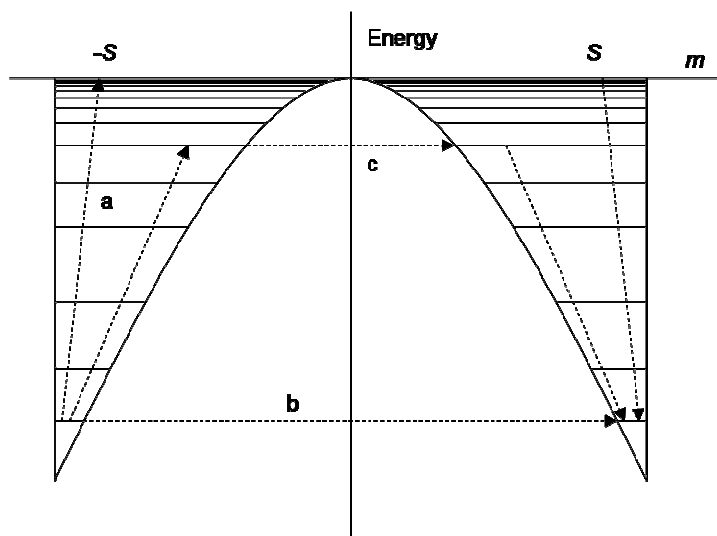


Figure I.1: Possible relaxation process in vanishing field. See text for description

First SMM were based on the famous and widely studied $Mn_{12}ac$ cluster synthesized by Lis². This latter was the first cluster to display slow relaxation of the magnetization at low temperature³. Moreover the presence of a hysteresis of molecular origin shows that this tiny magnet is able to maintain its magnetization state for months at 2K, and so to be able to magnetically store information. The system thus combines the advantage of a bulk magnet (*i.e.* the ability to store information) and of a nanosized material (*i.e.* presence of quantum effects). This latter aspect offers the possibility to manage the information through phenomena driven by quantum mechanics and the possible application to quantum computing has been reported⁴. The most relevant quantum effect seen on this type of material is the quantum tunneling of the magnetization⁵.

Despite the intense research activity the blocking temperature of SMM, *i.e.* the temperature below which the hysteresis cycle is open, remains quite low. A promising strategy to increase this temperature is the organization of anisotropic magnetic centers in one-dimensional structures. This has led to a novel class of molecular magnetic materials, named for analogy as Single Chain Magnets (SCM).⁶

Equally groundbreaking has been also the discovery that some mononuclear lanthanide complexes can behave as SMM. The first reported example is the complex Terbium(III) bis-phthalocyaninato, with a double decker structure.⁷

Lanthanides ions are widely employed in magnetism for their large magnetic moments, in most cases associated to huge magnetic anisotropy originated by the large spin-orbit coupling. Dysprosium(III), with its 4f⁹ electronic configuration, has a ground ⁶H_{15/2} state and is generally characterized by large magnetic anisotropy of the easy-axis type.

The magnetic anisotropy of lanthanide ions has been widely investigated in the past⁸ but mainly in high symmetry environment. Its characterization in low symmetry is much more demanding, from both experimental and theoretical point of views, but a necessary step for a rational design of molecular magnetic materials.

This thesis is devoted to the magnetic investigation of different types of molecular magnetic systems comprising dysprosium(III) ions.

The first chapter of this thesis reports the experimental determination of the magnetic anisotropy of a model exchange-coupled system comprising a Dy^{III} ion and organic radicals. Single-crystal magnetic measurements through angle-resolved magnetometry have been performed since this system is EPR silent. These measurements were then combined to ab-initio calculations.

In a second part, an hexanuclear dysprosium(III) cluster, made of two Dy triangles, synthesized in the laboratory of Prof. Annie Powell, at the University of Karlsruhe, Germany, is studied. Triangular systems are attracting increasing interest because they can show exotic phenomena, like spin chirality and slow relaxation of the magnetization of the excited state. As an introduction of this study, Chapter 2 briefly describes the magnetic properties of the triangular building block. Then, Chapter 3 reports the magnetic characterization of the hexanuclear cluster. In order to characterize the magnetic anisotropy of this compound, the angle-resolved magnetometry protocol, used in chapter 1, was improved.

The combination of different spin carriers could be another way to fulfill the required conditions for the observation of SMM behavior: a high spin ground state and a large easy-axis anisotropy. Chapter 4 is dedicated to the magnetic study of two 4f-3d compounds synthesized by the group of Prof. Marius Andruh of the University of Bucharest (RO). A tetranuclear complex [Ni₂(valpn)₂Dy₂(pdca)₂(NO₃)(H₂O)₆](NO₃)·4H₂O and a ladder-like coordination polymer ∞¹[Ni₂(H₂O)₂(valpn)₂Dy₂(tfa)₃]·4CH₃CN have been magnetically characterized.

Finally, in chapter 5, we come back to the study of 4f-radicals complex. However this work is focused on a different aspect, the possibility to graft molecular compounds on surfaces. In addition to the magnetic characterization, a specific attention was given to the

study of the solubility of this complex since the stability in solution is one of the prerequisite for a compounds to be graft on surface as a Self Assembled Monolayer.

Bibliography

- (1) Willet R.D., Gatteschi D., Kahn O.; **1983**, *Magneto-structural correlations in exchange coupled systems*, Riedel Publishing, Dordrecht.
- (2) Lis, T., *Acta Crystallogr.*, **1980**, B36, 2042.
- (3) a) Caneschi, A., Gatteschi, D., Sessoli, R., Barra, A.-L., Brunel, L.C., Guillot, M., *J.Am.Chem.Soc.*, **1991**, 13, 5873. b) Sessoli, R., Gatteschi, D., Caneschi, A., Novak, M.A., *Nature*, **1999**, 365, 141.
- (4) Jones, J.A., *Science*, **1998**, 280, 229.
- (5) Christou, G., Gatteschi, D., Sessoli, R., *MRS Bull.*, **2000**, 26, 66.
- (6) Clerac, R.; Miyasaka, H.; Yamashita, M.; Coulon, C. *J. Am. Chem. Soc.*, **2002**, 124, 12837.
- (7) Ishikawa, N., Sugita, M. and Wernsdorfer, W. *Angewandte Angew. Chem., Int. Ed.*, **2005** 44: 2931
- (8) Abragham, A., Bleaney, B., *Electron paramagnetic resonance of transition ions*, **1986**, Dover, New York.

Chapter 1

Magnetic anisotropy of Dysprosium(III) in a low symmetry environment: a theoretical and experimental investigation

<u>1.1 INTRODUCTION</u>	9
<u>1.2 SYNTHESIS AND CRYSTAL STRUCTURE</u>	11
<u>1.3 MAGNETIC MEASUREMENTS.</u>	15
<u>1.4 AB INITIO CALCULATIONS.</u>	20
<u>1.5 QUANTITATIVE ANALYSIS OF THE MAGNETIC DATA</u>	22
<u>1.6 CONCLUSION</u>	25

1.1 Introduction

Magnetic anisotropy plays a crucial role in magnetic bistability and related memory effects, in both traditional magnets and low-dimensional molecular materials such as single molecule magnets (SMMs)¹ and single-chain magnets (SCMs).² In the design of new SMMs and SCMs with increased blocking temperatures (T_B), good control of the magnetic exchange (J), and consequently of the spin ground state of SMMs, has been achieved, leading to a record spin value as high as $83/2$.³ Much more remains to be done to also engineer the magnetic anisotropy, and in fact, the record T_B value of $Mn_{12}OAc$, the archetypal SMM, has only recently been broken.⁴

The magnetic anisotropy of an exchange-coupled system depends not only on the individual anisotropies of the metal ions but also on the relative orientation of the local axes. When the anisotropy is large, this may give rise to spin noncollinearity, which is responsible for several interesting magnetic properties, such as weak ferromagnetism,⁵ which has recently also been observed in SCMs.⁶ In SMMs, spin noncollinearity has been associated with the generation of high-order terms in the magnetic anisotropy, which are mostly responsible for tunneling of the magnetization.⁷ More recently, spin noncollinearity has been observed in a triangular dysprosium(III) cluster⁸ (See Chapter 2) and indeed predicted theoretically,⁹ giving rise to spin chirality and slow magnetic relaxation together with a nonmagnetic ground state.

Anisotropic lanthanide ions are attracting increasing interest in molecular magnetism,¹⁰ where they are often combined with 3d metal ions¹¹ or other magnetic centers.^{12,13} Adequate analysis of the magnetic properties is in most cases lacking because of its complexity, thus hampering the development of a rational and efficient strategy to increase T_B in these systems. In fact, in low-symmetry environments, crystal-field analysis is not fully reliable because of the large number of parameters that must be included in the treatment. Ab initio post-Hartree-Fock calculations have recently been employed successfully to determine the magnetic anisotropy of a triangular Dy_3 cluster, but only an indirect comparison of the theoretical prediction with the single-ion anisotropy was possible.⁹

In this thesis, I have contributed to the experimental investigations of a model exchange-coupled system comprising a Dy^{III} ion and organic radicals to shed light on the magnetic anisotropy and exchange interactions involving this otherwise intractable lanthanide ion. The interest in this type of system is many-sided. In fact, compounds comprising nitronyl nitroxide (NIT-R) radicals (NIT-R)₂-R-4,4,5,5-tetramethylimidazolidine-3-oxide-1-oxyl) and rare earths give rise to a multitude of interesting phenomena, including (i) relatively high

temperature transitions to three-dimensional ferromagnetic order,¹⁴ (ii) SMMs,^{12,13} (iii) SCMs,¹⁵ and (iv) chiral magnetic phases.¹⁶ This last point is associated with the ability of rare earths, both diamagnetic and paramagnetic, to transmit relatively strong next-nearest-neighbor (NNN) exchange interactions between NIT-R radicals,¹⁷ giving rise to spin frustration. The need to include NNNs in the analysis of the interactions inside exchange-coupled clusters is a general one, and it is very important to establish structural magnetic correlations in order to properly handle complex systems.¹⁸

It has been recently reported by our group the synthesis and magnetic analysis of a family of 4f-based SCMs,¹⁵ of which the Dy derivative having the formula $[\text{Dy}(\text{hfac})_3(\text{NIT-C}_6\text{H}_4\text{OPh})]_\infty$ was the most deeply characterized.^{15,19} Nevertheless, no analysis of the magnetic anisotropy of the rare earths could be provided, since simulation of the magnetic behavior of rare-earth-containing compounds is rather tricky. In fact, the spin-Hamiltonian approach, which works well for transition-metal ions, is less appropriate for rare earths because of the unquenched orbital momentum, and crystal-field analysis suffers from overparametrization problems. In the absence of detailed knowledge of the local magnetic anisotropy, no clear evidence of NNN interactions mediated by the anisotropic rare earth can in fact be detected through a simple analysis of the magnetic behavior.

In order to obtain information on complex systems, single crystal EPR measurements allow for a full characterization of the magnetic anisotropy in compounds based on transition metals,²⁰ and a report is available on a cerium-iron derivative.²¹ Unfortunately, most Dy^{III} derivatives, as well as $[\text{Dy}(\text{hfac})_3(\text{NIT-C}_6\text{H}_4\text{OPh})_2]$, the monomeric analogue of the chain, are EPR silent, since anisotropic rare earths present very fast electronic relaxation that broadens the EPR signal, hampering a precise determination of the *g* tensor.

Single-crystal magnetic measurements can provide information on the magnetic anisotropy through angle-resolved magnetometry. This technique was developed in the 1960s and has been used in the past to characterize the magnetic anisotropies of a huge variety of samples, mainly thanks to the fiberglass torque method.²² However, it has scarcely been employed in molecular magnetism because of its complex procedure and low sensitivity, a problem recently solved with the integration of sample rotators in SQUID magnetometers. Another problem that has been detrimental to its widespread use is that, in many cases, the observed magnetization is the crystal average of molecules that are structurally identical but oriented differently in the crystal. This occurs when the site symmetry of the magnetic molecules is lower than that of the space group. For instance, a problem like this occurs in widely spread monoclinic lattices when the molecule is in a general position or on an

inversion center. Triclinic crystals do not suffer this drawback but are more difficult to handle.

Monomeric species having the general formula $[\text{Dy}(\text{hfac})_3\text{-(NIT-R)}_2]$, when suited to single-crystal magnetization measurements, can allow the determination of the local magnetic anisotropy of the Dy ions, thus affording valuable information about Dy-based magnetic materials and $[\text{Dy}(\text{hfac})_3(\text{NIT-C}_6\text{H}_4\text{OPh})]_\infty$ SCM in particular. Screening of the outcome of the reaction of $\text{Dy}(\text{hfac})_3 \cdot 2\text{H}_2\text{O}$ with NIT- $\text{C}_6\text{H}_4\text{OR}'$ radicals revealed that with $\text{R}' = \text{ethyl}$, crystallization occurs in the triclinic *P-1* space group with only one Dy center in the asymmetric unit. We thus investigated $[\text{Dy}(\text{hfac})_3(\text{NIT-C}_6\text{H}_4\text{OEt})_2]$ and measured the susceptibility tensor at various temperatures. We then succeeded in rationalizing the observed magnetic anisotropy with predictions from an ab initio calculation, demonstrating that this theoretical approach can be used to reliably predict the nature, strength, and orientation of the magnetic anisotropy of rare earths.

1.2 Synthesis and Crystal Structure

Reaction of NIT-R radicals with $\text{Dy}(\text{hfac})_3 \cdot 2\text{H}_2\text{O}$ salts has previously been employed to obtain both chain compounds and various monomeric species,^{13-15,17,30} depending on the stoichiometry of the reagents and the presence of water. The $\text{Dy}(\text{NIT-R})_2$ stoichiometry was chosen to mimic the coordination around Dy^{III} in the chain compound. Additionally, it also allows information on the radical-radical NNN interactions to be gathered.

The general synthetic procedure to obtain this stoichiometry is based on dissolving 0.025 mmol of $[\text{Dy}(\text{hfac})_3 \cdot 2\text{H}_2\text{O}]$ in boiling n-heptane (40 mL) under stirring. When the volume reaches 10-12 mL, the stirring proceeds on a cold rotator and, at 75°C, 0.1 mmol (32 mg) of radical are quickly added.

The mononuclear compound with the same NIT- $\text{C}_6\text{H}_4\text{OPh}$ radical of the SCM analogue obtained in this way crystallizes in a monoclinic space group with the metal ion in a general position. The presence in the crystal cell of identical molecular units differently oriented does not make it suitable for angle resolved magnetic measurements, as angle-resolved magnetometry provides the crystal magnetic susceptibility tensor, which corresponds to the molecular one only when the molecule has the same point symmetry as the crystal space group. However, a quantitative determination of the molecular χ tensor is possible for the triclinic system.³¹

A screening of the outcomes of the reactions of $\text{Dy}(\text{hfac})_3 \cdot 2\text{H}_2\text{O}$ with NIT- $\text{C}_6\text{H}_4\text{OR}'$ radicals revealed that $[\text{Dy}(\text{hfac})_3(\text{NIT}-\text{C}_6\text{H}_4\text{OEt})_2]$ (abbreviated in **Dy_{mono}** for of the remaining of the chapter) crystallizes in the triclinic *P-1* space group with $a=12.259(5)$, $b=14.235(4)$, $c=17.560(1)$, $\alpha=98.111(2)$, $\beta=103.836(5)$, $\gamma=111.260(8)$, $V=2683.6(16)$ Å³, and $Z=2$. Thus only one Dy center is present in the asymmetric unit.

To solve the crystal structure X-Ray data were collected at 150 K with an Oxford Diffraction Xcalibur3 diffractometer using Mo- $K\alpha$ radiation ($\lambda=0.71073$ Å). Data reduction was accomplished using CRYALIS.RED p 171.29.2. Absorbtion correction was performed using both ABSGRAB and ABSPACK software included in the CrysAlis package.²⁴ The ABSGRAB correction allows for the determination of μ parameter. The structure was solved by direct methods, developed by successive difference Fourier syntheses, and refined by full-matrix least-squares on all F² data using SHELXL 97.25 Hydrogen atoms were included in calculated positions and allowed to ride on their parent atoms.

In **Dy_{mono}**, the Dy ion is octacoordinated by three hfac- ligands and two oxygens belonging to the NIT-R radicals, as shown in Figure 1.1.

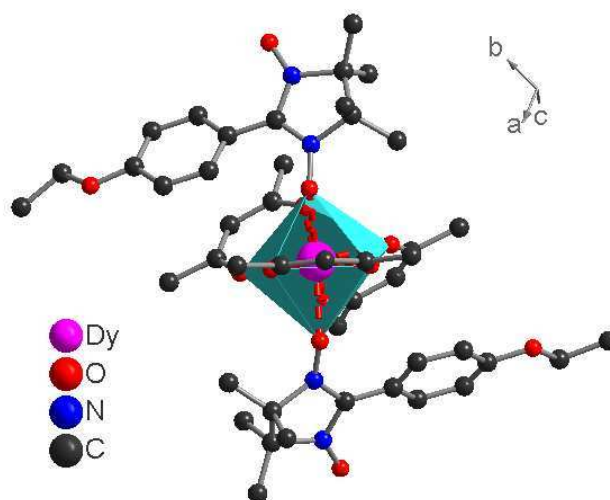


Figure 1.1: Representation of **Dy_{mono}**, as seen from the idealized C_2 molecular symmetry axis. The coordination environment of the Dy^{III} ion is highlighted with an azure polyhedron. Fluorine and hydrogen atoms are omitted for clarity.

The coordination polyhedron of each Dy^{III} ion is quite regular, with six Dy-O_{hfac} distances ranging from 2.333(4) to 2.371(3) Å and two almost identical Dy-O_{rad} distances of 2.328(3) and 2.331(3) Å. Selected bond distances and angles are listed in Table 1.1.

Bonds	Bond length (Å)	Delta 1* (Å)	Angle (°)	Angle (°)	Delta 1* (Å)
Dy-O1	2.316 (3)	-0.07	O1-Dy-O5	138.5(3)	-1.61
Dy-O5	2.351 (3)	-0.007	O7-Dy-O8	73.5(2)	0.38
Dy-O9	2.336 (4)	-0.0181	O9-Dy-O10	72.7(2)	0.32
Dy-O7	2.322 (4)	-0.0395	O11-Dy-O12	73.6(7)	0.30
Dy-O12	2.358 (3)	0.0298	O5-Dy-O12	74.4(4)	-2.93
Dy-O8	2.375 (4)	0.0469	O1-Dy-O11	70.6(6)	-5.27
Dy-O11	2.349 (3)	0.006			
Dy-O10	2.368 (4)	0.0254			
N1-O5	1.296 (4)	0.002			
N3-O1	1.314 (5)	0.02			

*Delta is the difference calculated with respect to chain as (Dy_{mono} - chain)

Table 1.1: Selected bond length and angles for Dy_{mono} , and comparison with the chain analogue.

The coordination geometries of the Dy ions in the SCM and in Dy_{mono} are very similar to each other, with the highest discrepancies being 0.055 Å in the Dy-O bond length and 4.2° in the bond angle. This is clearly demonstrated by bond distances and angles (Table 1.1) and a superposition of the coordination polyhedra of the two compounds (Figure 1.2 and 1.3), which can be schematized as distorted square antiprisms.³² This similarity is mainly due to the fact that despite the stoichiometry change, the same stacking interactions take place between the aromatic rings of the radicals and two of the three hfac- ligands, governing the geometrical arrangement of the complex. Consequently, as for the SCM analogue, the two radicals point in almost opposite directions.



Figure 1.2: Superimposition of the coordination polyhedron the Dy^{III} from Dy_{mono} (colored sticks) on the Dy^{III} and its coordinated atoms from the chain (black balls).

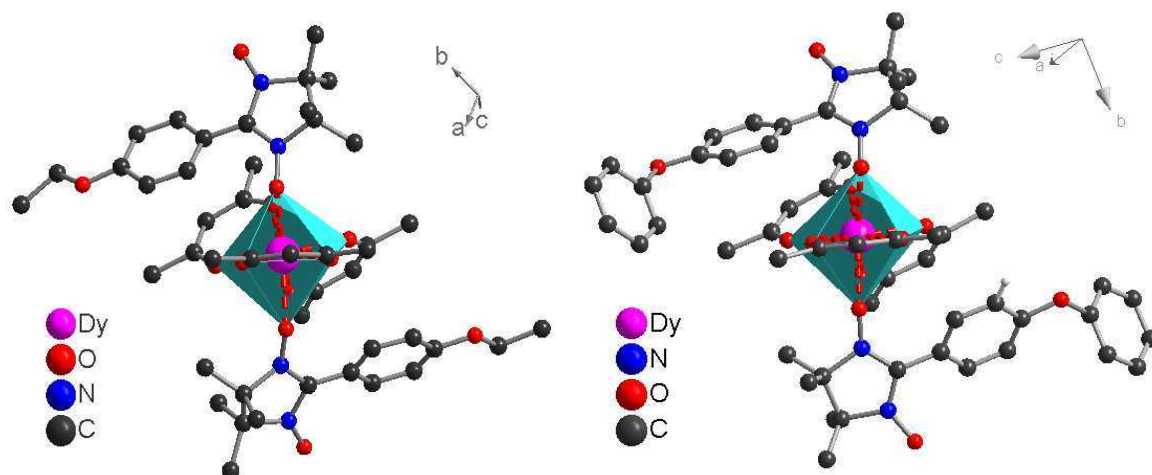


Figure 1.3: Representations of $[Dy(hfac)_3(NITC_6H_4-OEt)_2]$ (Dy_{mono}) (left picture) and $[Dy(hfac)_3(NITC_6H_4-OPh)]_{\infty}$ ($chain$) (right picture). Fluorine and hydrogen's atoms are omitted for clarity.

The monomers are well-isolated one from another, with a minimum Dy-Dy distance of 10.06 Å. Neither intermolecular contact through the noncoordinated NO groups of the radicals (minimum distance 4.26 Å) nor hydrogen bonds that could be responsible for intermolecular magnetic interactions are observed in the system. A representation of the crystal packing in Dy_{mono} is provided in Figure 1.4.

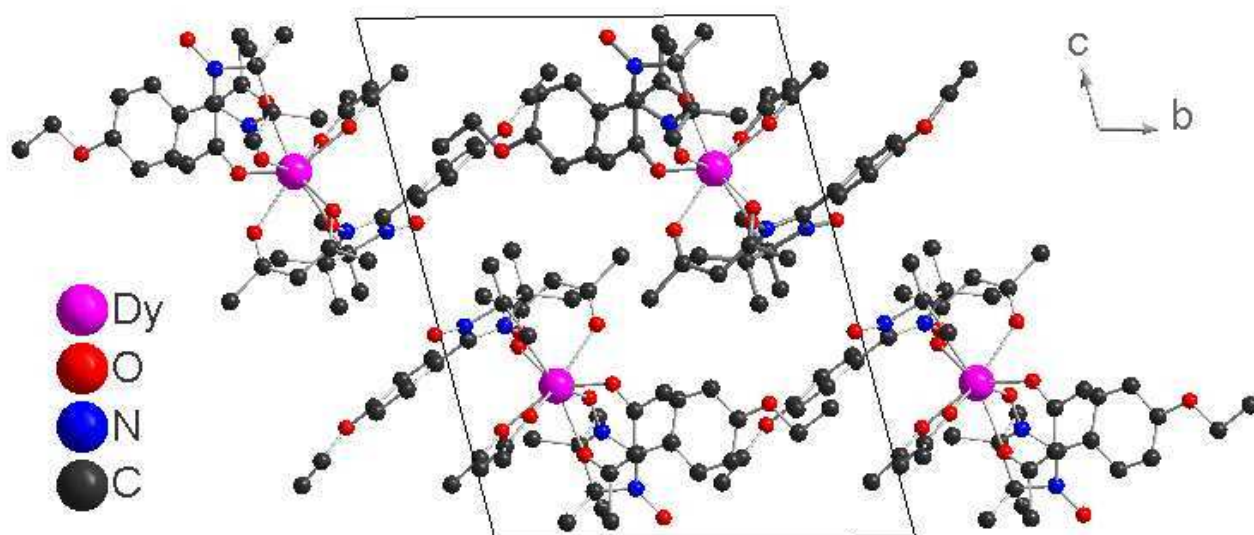


Figure 1.4: View of the crystal packing of $[Dy(hfac)_3(NITC_6H_4-OEt)_2]$ (3) along the a axis. Fluorine and hydrogen atoms are omitted for clarity.

1.3 Magnetic Measurements.

The angle-dependent magnetic measurements were obtained with a Cryogenic S600 SQUID magnetometer equipped with an automatic horizontal sample rotator (see Appendix). Single crystal ac susceptibility was measured with a Quantum Design MPMS SQUID magnetometer. The magnetization curve was obtained with a Vibrating Sample Magnetometer (Oxford Inst. MAGLAB2000 platform).

A crystal of Dy_{mono} (1.48 mg) was placed on its (001) crystallographic face on a Teflon cube and stuck with Apiezon N grease on one face of the cube, with an estimated error of $\pm 3^\circ$. Three orthogonal faces of the cube were then employed to fix the sample on the platelet of a Quantum Design Horizontal Sample Rotator adapted to work in a Cryogenic S600 SQUID magnetometer. The angular dependence was investigated over an angular range of more than 180° in three consecutive rotations performed along the three orthogonal crystallographic axes \mathbf{a} , \mathbf{b}' , \mathbf{c}^* , where \mathbf{c}^* is defined as $\mathbf{a} \times \mathbf{b}$ and \mathbf{b}' is orthogonal to \mathbf{a} and \mathbf{c}^* defining a right-handed frame. The signal has been corrected for the diamagnetic contribution of the Teflon cube, which, however, has been fundamental to better control the orthogonality of the three rotations. Measurements have been performed in a magnetic field of 1 kOe to avoid a strong torque on the crystal.

The angular dependence of the M/H ratio was measured in a static field of 1 kOe. At this field, the magnetization is almost linear in H , and the M/H ratio can be assumed to correspond to the susceptibility. Figure 1.5 shows that the susceptibility is highly dependent on the angle, particularly for the rotation around \mathbf{b}' , where values span the range from 0.74 to 12.9 emu mol⁻¹.

Similar to what is commonly done in single-crystal EPR analysis,²⁰ the data were fitted assuming the tensorial relation $\mathbf{M} = \boldsymbol{\chi} \mathbf{H}$. For \mathbf{H} rotating in the $\alpha\beta$ plane we can use the expression:

$$M(\theta) = \chi_{\alpha\alpha} H (\cos \theta)^2 + \chi_{\beta\beta} H (\sin \theta)^2 + 2\chi_{\alpha\beta} H \sin \theta \cos \theta \quad (1.1)$$

where α and β stay for the vectors of \mathbf{a} , \mathbf{b}' , and \mathbf{c}^* in a cyclic permutation and θ is the angle between \mathbf{H} and the α vector.

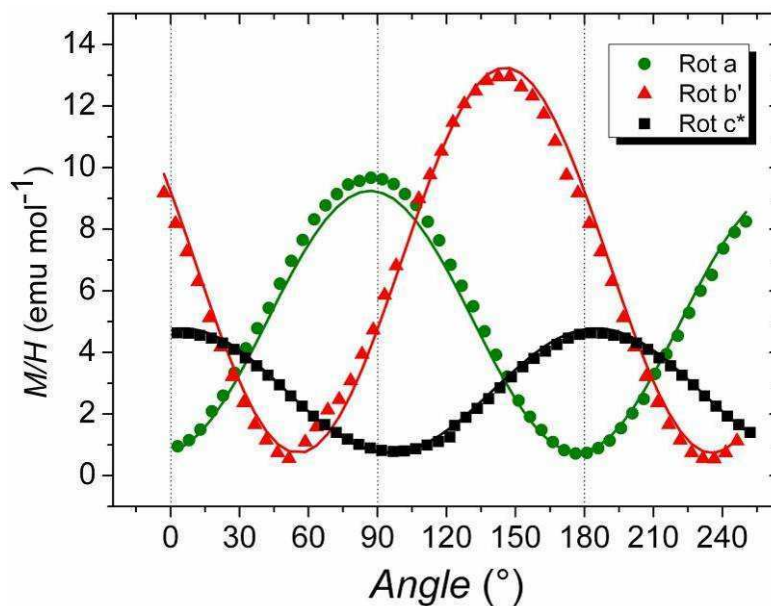


Figure 1.5: Angular variation of the molar susceptibility of Dy_{mono} at $T=2.5$ K along the three axes of the laboratory frame. At $\theta=0^\circ$ and 90° \mathbf{H} is parallel to, respectively: \mathbf{b}' and \mathbf{c}^* , for the rotation around \mathbf{a} ; \mathbf{c}^* and \mathbf{a} for the \mathbf{b}' rotation; \mathbf{a} and \mathbf{b}' for \mathbf{c}^* rotation.

The best fit procedure at $T=2.5$ K (Figure 1.5) provides the full susceptibility tensor (see tensor below), whose diagonalization afforded the three principal components $\chi_x=0.2\pm 0.1$, $\chi_y=1.3\pm 0.1$, $\chi_z=13.2\pm 0.2$ $\text{emu}\cdot\text{K}\cdot\text{mol}^{-1}$.

$$\chi = \begin{pmatrix} 0.58 & -0.57 & 0.56 \\ -0.69 & -0.72 & -0.01 \\ 0.41 & -0.38 & -0.82 \end{pmatrix}$$

Full susceptibility tensor of Dy_{mono}

The eigenvector matrix provides the molecular reference frame \mathbf{x} , \mathbf{y} , \mathbf{z} , and the easy axis \mathbf{z} is superimposed on the molecular structure in Figure 1.6. The outcome of this analysis is a strong Ising-type magnetic anisotropy for Dy_{mono} , with the easy axis along \mathbf{z} and the hard and intermediate axes along \mathbf{x} and \mathbf{y} , respectively. The experimental data refer to a three-spin system, but the assumption that the anisotropy is determined by Dy^{III} appears to be a reasonable one. This result represents, to the best of our knowledge, the first direct estimation of the magnetic anisotropy of a rare-earth center in the absence of symmetry, and it shows that

the easy axis lies not along any bond but rather through the approximate binary axis of the coordination environment (i.e., roughly the view axis of Figure 1.1).

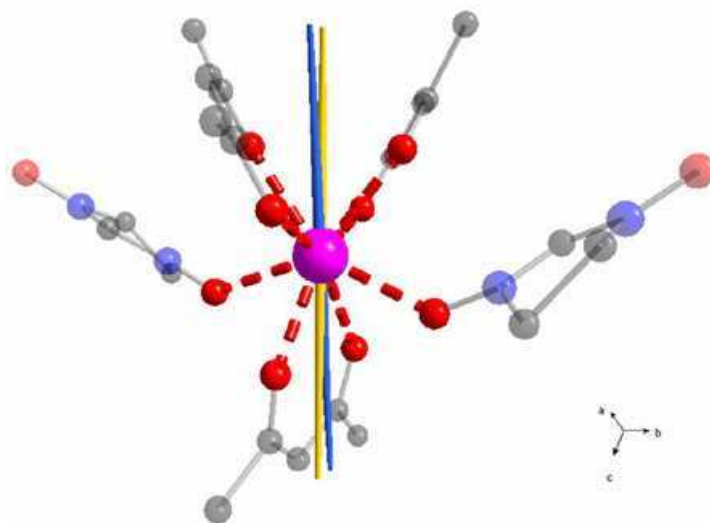


Figure 1.6: Representation of a molecule of Dy_{mono} together with the easy axis determined from the angular dependence of the susceptibility (yellow) and from *ab initio* calculation (blue). The angle formed by the two directions is ca. 7° .

Temperature-dependent measurements were then performed over the $T = 2$ -15 K range at $H = 1$ kOe (see Figure 1.7 for the rotation along *a*). The χ values depend strongly on T , with a 10-fold reduction of the maximum values in going from 2 to 15 K, independent of the rotation axis. On the contrary, the minimum values remain roughly the same, and no shift of the positions of the extrema is observed.

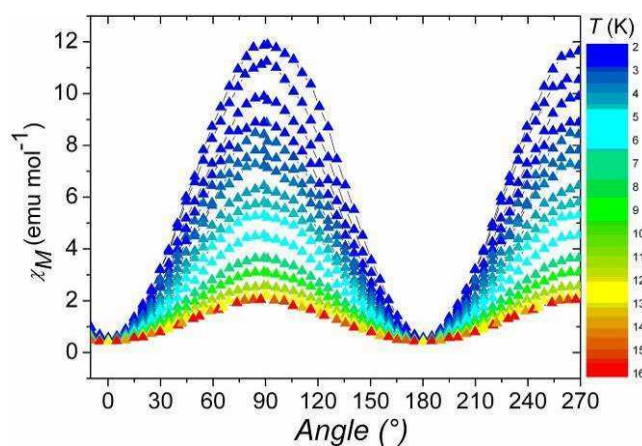


Figure 1.7: Angular variation of the susceptibility of Dy_{mono} measured at different temperatures, as reported in the color scale, from 2 (blue) to 15 K (red). Rotations are performed around the *a* axis and $\theta = 0^\circ$ and 90° correspond to measurements along *b'* and *c**, respectively.

Once angle-resolved magnetometry had provided the orientation of its anisotropy tensor we were able to measure the temperature dependence of the magnetic principal values of the magnetic susceptibility.

The same crystal was in fact placed on a specially designed support to measure its magnetization when the field is applied along the easy and hard axes previously determined. The temperature dependence of the magnetization has been measured with a Quantum Design SQUID magnetometer, while the field dependence has been measured up to 120 kOe with an Oxford Instruments Vibrating Sample Magnetometer. In this case, only the easy axis has been investigated because the application of a field larger than 40 kOe resulted in a torque sufficient to detach and break the crystal. Measurements on a powder sample were performed with the same instruments, grounding crystals in a pellet.

The results, which are shown in Figure 1.8, confirm that the magnetic anisotropy remains constant up to 30 K. Over the investigated temperature range, the $\chi_z T$ product shows a rounded maximum at ca. 15 K that reaches a value of 34 emu K mol⁻¹.

By using the same sample holder, we also measured the H-dependence of M at T = 1.6 K for H up to 120 kOe (Figure 1.9). A plateau is observed between 10 and 60 kOe with a magnetization value of ca. 10 μ_B ; beyond 70 kOe, M successively increases to reach a value of 11.8 μ_B . With an increase in T, the jump is transformed into a linear increase in M. Measurements with the field perpendicular to the easy axis were not possible, as they resulted in a torque strong enough to break the crystal or detach it from the sample holder. However, it was possible to measure the magnetization of a powder sample with blocked microcrystals in a pellet. The corresponding magnetization curve, which is also shown in Figure 1.9, differs significantly, being reduced by a factor of almost 2 and having no well-defined step even at low temperatures.

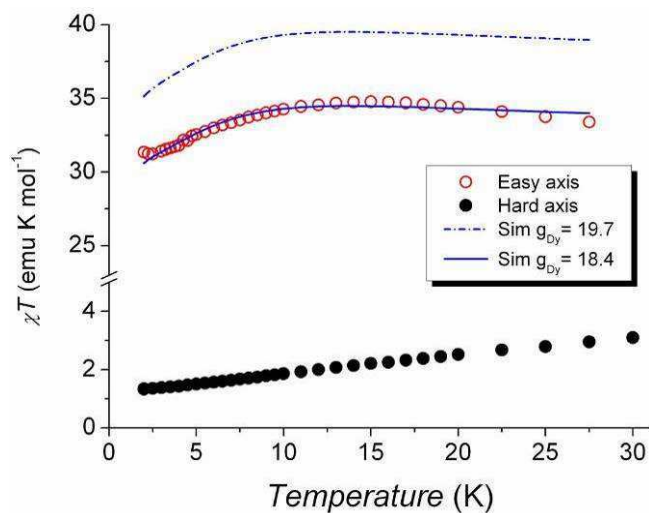


Figure 1.8: Temperature dependence of the χT product of Dy_{mono} measured along the hard axis (solid black circles) and the easy axis (empty red circles). Lines are theoretical simulations using an analytical expression derived from (2) considering $J_{NN} = -13.7 \text{ cm}^{-1}$ and $J_{NNN} = 15 \text{ cm}^{-1}$, with $g_{\text{Dy}} = 19.7$ (blue dash-dot curve) or $g_{\text{Dy}} = 18.4$ (blue solid curve), as reported in section 1.5.

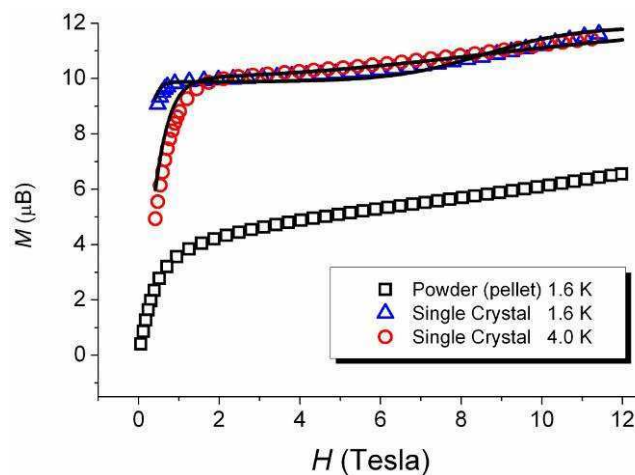


Figure 1.9: Field dependence of the magnetization of Dy_{mono} measured on single crystal with the field oriented along the easy axis at 1.6 K (blue triangles), at 4 K (red circles) and on a powder pellet (black squares). The solid lines represent curves obtained using the analytical expression derived from the spin-hamiltonian (eq 1.2), as discussed in section 1.5.

1.4 Ab Initio Calculations.

Thanks to the collaboration with Dr. Javier Luzon it has been possible to evaluate the low lying energy levels of the Dy ion in the coordination environment of the X-ray structure via CASSCF calculations. Only a brief summary of the methods and results will be provided here.

A simplified molecular model was considered in order to reduce the otherwise too large computational time. The fluorides in the hfac- ligands were replaced by H atoms and the NIT-C₆H₄-OEt radicals by NIT-CH₃, and H atoms were added to the external oxygen atoms of the radicals, transforming them into closed shell molecules in order to reduce the active space of the CASSCF calculations. In view of the internal nature of the 4f orbitals, they should be the most sensitive to ionic interactions, justifying the above assumptions.

All of the atoms were represented by basis sets of atomic natural orbitals from the ANO-RCC library, as implemented in the MOLCAS 7.0 quantum chemistry package. The following contractions were used: [8s7p4d3f2g] for Dy; [3s2p] for O, C, and N; and [2s] for H. The CASSCF active space consisted of the Dy 4f orbitals, containing nine electrons in seven orbitals [CASSCF(9,7)]. CASSCF state average calculations of all of the sextets (21 roots) and all of the quadruplets (224 roots) were computed. As for the doublets, because of hardware limitations, a subset of 200 out of a total of 490 roots was considered in the state average calculations. With these CASSCF states, three different RASSI state interactions were computed in order to check the effect of the other energy levels on the spin-orbit splitting of the ⁶H_{15/2} ground multiplet: first, a calculation (labeled as A in Table 1.2) including all of the multiplets having an energy gap of less than 40 000 cm⁻¹ with respect to the ⁶H_{15/2} multiplet (the 6H, 6F, and 6P sextets, 108 quadruplets, and 32 doublets); second, a calculation (B) considering only the three sextets (6H, 6F, and 6P); and finally, a calculation (C) using only the 6H multiplet. The computed energies of the split levels of the ground ⁶H_{15/2} multiplet and the principal g values of the ground Kramers doublet are listed in Table 1.2. The energy pattern is basically the same in the three calculations, indicating a small mixture of the 6H multiplet with the other ones due to the spin-orbit coupling. Therefore, we performed a last CASSCF/RASSI calculation (D) considering only the 11 roots of the 6H multiplet in the CASSCF state average and using them for the RASSI-SO state interaction. The energies of the ⁶H_{15/2} multiplet and the g values from this last calculation are also listed in Table 1.2.

Calc:	A	B	C	D
Energy level (cm ⁻¹)				
E_1	30.2	30.3	29.9	40.4
E_2	62.1	63.0	62.6	75.0
E_3	66.6	67.4	67.4	79.1
E_4	99.6	101.5	101.5	111.4
E_5	114.7	116.0	115.8	128.9
E_6	215.9	220.6	221.0	237.8
E_7	372.8	380.2	380.0	411.1
Gyromagnetic factors				
g_x	1.5	1.7	1.8	1.0
g_y	1.3	1.4	1.4	0.9
g_z	17.6	17.5	17.4	18.2

Table 1.2: Energy levels of the ${}^6H_{15/2}$ multiplet and gyromagnetic factors for the ground Kramer's doublet state computed for Dy^{III} in Dy_{mono} using the CASSCF-RASSI-SO ab initio method. A: including in the RASSI-SO calculation all the CASSCF roots in the 0-40.000 cm⁻¹ energy range. B: Same as in A, but considering only the sextets roots. C: Considering only the 6H roots from an average CASSCF calculation with the total 18 sextet roots. D: As C, but from average CASSCF calculation with the 11 lowest sextet roots.

The magnetization easy axis, corresponding to the direction of the largest g component obtained from the last RASSI-SO computation, is represented together with the experimental one in Figure 1.6. The angle between the ab initio-computed and experimental easy axes is only 7°. This result allows us not only to confirm the experimental determination of the single ion anisotropy axis but also to support the use of the CASSCF/ RASSI-SO method as a suitable technique for the determination of single-ion easy anisotropy axes in lanthanide-based molecules.

1.5 Quantitative analysis of the magnetic data

The ab initio calculations suggest a strong Ising-type magnetic anisotropy of the Dy ion at low temperature. A first rationalization of the observed magnetic behavior can be given by considering that the ${}^6H_{15/2}$ ground electronic state of the Dy^{III} ion is characterized by $g_J=4/3$.^{17,33} The crystal-field interaction removes the $(2J+1)$ degeneracy, yielding eight Kramers doublets. In the Ising limit, the ground doublet can be reasonably approximated $m_J=\pm 15/2$, with the first excited doublet separated by ca. 60 K. Therefore, the low-T data can be interpreted by taking into account only the ground Kramers doublet, which can be treated as having the effective values $S_{eff}=1/2$ with $g_{eff,z}=2 \cdot 15/2 \cdot g_J=20$ and $g_{eff,x,y}=0$. These data are in good agreement with the data in column D of Table 1.2. With respect to the magnetization, the M value observed at the plateau, 9.9 μ B, is very close to the value of 10 μ B expected for this limiting case. The estimated g values compare well with those obtained by fitting the susceptibility data of Dy-NIT-R square dimers¹³ and those reported in the literature that have been extracted from Mössbauer experiments³⁴ and other techniques.^{33,35,36}

The observed magnetic behavior also suggests that the radicals are antiferromagnetically coupled and do not contribute significantly to M at low H. The increase in M at high H to reach the 11.92 μ B value confirms the presence of an NNN antiferromagnetic interaction (J_{NNN}) between the radicals, which is broken by the applied magnetic field at H = 120 kOe.

The ability to obtain single-crystal magnetic data with H applied along the easy axis of the Dy^{III} ion allows a much simpler analytical treatment to be performed. With the assumption that the two radicals interact isotropically between themselves via a J_{NNN} coupling while an Ising interaction, J_{NN} , occurs with the $S_{eff}=1/2$ of Dy^{III}, the spin Hamiltonian becomes:

$$\mathcal{H} = J\mathbf{S}_{R1} \cdot \mathbf{S}_{R2} + J'(S_{R1z} + S_{R2z})\sigma + g_{R1z}S_{R1z}\mu_B H_z + g_{R2z}S_{R2z}\mu_B H_z + g_{Dy}\mu_B\sigma H_z \quad (1.2)$$

where $\sigma = \pm 1/2$ due to the Ising nature of Dy^{III}. The splitting of the four Kramers' doublets present in zero magnetic field is given by:

$$\begin{aligned} E_{1,2} &= \pm(1/2g_{Dy}) \mu_B H \\ E_{3,4} &= J_{NNN} + 1/2 J_{NN} \pm(g_R + 1/2g_{Dy}) \mu_B H \\ E_{5,6} &= J_{NNN} \pm(1/2g_{Dy}) \mu_B H \end{aligned}$$

$$E_{7,8} = J_{NNN} - \frac{1}{2} J_{NN} \pm (g_R - \frac{1}{2} g_{Dy}) \mu_B H.$$

From these expressions, an analytical formula to reproduce the field and temperature dependence of the magnetization along the easy axis can easily be derived. Qualitative agreement with the experimental data is found for antiferromagnetic J_{NNN} and ferromagnetic J_{NN} values, with a sign alternation reminiscent of that observed for Gd-based compounds containing NIT-R radicals.³⁷ In this case, the E1,2 doublet lies lowest for zero and weak applied fields. At a field $H_{co} = (J_{NNN} + \frac{1}{2} J_{NN}) / (g_R \mu_B)$, a crossover with the first excited doublet E3,4 occurs. As far as the level crossing is concerned, the two coupling constants J_{NNN} and J_{NN} are therefore strongly correlated to one another, and many sets of J_{NNN} and J_{NN} values reproduce the observed step. To solve this point, we synthesized $[Y(\text{hfac})_3(\text{NIT-C}_6\text{H}_4\text{OEt})_2]$, which is structurally identical to **Dy_{mono}** except for the substitution of Dy^{III} with the diamagnetic Y^{III} center. Analysis of the temperature dependence of the susceptibility of **Y_{mono}** with a Bleaney-Bowers formula (see Figure 1.10) affords a J_{NNN} value of 15(1) cm⁻¹. When this J_{NNN} magnitude is used for **Dy_{mono}**, the best-fit values $g_{Dy} \cong 19.7(3)$ and $J_{NN} = -13.5(7)$ cm⁻¹ for the Dy-radical interaction are found. Such a large value for the Dy-radical coupling constant J_{NN} is a direct consequence of using $S_{eff} = \frac{1}{2}$ for Dy^{III} but indeed corresponds to an exchange energy comparable to that observed for Gd^{III}-NIT-R derivatives.³⁸

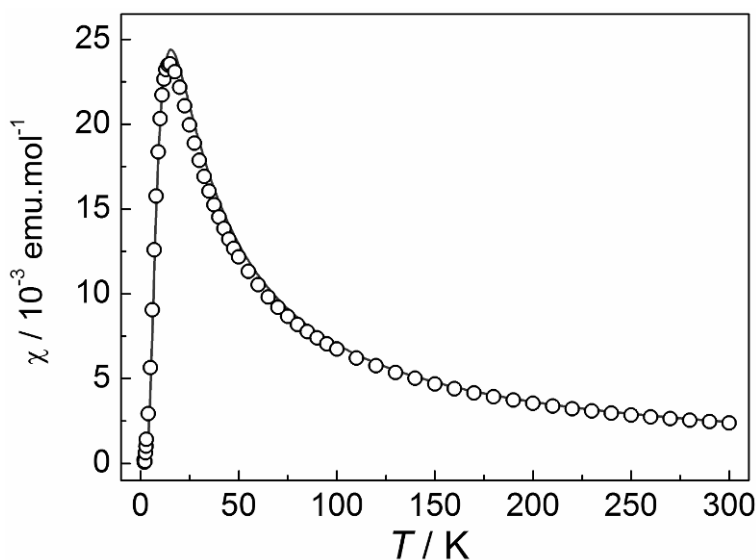


Figure 1.10: Temperature dependence of the magnetic susceptibility of $Y(\text{hfac})_3(\text{NITC}_6\text{H}_4\text{-OEt})_2$. The solid line represents the calculated values using the Bleaney-Bowers^{vi} formula for a pair of interacting spins $S=1/2$ with the best-fit parameters $g=2.0$, $J=15.5$ cm⁻¹ and $H=JS_1 \cdot S_2$.

Despite the excellent agreement between the shapes of the simulated and experimental curves reported in Figure 1.9, the simulated ones show a more drastic jump of the magnetization near H_{co} and a flatter signal in the initial part of the plateau than do the experimental ones. Moreover, the simulation of the T dependence of χT along the single-ion easy axis using the with experimental data, confirming that the JNNN and JNN values are correctly estimated; however, for quantitative agreement, the simulation requires a slightly reduced g_{Dy} value of 18.4, which is indeed closer to the value estimated from the ab initio calculations.

The origin of the differences between the simulated and experimental data, in particular the discrepancy between the g values estimated from the high and low magnetic field experiments, can be envisaged by considering that CASSCF/RASSISO calculations suggest a relatively small separation between the ground and excited states inside the ${}^6H_{15/2}$ multiplet. The g_z value, in fact, does not approach the limiting value of 20 expected for a ground doublet corresponding to the pure $m_J = \pm 15/2$ value, contrary to what is observed for the Dy_3 cluster.^{11,12} In the case of Dy_{mono} , as the ground Kramer's doublet is not an eigenstate of J_z , the Zeeman term of the Hamiltonian produces an admixture of the ground and excited states, resulting in a nonlinear dependence of its energy as a function of H. These nonlinear terms in the Zeeman effect would account for the discrepancies observed at low field in Figure 1.9, namely, the smoother increase of the experimental magnetization versus the faster saturation of the simulated curve and the slightly smaller g_{Dy} value necessary to reproduce the experimental T dependence of χT along the single ion easy axis measured at the relatively low applied field of 1000 Oe.

Other possibly relevant factors that were not considered in the model are the effects of thermal population of the other ${}^6H_{15/2}$ Kramers doublets of the Dy^{III} ion and a more complicated magnetic interaction between the radicals than just an isotropic one, since this interaction is mediated by the anisotropic spin density of Dy^{III} . Of course, it cannot be excluded that the energy levels may be somewhat populated above 15 K, but there is no doubt that the strong magnetic anisotropy requires that the low temperature behavior is dominated by the population of the most anisotropic state. The small upturn observed in χT at the lowest investigated temperature cannot be ascribed to the excited states but could be due to either intermolecular weak dipolar interactions or an artifact introduced by the torque exerted on a non perfectly aligned crystal.

1.6 Conclusion

The power of a mixed experimental-theoretical approach in the analysis of the magnetic anisotropy and exchange interactions in molecular magnetic materials having a low-symmetry environment around the anisotropic lanthanide ion has been here demonstrated. In particular, using angle-resolved single-crystal magnetometry, we have obtained the orientation of the principal axes of the magnetization of a model system comprising Dy^{III} and organic radicals.

With this information, a clear analysis of the T and H dependence of M has been possible, even in the presence of a strong orbital contribution.

A ferromagnetic Dy radical interaction has been evidenced, as has the presence of antiferromagnetic NNN interactions between the radicals that are mediated by the Dy^{III} ion, analogous to what has previously been observed for diamagnetic³⁹ Y^{III} and Eu^{III} or isotropic Gd^{III} magnetic centers.³⁸ The collected information have been successfully employed by the group to analyze the more complex behavior of the first rare-earth-based SCM,^{1,15,19} and a successful rationalization can be obtained by also assuming NNN antiferromagnetic interactions between Dy^{III} ions and a resulting spin-canted structure similar to that observed in Mn^{III}-porphyrine SCMs.⁶

At a later stage in this work thesis this approach has been applied to a more complex discrete system comprising six coupled Dy(III) ions, as described in the following chapters.

Bibliography

- (1) Gatteschi, D.; Sessoli, R.; Villain, J. *Molecular Nanomagnets*; Oxford University Press: Oxford, U.K., **2006**.
- (2) (a) Coulon, C.; Miyasaka, H.; Clérac, R. *Struct. Bonding (Berlin)* **2006**, 122, 163. (b) Bogani, L.; Vindigni, A.; Sessoli, R.; Gatteschi, D. *J. Mater. Chem.* **2008**, 18, 4750.
- (3) Ako, A. M.; Hewitt, I. J.; Mereacre, V.; Clérac, R.; Wernsdorfer, W.; Anson, C. E.; Powell, A. K. *Angew. Chem., Int. Ed.* **2006**, 45, 4926.
- (4) Milios, C. J.; Vinslava, A.; Wernsdorfer, W.; Moggach, S.; Parsons, S.; Perlepes, S. P.; Christou, G.; Brechin, E. K. *J. Am. Chem. Soc.* **2007**, 129, 2754.
- (5) Morrish, A. H. *The Physical Principles of Magnetism*; John Wiley & Sons, Inc.: New York, **1966**.
- (6) (a) Bernot, K.; Luzon, J.; Sessoli, R.; Vindigni, A.; Thion, J.; Richeter, S.; Leclercq, D.; Larionova, J.; Van Der Lee, A. *J. Am. Chem. Soc.* **2008**, 130, 1619. (b) Palii, A. V.; Ostrovsky, S. M.; Klokishner, S. I.; Reu, O. S.; Sun, Z. M.; Prosvirin, A. V.; Zhao, H. H.; Mao, J. G.; Dunbar, K. R. *J. Phys. Chem. A* **2006**, 110, 14003.
- (7) Barra, A. L.; Caneschi, A.; Cornia, A.; Gatteschi, D.; Gorini, L.; Heiniger, L. P.; Sessoli, R.; Sorace, L. *J. Am. Chem. Soc.* **2007**, 129, 10754.
- (8) (a) Tang, J. K.; Hewitt, I.; Madhu, N. T.; Chastanet, G.; Wernsdorfer, W.; Anson, C. E.; Benelli, C.; Sessoli, R.; Powell, A. K. *Angew. Chem., Int. Ed.* **2006**, 45, 1729. (b) Luzon, J.; Bernot, K.; Hewitt, I. J.; Anson, C. E.; Powell, A. K.; Sessoli, R. *Phys. Rev. Lett.* **2008**, 100, 247205.
- (9) Chibotaru, L. F.; Ungur, L.; Soncini, A. *Angew. Chem., Int. Ed.* **2008**, 47, 4126.
- (10) (a) Ishikawa, N.; Sugita, M.; Ishikawa, T.; Koshihara, S.; Kaizu, Y. *J. Am. Chem. Soc.* **2003**, 125, 8694. (b) Takamatsu, S.; Ishikawa, T.; Koshihara, S.; Ishikawa, N. *Inorg. Chem.* **2007**, 46, 7250. (c) Aldamen, M. A.; Clemente-Juan, J. M.; Coronado, E.; Martí-Gastaldo, C.; Gaita-Arino, A. *J. Am. Chem. Soc.* **2008**, 130, 8874. (d) Gamer, M. T.; Lan, Y.; Roesky, P. W.; Powell, A. K.; Clérac, R. *Inorg. Chem.* **2008**, 47, 6581. (e) Westin, L. G.; Kritikos, M.; Caneschi, A. *Chem. Commun.* **2003**, 1012.
- (11) (a) Zaleski, C. M.; Depperman, E. C.; Kampf, J. W.; Kirk, M. L.; Pecoraro, V. L. *Angew. Chem., Int. Ed.* **2004**, 43, 3912. (b) Osa, S.; Kido, T.; Matsumoto, N.; Re, N.; Pochaba, A.; Mrozinski, J. *J. Am. Chem. Soc.* **2004**, 126, 420. (c) Mishra, A.; Wernsdorfer, W.; Abboud, K. A.; Christou, G. *J. Am. Chem. Soc.* **2004**, 126, 15648. (d) He, F.; Tong, M.-L.; Chen, X.-M. *Inorg. Chem.* **2005**, 44, 8285. (e) Mishra, A.; Wernsdorfer, W.; Parsons, S.; Christou, G.; Brechin, E. K. *Chem. Commun.* **2005**, 2086. (f) Costes, J.-P.; Auchel, M.; Dahan, F.; Peyrou, V.; Shova, M.; Wernsdorfer, W. *Inorg. Chem.* **2006**, 45, 1924. (g) Mori, F.; Nyui, T.; Ishida, T.; Nogami, T.; Choi, K.-Y.; Nojiri, H. *J. Am. Chem. Soc.* **2006**, 128, 1440. (h) Aronica, C.; Pilet, G.; Chastanet, G.; Wernsdorfer, W.; Jacquot, J.-F.; Luneau, D. *Angew. Chem., Int. Ed.* **2006**, 45, 4659. (i) Ferbinteanu, M.; Kajiwarra, T.; Choi, K.-Y.; Nojiri, H.; Nakamoto, A.; Kojima, N.; Cimpoesu, F.; Fujimura, Y.; Takaishi, S.; Yamashita, M. *J. Am. Chem. Soc.* **2006**, 128, 9008. (j) Mereacre, V. M.; Ako, A. M.; Clérac, R.; Wernsdorfer, W.; Filoti, G.; Bartolome, J.; Anson, C. E.; Powell, A. K. *J. Am. Chem. Soc.* **2007**, 129, 9248. (k) Zaleski, C. M.; Kampf, J. W.; Mallah, T.; Kirk, M. L.; Pecoraro, V. L. *Inorg. Chem.* **2007**, 46, 1954. (l) Mereacre, V.; Ako, A. M.;

- Clérac, R.; Wernsdorfer, W.; Hewitt, E. J.; Anson, C. E.; Powell, A. K. *Chem. Eur. J.* **2008**, *14*, 3577.
- (m) Stamatatos, T. C.; Teat, S. J.; Wernsdorfer, W.; Christou, G. *Angew. Chem., Int. Ed.* **2009**, *48*, 521.
- (n) Chandrasekhar, V.; Pandian, B. M.; Azhakar, R.; Vittal, J. J.; Clérac, R. *Inorg. Chem.* **2009**, *48*, 521.
- (o) Novitchi, G.; Wernsdorfer, W.; Chibotaru, L. F.; Costes, J.-P.; Anson, C. E.; Powell, A. K. *Angew. Chem., Int. Ed.* **2009**, *48*, 1614.
- (12) (a) Luneau, D.; Rey, P. *Coord. Chem. Rev.* **2005**, *249*, 2591. (b) Sutter, J.-P.; Kahn, M. L.; Golhen, S.; Ouahab, L.; Kahn, O. *Chem. Eur. J.* **1998**, *4*, 571. (c) Caneschi, A.; Dei, A.; Gatteschi, D.; Sorace, L.; Vostrikova, K. *Angew. Chem., Int. Ed.* **2000**, *39*, 246. (d) Caneschi, A.; Dei, A.; Gatteschi, D.; Massa, C. A.; Pardi, L. A.; Poussereau, S.; Sorace, L. *Chem. Phys. Lett.* **2003**, *371*, 694.
- (13) Poneti, G.; Bernot, K.; Bogani, L.; Caneschi, A.; Sessoli, R.; Wernsdorfer, W.; Gatteschi, D. *Chem. Commun.* **2007**, 1807.
- (14) (a) Benelli, C.; Caneschi, A.; Gatteschi, D.; Sessoli, R. *Inorg. Chem.* **1993**, *32*, 4797. (b) Benelli, C.; Caneschi, A.; Gatteschi, D.; Sessoli, R. *Adv. Mater.* **1992**, *4*, 504.
- (15) (a) Bogani, L.; Sangregorio, C.; Sessoli, R.; Gatteschi, D. *Angew. Chem., Int. Ed.* **2005**, *44*, 5817. (b) Bernot, K.; Bogani, L.; Caneschi, A.; Gatteschi, D.; Sessoli, R. *J. Am. Chem. Soc.* **2006**, *128*, 7947. (c) Bernot, K.; Bogani, L.; Sessoli, R.; Gatteschi, D. *Inorg. Chim. Acta* **2007**, *360*, 3807.
- (16) (a) Bartolome, F.; Bartolome, J.; Benelli, C.; Caneschi, A.; Gatteschi, D.; Paulsen, C.; Pini, M. G.; Rettori, A.; Sessoli, R.; Volokitin, Y. *Phys. Rev. Lett.* **1996**, *77*, 382. (b) Cinti, F.; Rettori, A.; Barucci, M.; Olivieri, E.; Risegari, L.; Ventura, G.; Caneschi, A.; Gatteschi, D.; Rovai, D.; Pini, M. G.; Affronte, M.; Mariani, M.; Lascialfari, A. *J. Magn. Magn. Mater.* **2007**, *310*, 1460.
- (17) Benelli, C.; Gatteschi, D. *Chem. Rev.* **2002**, *102*, 2369.
- (18) De Graaf, C.; de P. R. Moreira, I.; Illas, F.; Iglesias, O.; Labarta, A. *Phys. Rev. B* **2002**, *66*, 014448.
- (19) Bernot, K.; Luzon, J.; Bogani, L.; Caneschi, A.; Gatteschi, D.; Sessoli, R.; Vindigni, A.; Rettori, A.; Pini, M. G. *Phys. Rev. B*, **2009**, *79*, 134419.
- (20) (a) Bencini, A.; Gatteschi, D. *Transition Met. Chem.* **1982**, *8*, 1. (b) Pilbrow, J. R. *Transition Ion Electron Paramagnetic Resonance* Oxford University Press: Oxford, U.K., **1990**. (c) Caneschi, A.; Gatteschi, D.; Lalioti, N.; Sessoli, R.; Sorace, L.; Tangoulis, V.; Vindigni, A. *Chem. Eur. J.* **2002**, *8*, 286.
- (21) Sorace, L.; Sangregorio, C.; Figuerola, A.; Benelli, C.; Gatteschi, D. *Chem. Eur. J.* **2009**, *15*, 1377.
- (22) (a) Mitra, S. *Prog. Inorg. Chem.* **1977**, *22*, 309. (b) Gerloch, M.; Mackey, D. J. *J. Chem. Soc., Dalton Trans.* **1972**, *3*, 415.
- (23) Ullmann, E. F.; Osiecki, J. H.; Boocock, D. G. B.; Darcy, R. J. *Am. Chem. Soc.* **1972**, *94*, 7049.
- (24) CrysAlis CCD and CrysAlis RED, version 1.171.32.15; Oxford Diffraction Ltd.: Abingdon, U.K., **2008**.
- (25) Sheldrick, G. M. *SHELX-97: An Integrated System for Solving and Refining Crystal Structures From Diffraction Data*; University of Goettingen: Goettingen, Germany, **1997**.
- (26) Karlstrom, G.; Lindh, R.; Målmqvist, P. A.; Roos, B. O.; Ryde, U.; Veryazov, V.; Widmark, P. O.; Cossi, M.; Schimmelpfennig, B.; Neogrady, P.; Seijo, L. *Comput. Mater. Sci.* **2003**, *28*, 222.
- (27) Hess, B. A.; Marian, C. M.; Wahlgren, U.; Gropen, O. *Chem. Phys. Lett.* **1996**, *251*, 365.
- (28) Målmqvist, P. A.; Roos, B. O.; Schimmelpfennig, B. *Chem. Phys. Lett.* **2002**, *357*, 230.

- (29) Vancoille, S.; Målmqvist, P. A.; Pierlot, K. *ChemPhysChem* **2007**, 8, 1803.
- (30) Lescop, C.; Belorizky, E.; Luneau, D.; Rey, P. *Inorg. Chem.* **2002**, 41, 3375.
- (31) De W. Horrocks, W., Jr.; De W. Hall, D. *Coord. Chem. Rev.* **1971**, 6, 147.
- (32) King, R. B. J. *Am. Chem. Soc.* **1969**, 91, 7211.
- (33) Abragam, A.; Bleaney, B. *Electron Paramagnetic Resonance of Transition Ions*; Dover: New York, **1986**.
- (34) (a) Wickman, H. H.; Nowik, I. *Phys. Rev.* **1966**, 142, 115. (b) Nowik, I.; Wickman, H. H. *Phys. Rev.* **1965**, 140, 869. (c) Ofer, S.; Rakavy, M.; Segal, E.; Khurgin, B. *Phys. Rev.* **1965**, 138, 241.
- (35) (a) Bramwell, S. T.; Harris, M. J. J. *Phys.: Condens. Matter* **1998**, 10, L215. (b) Flood, D. J. J. *Appl. Phys.* **1974**, 45, 404. (c) Blote, H. W.; Wielinga, R. F.; Huiskamp, W. J. *Physica (Amsterdam)* **1969**, 43, 549. (d) Janaa, Y. M.; Sengupta, A.; Ghosh, D. J. *Magn. Magn.Mater.* **2002**, 248, 7.
- (36) (a) Borowiec, M. T.; Dyakonov, V.; Prokhorov, A.; Szymczak, H. *Phys. Rev. B* **2000**, 62, 5834. (b) Carlin, R. D. L. *Magnetochemistry*; Springer-Verlag: Berlin, **1986**. (c) Bellesis, G. H.; Simizu, S.; Friedberg, S. A. J. *Appl. Phys.* **1987**, 61, 3286.
- (37) Benelli, C.; Caneschi, A.; Gatteschi, D.; Laugier, J.; Rey, P. *Angew. Chem., Int. Ed.* **1987**, 26, 913.
- (38) Benelli, C.; Caneschi, A.; Gatteschi, D.; Pardi, L.; Rey, P. *Inorg. Chem.* **1989**, 28, 275.
- (39) Benelli, C.; Caneschi, A.; Gatteschi, D.; Pardi, L.; Rey, P. *Inorg. Chem.* **1989**, 28, 3230.

Chapter 2

Preliminary study for chapter 3

During this thesis work we have applied angular dependent magnetometry, employed to characterize the mononuclear Dysprosium-radical complex, to investigate more complex systems, like 4f polynuclear clusters. The compound we have investigated is an hexanuclear dysprosium(III) cluster synthesized in the laboratory of Prof. Annie Powell, at the University of Karlsruhe, Germany. The interest in this compound relies on the fact that it is constituted by two interacting dysprosium triangles. Triangular systems are attracting increasing interest because they can show exotic phenomena, like spin chirality and slow relaxation of the magnetization of the excited state.

Before entering in the description of the original work of this thesis that concerns the investigation of the hexanuclear system we find appropriate to include a brief description of the magnetic properties of the triangular building block.

Recently synthesized a trinuclear Dy^{3+} cluster $[\text{Dy}_3(\mu_3\text{-OH})_2\text{L}_3\text{Cl}(\text{H}_2\text{O})_5]\text{Cl}_3$ (where L is the anion of ortho-vanillin)¹, hence abbreviated as Dy_3 , seems to combine for the first time both types of features specific to molecular magnetism, *i.e.*, a system with almost nonmagnetic moment showing the slow magnetic relaxation typical of some high spin clusters. Preliminary powder magnetic measurements revealed an unprecedented magnetic behavior where the magnetization vs field curve at low temperature is almost flat, suggesting a nonmagnetic ground state. It suddenly increases to its saturation value¹ in contrast to the common multistep behavior of antiferromagnetic triangular clusters.² A possible explanation lies in the almost trigonal (C_{3h}) symmetry of the molecule (see Figure 2.1 and 2.2) combined with the large Ising anisotropy of Dy^{3+} ions.³ With this molecular symmetry, if the single-ion easy anisotropy axes are in the Dy_3 plane and not perpendicular to it, they must be at 120° from one another, as represented in the scheme of Figure 2.1. In that case, an antiferromagnetic interaction among the Dy^{3+} would result in a nonmagnetic ground state characterized by a vortex spin-chirality.

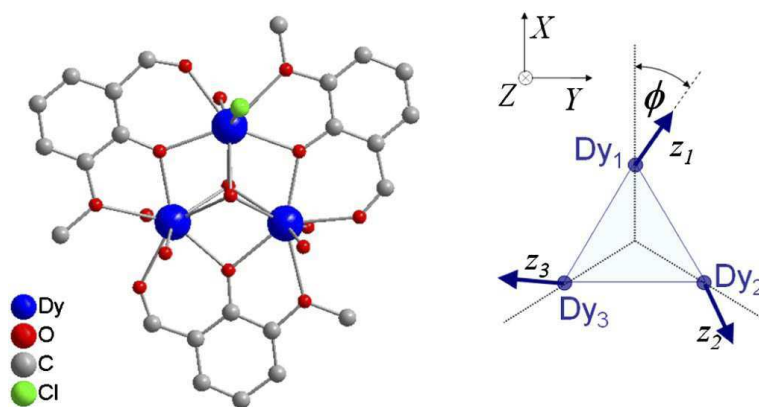


Figure 2.1: Left: View of the molecular structure of Dy_3 cluster where the hydrogen atoms, the chloride counteranions and the solvent molecules of crystallization have been omitted. Right: Schematic view of the spin structure of the Dy_3 triangular cluster and of the local easy axes orientation in respect of the laboratory XYZ reference frame.

Dy_3 is an unprecedented experimental realization of this simple but fascinating spin structure, which represents the archetype of noncollinear spin systems^{4, 5, 6}. Moreover thanks to its rich magnetization dynamics, with quantum acceleration at the level crossings, it represents a new type of magnetic memory despite the nonmagnetic ground state.

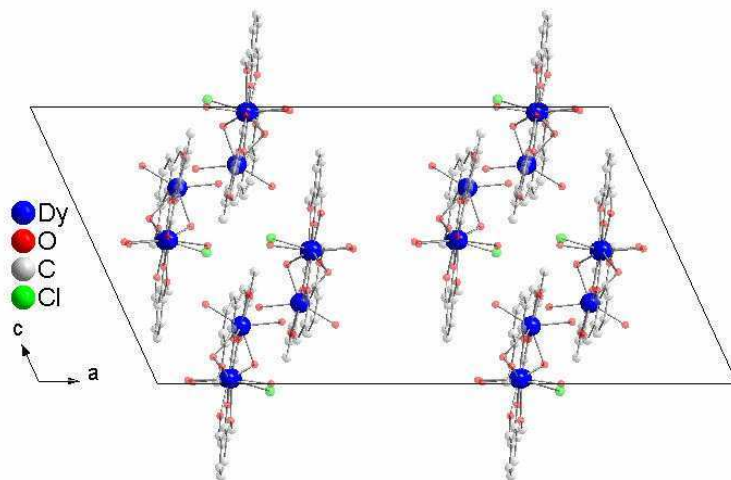


Figure 2.2: View along the $b=Y$ crystallographic axis (entering the page) of the crystal packing of Dy_3 . Hydrogen atoms, Chloride counterions and solvent molecules of crystallization have been omitted for the sake of clarity. The labelling color scheme is drawn in the picture. Both crystallographic (a , c) and laboratory (X , Z) reference frames are given

The two structurally equivalent Dy_3 molecules in the unit cell have the Dy_3 planes almost perpendicular to Z and one side of the triangle parallel to Y (see Figure 2.1). The Magnetization vs field behaviour in-plane X and Y directions are very similar and M tends to zero at low temperatures, confirming a nonmagnetic ground state, while a weaker signal is observed along Z (see figure 2.3).

The observed behavior has been modeled with the canonical formalism of the statistical thermodynamics by taking into account that intermolecular interactions can be neglected¹ and that Dy^{3+} ions have a very large magnetic single-ion anisotropy due to the crystal field splitting of the ${}^6H_{15/2}$ ground state. In a first approximation each Dy^{3+} ion, which is supposed to have the doublet ground state well separated in energy from the other excited Stark sublevels, can be represented by an effective spin $S = 1/2$ and the Dy_3 system can be modeled by an Ising Hamiltonian:

$$H = - \sum_{i,k=1,2,3}^{i>k} j_{zz} S_{z_i} S_{z_k} - \mu_B \sum_{i=1,2,3} g_z H_z S_{z_i} \quad (2.1)$$

Where for each Dy^{3+} ion the z_i local axis is considered to be in the plane of the triangle at 120° one from each other as schematized in Figure 2.1. The basis set of the full system consists therefore of 8 vectors: $|\uparrow\uparrow\uparrow\rangle$, $|\downarrow\downarrow\downarrow\rangle$, $|\uparrow\downarrow\uparrow\rangle$, $|\uparrow\uparrow\downarrow\rangle$, $|\uparrow\downarrow\downarrow\rangle$, $|\downarrow\uparrow\uparrow\rangle$, $|\downarrow\downarrow\uparrow\rangle$, $|\downarrow\uparrow\downarrow\rangle$, where, however, up and down refers to the local z axes. Actually, these vectors are already the eigenvectors of (2.1).

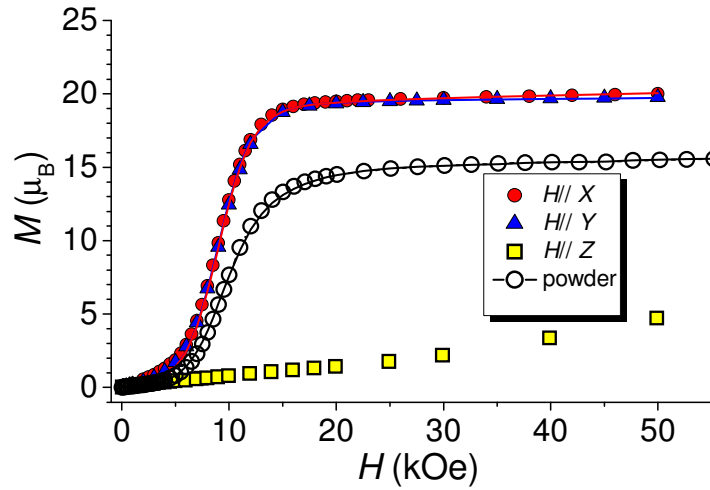


Figure 2.3: Field dependence of the magnetization measured along the X, Y, and Z axes at $T = 1,9$ K. In the inset a magnified view of the high field region is reported.

It is interesting to focus on the energy of the eight eigenstates of the Hamiltonian (2.1) as a function of the applied magnetic field in the Dy_3 plane, as shown in Figure 2.4. At zero field two states with a zero net magnetic moment, are degenerate with energy equal to $-3j_{zz}/4$, whereas the other 6 states are also degenerate with energy equal to $j_{zz}/4$. In an applied magnetic field the energy of the last six levels depends on the angle the magnetic field forms with the local easy z axes. Let us suppose that the field is applied along one bisector of the triangle as shown in Figure 2.4. Two limiting scenarios can be observed depending whether the local easy axes are along the edges of the triangle (Figure 2.4(a)) or along the bisectors (Figure 2.4(b)). A jump to saturation magnetization at the first level crossing, H_1 , is expected in both cases, as indeed observed in Dy_3 . In general, thanks to the structural noncollinearity of the easy axes, the two states of the ground doublet have opposite vortex chirality, with clockwise or anticlockwise rotation of the spins.

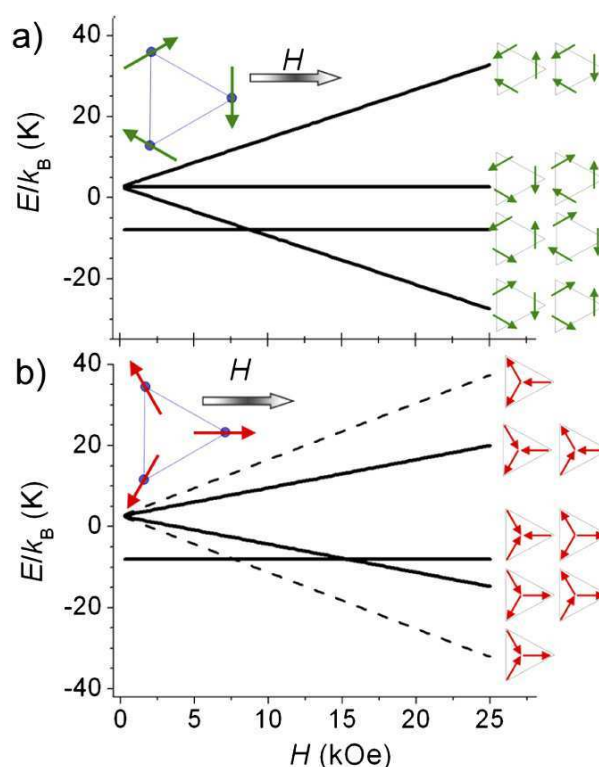


Figure 2.4: (a) Zeeman splitting of the levels due to the application of the field along the X axis (bisector) calculated with the Spin Hamiltonian (1) and the parameters indicated in the text, assuming $\phi = 90^\circ$. (b) Same diagram calculated with $\phi = 0^\circ$. The spin structure for each state is schematized by the arrows. The nondegenerate states are highlighted by dashed lines.

Susceptibility measurements using standard induction coils in alternating magnetic field allowed us to estimate the relaxation rate from the frequency dependence of the imaginary component of the susceptibility χ'' assuming that, according to the Debye model, at the maximum of χ'' vs ω curve the simple relation $\tau = 1/\omega$ is valid. When the ac field is applied in the plane of the triangle the relaxation rate decreases on lowering the temperature following an Arrhenius law, $\tau = \tau_0 \exp(\Delta/k_B T)$, with $\tau_0 = 2.5(5) \cdot 10^{-7}$ s and $\Delta = 36(2)$ K. At temperatures below *ca.* 7 K the relaxation increases less rapidly. The Arrhenius behavior of the relaxation time is similar to that of Single Molecule Magnets, SMMs,⁷ where the easy axis magnetic anisotropy generates a barrier for the reversal of the magnetization giving rise at low temperature to magnetic bistability and memory effect of pure molecular origin.^{8,9} Dy₃, however, represents the first example where such a slowing down of the magnetization dynamics occurs even if the overall magnetization lies in an almost isotropic plane rather than along an easy axis. That is because the system can be better schematized by three interacting SMMs.

The application of a static field has indeed a strong influence on the dynamics of the magnetization of Dy_3 , as shown in Figure 2.5(a) where the real component of the susceptibility, χ' for different frequencies in 1–1000 Hz range is shown as a function of the field. Around zero field and the first level crossing, H_1 , the dynamic susceptibility approaches the equilibrium value, *i.e.*, that obtained from the derivative of the static magnetization curve recorded at the same temperature, while for intermediate fields a strong frequency dependent reduction, arising from the impossibility to follow the oscillating field, is observed. Similar results have been obtained along Y , as shown in Figure 2.5(b) where the field dependence of the relaxation rate at $T = 7$ K for this orientation is given. When the temperature dependence of the relaxation time is investigated far from the level crossings, *i.e.*, at $H=3$ kOe, the relaxation times show a significant increase of the barrier ca. 120 K with τ_0 ca. 3×10^{-10} s.

The present results are well rationalized by the model previously introduced. The response in the ac field mainly involves transfer of population from (to) the ground doublet to (from) the first magnetic excited state, implying the reversal of one spin inside the triangle. Far from any level crossings this seems to occur through an Orbach process involving the first excited Kramers doublet of each of the Dy^{3+} ions, and its energy gap δ , estimated from the static properties as well as from ab initio calculations⁵, is found indeed to be in good agreement with the observed activation energy Δ . On the contrary, at $H = 0$ the reduction of the barrier suggests that an alternative mechanism takes place. Tunnelling of the magnetization has already been observed for many lanthanide-based SMMs and is attributed to the admixture in zero external field of the ground Kramers doublet states, made possible by the hyperfine interaction.^{10, 11} At the first level crossing the situation of zero local field is re-established for a Dy^{3+} ion resulting in the observed fast dynamics.

To conclude, Dy_3 has revealed to be a benchmark system to investigate noncollinearity in Ising systems. It is worth stressing that noncollinearity is a key feature of molecular magnetism, where complex building-blocks characterized by low symmetry are assembled in more symmetric architectures. Dy_3 combines the slow dynamics of SMM and the level crossing observed in antiferromagnetic rings.^{12, 13} Both types of systems are currently being investigated for their potential application in quantum computation^{14, 15, 16, 17} and systems with a nonmagnetic nature of the ground doublet state could be used in order to reduce decoherence effects due to the fluctuation of local magnetic fields. The dynamics involving the ground doublet is in principle not directly accessible with magnetometry and requires to be further investigated with more sophisticated techniques, for instance using local probes like muons or neutrons.

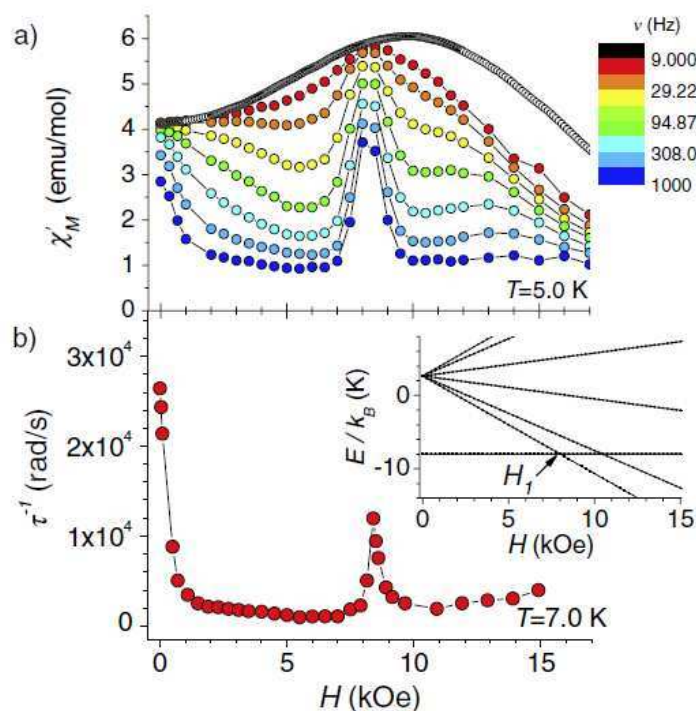


Figure 2.5: (a) Field dependence of the real component at 5 K of the ac susceptibility measured with the field along X at logarithmic spaced frequencies. The empty circles represent the experimental static susceptibility obtained by derivation of the experimental magnetization curve. (b) Field dependence of the relaxation time measured at $T = 7$ K with the field applied along Y . In the inset the Zeeman splitting calculated for H parallel to Y with the best-fit parameters discussed in the text.

Bibliography

- (1) Tang, J. et al., *Angew. Chem., Int. Ed.* **2006**, 45, 1729.
- (2) Luban, M. et al., *Phys. Rev. B* **2002**, 66, 054407.
- (3) Ishikawa, N.; Sugita, M.; Ishikawa, T.; Koshihara, S. and Kaizu, Y., *J. Am. Chem. Soc.* **2003**, 125, 8694.
- (4) Luzon, J.; Bernot, K.; Hewitt, I. J.; Anson, C. E.; Powell, A. K. and Sessoli, R., *PRL* **2008**, 100, 247205.
- (5) Chibotaru, L. F.; Ungur, L. and Soncini, A., *Angew. Chem., Int. Ed.* **2008**, 47, Issue 22, 4126–4129.
- (6) Ungur, L.; Van den Heuvel, W. and Chibotaru, L. F., *New J. Chem.*, **2009**, 33, 1224-1230.
- (7) Eppley, H. et al., *Mol. Cryst. Liq. Cryst. Sci. Technol., Sect. A* **1997**, 305, 167.
- (8) Gatteschi, D.; Sessoli, R. and Villain, J., *Molecular Nanomagnets* (Oxford University Press, Oxford, **2006**).
- (9) Sessoli, R.; Gatteschi, D.; Caneschi, A. and Novak, M., *Nature (London)* **1993**, 365, 141.
- (10) Giraud, R.; Wernsdorfer, W.; Tkachuk, A.M.; Maily, D. and Barbara, B., *Phys. Rev. Lett.* **2001**, 87, 057203.
- (11) Ishikawa, N.; Sugita, M. and Wernsdorfer, W., *Angew. Chem., Int. Ed.* **2005**, 44, 2931.
- (12) Taft K. et al., *J. Am. Chem. Soc.* **1994**, 116, 823.
- (13) Normand, B.; Wang, X.; Zotos, X. and Loss, D., *Phys. Rev. B* 2001, 63, 184409.
- (14) Ardavan A. et al., *Phys. Rev. Lett.* 2007, 98, 057201.
- (15) Bertaina S. et al., *Nature (London)* 2008, 453, 203.
- (16) Leuenberger, M. and Loss, D., *Nature (London)* 2001, 410, 789.
- (17) Meier, F.; Levy, F. and Loss, D., *Phys. Rev. B* 2003, 68, 134417.

Chapter 3

Coupling Dy₃ Triangles to Enhance their Slow Magnetic Relaxation

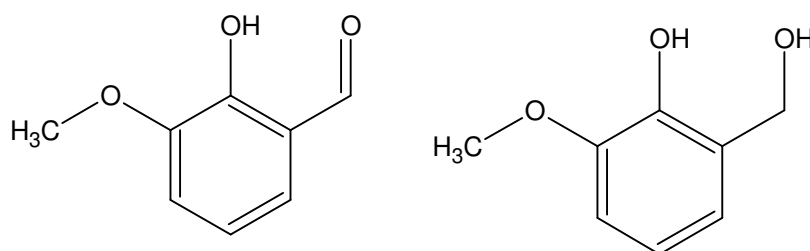
<u>3.1 INTRODUCTION</u>	41
<u>3.2 SYNTHESIS AND CRYSTAL STRUCTURE</u>	41
<u>3.3 MAGNETIC MEASUREMENTS</u>	43
<u>3.4 AB INITIO CALCULATIONS</u>	46
<u>3.5 ANGLE RESOLVED MAGNETOMETRY</u>	48
<u>3.6 ENERGY SPECTRUM FOR DY₆</u>	52
<u>3.7 CONCLUSION</u>	54

3.1 Introduction

As part of the continuing studies on Lanthanides based SMM^{1, 2, 3} and especially of trinuclear system,³ⁱ carried out at in the laboratory of Prof. Annie Powell, it has been discovered a means of linking two Dy₃ L^{3d} to give a Dy₆ molecule with even more exotic magnetic properties that have been investigated during this thesis.

3.2 Synthesis and Crystal Structure

In the course of synthesizing analogous Ln₃ triangles for a systematic study of the system, which will be described elsewhere, and again using vanillin as ligand, it was found that for the thulium(III) compound, the hexanuclear complex, [Tm₆(μ₃-OH)₄L₄L'₂(H₂O)₁₀]Cl₆·18H₂O (**Tm₆**) formed, where L= o-vanillato and L' is its reduced form (see Scheme 1) This formation results from the reduction of the aldehyde to an alcohol for one of the three o-vanillinato ligands on each triangle. The resulting alkoxides lead to a double bridge between two of the triangular Tm₃ motifs.



Scheme 3.1: Structural formulae for o-vanillin, HL, (left) and 2-hydroxymethyl-6-methoxyphenol, H₂L' (right).

Given the interesting magnetic properties of Dy₃ the synthesis to the Dy₆ analogue has been attempted by deliberately adding 2-hydroxymethyl-6-methoxyphenol, H₂L', to the reaction, leading to the formation of [Dy₆(μ₃-OH)₄L₄L'₂(H₂O)₉Cl]Cl₅·15H₂O (**Dy₆**) in good yields. Such metal-ion catalyzed ligand transformations are now relatively frequently reported in the literature, and the most relevant example to this work is the dysprosium(III)-activated^{3h} transformation involving acetone and o-vanillin.

The triangular Dy₃ unit in **Dy₆** is less equilateral than found for the archetypal Dy₃ compound,^{3d} with Dy...Dy distances of 3.5127(3), 3.5371(3), and 3.5797(3) Å. The inter-triangle Dy₃...Dy₃' distance is 3.7262(4) Å. The planes of the two triangles in the Dy₆ unit are strictly co-parallel, but not coplanar, and the perpendicular distance between them is 2.4757(6) Å, with the Dy₃...Dy₃' vector at 48.48° to the normal of the Dy₃ planes.

3.3 Magnetic Measurements

A dc magnetic susceptibility measurement of **Dy₆** showed a χT product at room temperature of 82.3 emuKmol⁻¹, as expected for six non-interacting f⁹ ions, and a monotonic decrease upon lowering the temperature (Figure 3.2). The low-temperature behavior of the susceptibility is more informative (Figure 3.3, inset), in which a maximum around T=3 K is observed with an external field of 1 kOe. In contrast, this maximum occurs at T=7 K in **Dy₃**. A constant increase is observed with an applied field of 10 kOe.

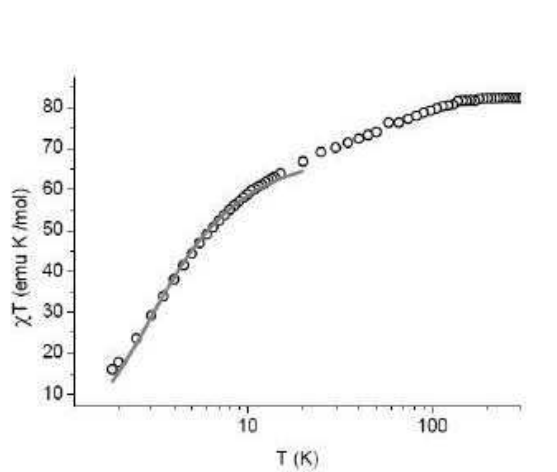


Figure 3.2: Temperature dependence of the product of the magnetic susceptibility (M/H) and temperature. The grey line represents the calculated values using the model described in the text.

The application of a moderate field is able to overcome the weak antiferromagnetic (AF) interactions and to suppress the maximum in the susceptibility. The magnetization measured under variable field at 1.8 K shows an inflection around 0.5 kOe, see Figure 3.3, and reaches a plateau at about 30 kOe with a value of $28\mu_B$, corresponding to twice the value observed for **Dy₃**, with a similar weak linear increase at higher fields. The behavior is therefore broadly similar to that of the Dy₃ clusters^{3d} but the latter shows a more pronounced

antiferromagnetism (*cf.* Figure 2.3), in spite of the fact that Dy_6 comprises an even number of interacting centers.

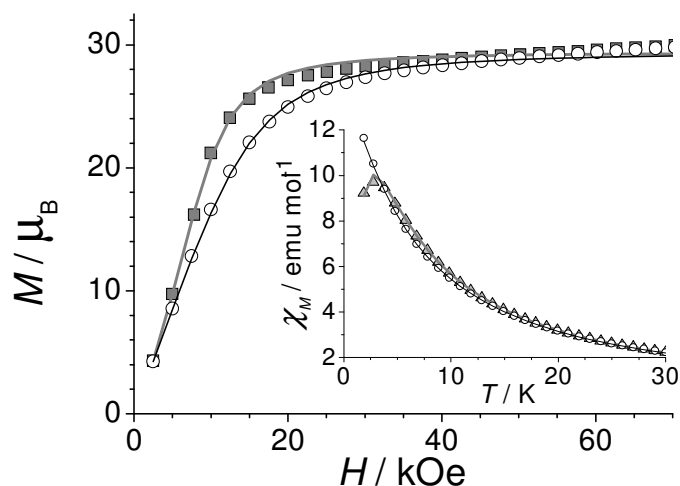


Figure 3.3: Field dependence of the molar magnetization measured on a pellet of polycrystalline powder of Dy_6 at $T=1.8 \text{ K}$ (open circles) and $T=4.0 \text{ K}$ (solid squares). Inset: temperature dependence of the magnetic susceptibility on a polycrystalline powder at $H=1 \text{ kOe}$ (solid triangles) and $H=10 \text{ kOe}$ (open circles). Lines correspond to the calculated values (*see text*) obtained from the simultaneous simulation of single-crystal data.

The dynamics of the magnetization were investigated using ac susceptibility measurements, with the temperature dependence of the imaginary components in zero static field given in Figure 3.4a. Most striking is the presence of two regions in which the susceptibility shows a strong frequency dependence. The out-of-phase component χ'' shows a series of frequency-dependent peaks around 25 K, with a second set around 5 K. In contrast, Dy_3 showed a unique set of maxima around 8 K.⁴ The curves of $\chi''T$ versus T (Figure 3.4b) are more helpful in quantifying the relative fraction of magnetization involved in the two relaxation processes and suggest that the high-temperature slow relaxation process involves a significant fraction (about 25%) of the magnetization.

The difference in the magnetization dynamics compared with Dy_3 is also clear from the field dependence of the ac susceptibility. The application of a field of 1 kOe has practically no effect on the dynamics (Figure 3.5), while a dramatic slowing down was observed in the case of for Dy_3 (*cf.* Figure 2.5) suggesting that the tunneling in zero field is less efficient in Dy_6 than in Dy_3 .

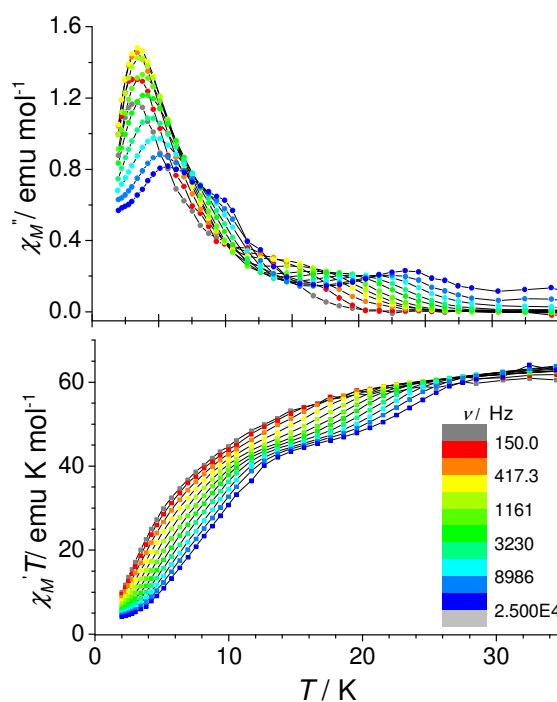


Figure 3.4 : Temperature dependence of a) ac magnetic susceptibility for Dy_6 of imaginary component and b) χT product in zero static field.

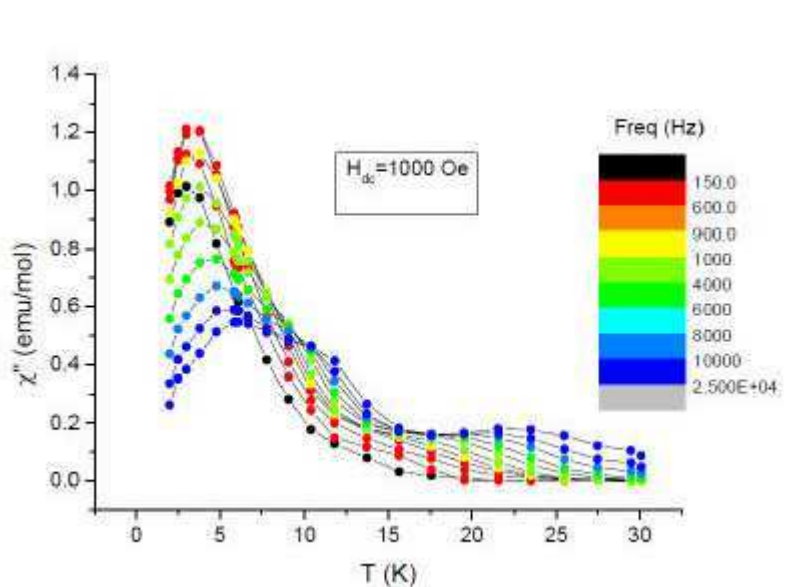


Figure 3.5: Temperature dependence of the out-of-phase component of the ac susceptibility of Dy_6 measured in a static field of 1 kOe.

To investigate this complex behavior further, the relaxation time τ was extracted from the isothermal frequency dependence of the out-of-phase component of the susceptibility, assuming that at its maximum $\tau = (2\pi\nu)^{-1}$ shown in Figure 3.6

The results, reported in Figure 3.7 show a marked deviation from an Arrhenius law, with a leveling of τ on lowering the temperature more evident for the low temperature process. The Arrhenius analysis for the higher temperature data gives $\Delta E=200(10)$ K, $\tau_0=1.5(5)\times 10^{-9}$ s.

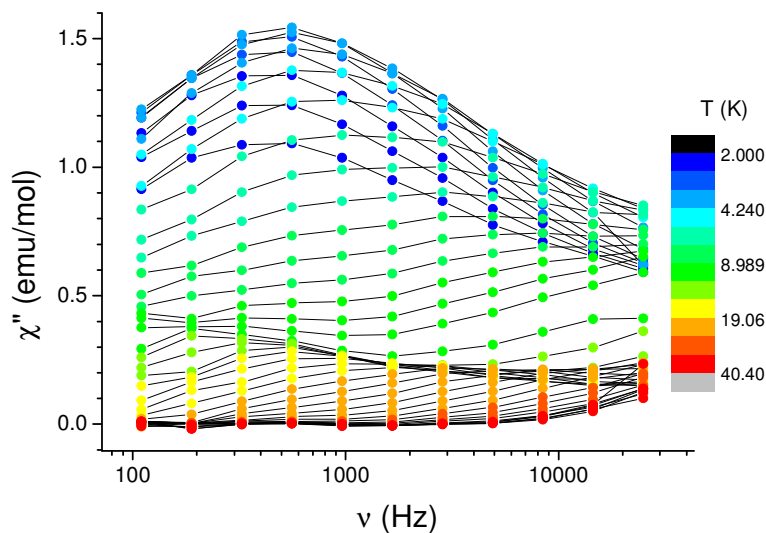


Figure 3.6: Frequency dependence of the out-of-phase component of the ac susceptibility of Dy_6 measured in zero static field at different temperatures (see color scale).

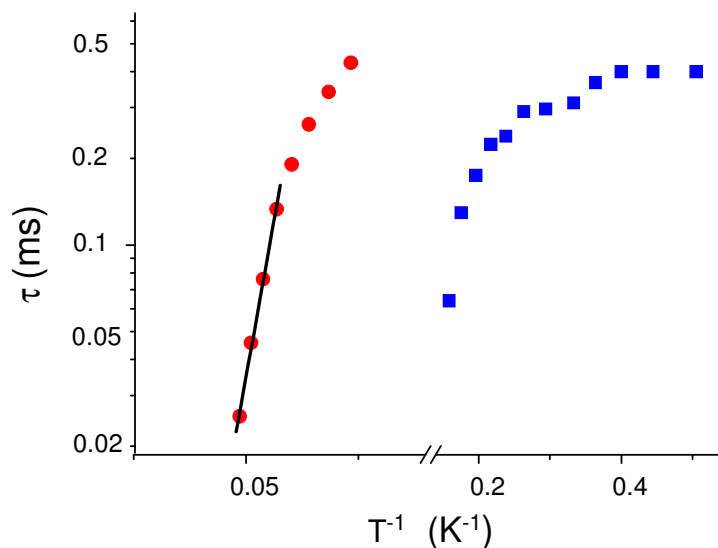


Figure 3.7: Temperature dependence of the relaxation time of Dy_6 for the high temperature (red circles) and low temperature (blue squares) processes. The black line is a linear fit in the Arrhenius plot of the high temperature data.

3.4 Ab Initio Calculations

As the unique features of the parent compound Dy_3 ^{3d, 4} originated from the arrangement of the Dy^{3+} easy axes at 120° to each other in the triangular plane, giving the first molecular example of a system showing the classic non collinear orientation of Ising spins seen in condensed phase materials, we decided to investigate the single-ion magnetic anisotropy in Dy_6 by performing complete active space (CASSCF) calculations for the three different Dy^{3+} ions, including the effect of the spin orbit coupling⁵. This high-level ab initio method was previously used to determine the single-ion easy anisotropy axes and gyromagnetic factors for the Dy^{3+} ions in Dy_3 and was in almost perfect agreement with the experimental results performed on single crystals.⁶ The validity of the method was confirmed for two further Dy^{3+} compounds.^{3i, 7, 8} The computed large anisotropy of the gyromagnetic factors ($g_z \gg g_x, g_y$) and the large energy gap between the ground and first excited Kramer's doublet justify the Ising approximation used. Also the g_z values of about 20 indicate an almost pure $|m_j = \pm 15/2\rangle$ ground-state doublet.⁹

Figure 3.8 shows the computed single-ion easy anisotropy axes, where θ is the angle subtended by an easy axis with respect to the plane of the triangle and ϕ is the angle between the projection of each easy axis on to the plane of the triangle and the corresponding bisector of the triangle. The directions of the local easy axes for $Dy1$ and $Dy2$ in Dy_6 lie almost in the plane of the triangle ($\theta < 3^\circ$) and are tangential to the triangle with ϕ ranging between 82.1 and 82.4° . These results are essentially the same as those found for the Dy_3 system, consistent with the similar ligand environments of $Dy1$ and $Dy2$ in the two compounds. However, there is the important difference that the local easy axis for the central Dy_3 ions deviates by about 10° out of the plane of the triangle and makes a smaller angle (64.2°) to the bisector, reflecting the rather different coordination environment resulting from the alkoxo bridges to the second triangle.

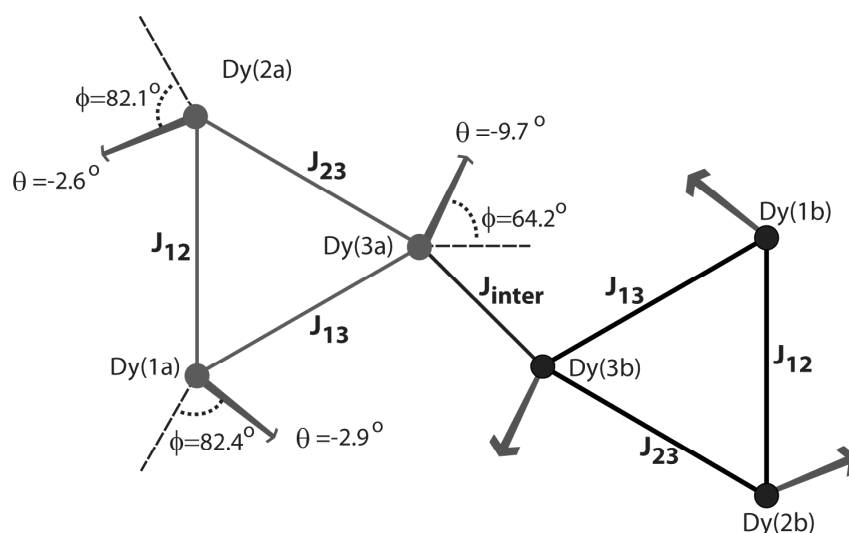


Figure 3.8 : The calculated six easy axes. The arrows represent the positive directions of the associated local z axes used in the spin Hamiltonian [Eq. (1)] and the angles of these to the plane defined by the triangular moiety (θ). The angles of their projections on to the triangular plane with the bisector of the triangle (ϕ) are also indicated. Lighter lines indicate that the first triangle lies behind the second, whilst the shape of the arrows is indicative of their relative orientation with respect to the plane of the page. The magnetic interactions derived from the spin Hamiltonian are also shown.

3.5 Angle resolved magnetometry

To evaluate the effects of the breaking of the trigonal symmetry characteristic of Dy_3 , we decided to perform a single-crystal magnetic characterization as described in chapter 1. The triclinic space group is well suited for this kind of investigation, as only one orientation of the cluster is present in the crystals. However, three orthogonal rotations are necessary to define the susceptibility tensor satisfactorily. Unfortunately, the presence of solvent molecules of methanol and acetonitrile in the crystal lattice makes the crystal very unstable, precluding precise indexing of the crystal faces and correct orientation of the crystal on the sample rotator. We therefore developed a new method to deal with this by embedding the crystal in glue (or grease) on one face of a millimeter-sized Teflon cube, which can then be mounted on a goniometer head, thus enabling crystal indexing using an X-ray diffractometer. As Teflon is a polymer and does not diffract, the metric matrix is defined by the crystal alone. Three rotations along the X, Y, and Z orthogonal axes defined as the normal to three faces of the cube were performed. These faces can be indexed with non-integer Miller indices within the reference frame of the crystal. This new procedure we have developed allows for much easier handling of crystals that are air sensitive, susceptible to solvent loss, or with poor habit, and

thus enables the results to be correlated accurately to the molecular structure (see appendix for a more detailed description).

This investigation showed, as expected, a large angular dependence of the magnetization (Figure 3.9). In stark contrast to what was observed in Dy₃ and monomeric Dy systems, the positions of the maxima and minima change significantly on going from 1.9 K to 10 K, but remain almost unaltered up to the highest investigated temperature (25 K). To extract more precise information on this extraordinary behavior, the data were fitted assuming a tensorial relation $\mathbf{M}=\chi\mathbf{H}$,^{8,10} using the equation 1.1. The susceptibility tensors χ can be diagonalized, and are presented pictorially in Figure 3.10 for T=2.0 K and T=10 K as ellipsoids superimposed on to the molecular structure of the cluster. The principal values are summarized in Table 3.1. It is clear that while at 2.0 K the magnetic anisotropy is of the easy-plane type and essentially isotropic within the plane, on increasing the temperature this assumes an Ising (easy axis) character. This behavior is unprecedented and can be attributed to the way in which the two triangles have been linked.

To explore this further, the angle-resolved single-crystal magnetic data of compound **Dy6** were fitted with an Ising spin Hamiltonian by considering each Dy³⁺ as an Ising spin with S=1/2, as we previously did for Dy₃:^{3d, 4}

$$H = -J_{\text{int}}^z S_{z_3}^{3a} S_{z_3}^{3b} - \sum_{\substack{n=a,b \\ i,j=1,2,3 \\ i<j}} J_{ij}^{zz} S_{z_i}^{in} S_{z_j}^{jn} - \sum_{i=1,2,3}^{n=a,b} g_{z_i} S_{z_i}^{in} H_{z_i} \quad (2.1)$$

where the index n refers to the two different triangular moieties, denoted as a and b, and the indexes *i* and *j* refer to the three different Dy³⁺ ions in each triangle (Figure 3.8). $S_{z_i}^{in}$ denotes the spin operator for the inner Dy³⁺ (Dy3) along its local easy anisotropy axis z_i . J_{ij}^{zz} corresponds to the Ising magnetic interactions inside the triangular moiety and J_{int}^z the magnetic interaction between the two Dy₃ ions in different triangles. Finally, g_{z_i} and H_{z_i} are the gyromagnetic factors and the applied magnetic field, respectively, along the z_i local axes. The fact that the two triangular moieties are related by an inversion center is taken into account and therefore the local axes z_i , the parameters J_{ij}^z and g_{z_i} do not depend on the triangle index *n*. Using the g_{z_i} gyromagnetic factors ($g_{z1} = 19.8$, $g_{z2} = 19.7$, $g_{z3} = 19.3$) and the directions of the z_i local axes obtained from the *ab initio* calculations, the unknown

parameters of the Hamiltonian model are the four independent magnetic interactions indicated in Figure 3.8.

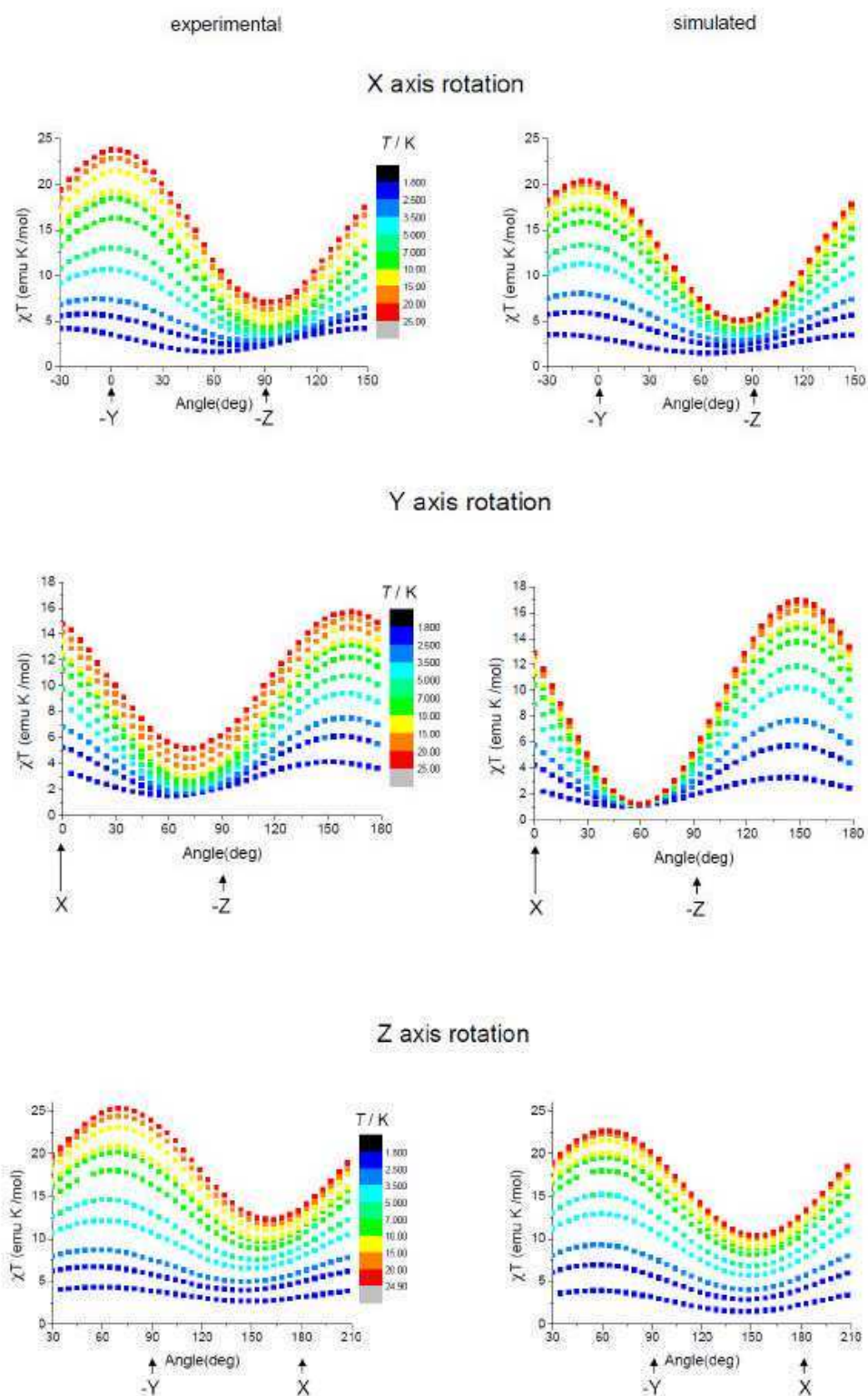


Figure 3.9: Experimental (left) and simulated (right) angular dependence of the magnetic susceptibility recorded for Dy_6 in the temperature range 1.9-25 K (see colour scheme) for three orthogonal rotations. The calculated values have been obtained as described in the text.

The simulation of the angle resolved magnetic susceptibility data resulted in the following values for them: $J_{12}^{zz} = 7.6$ K, $J_{13}^{zz} = 6.0$ K, $J_{23}^{zz} = 5.0$ K, and $J_{\text{int}}^z = 1.2$ K. It should be noted that the positive signs correspond to antiferromagnetic interactions, because in our spin Hamiltonian the local z axis vectors defined in Figure 3.8 of two interacting Dy^{3+} ions subtend an angle larger than 90° .

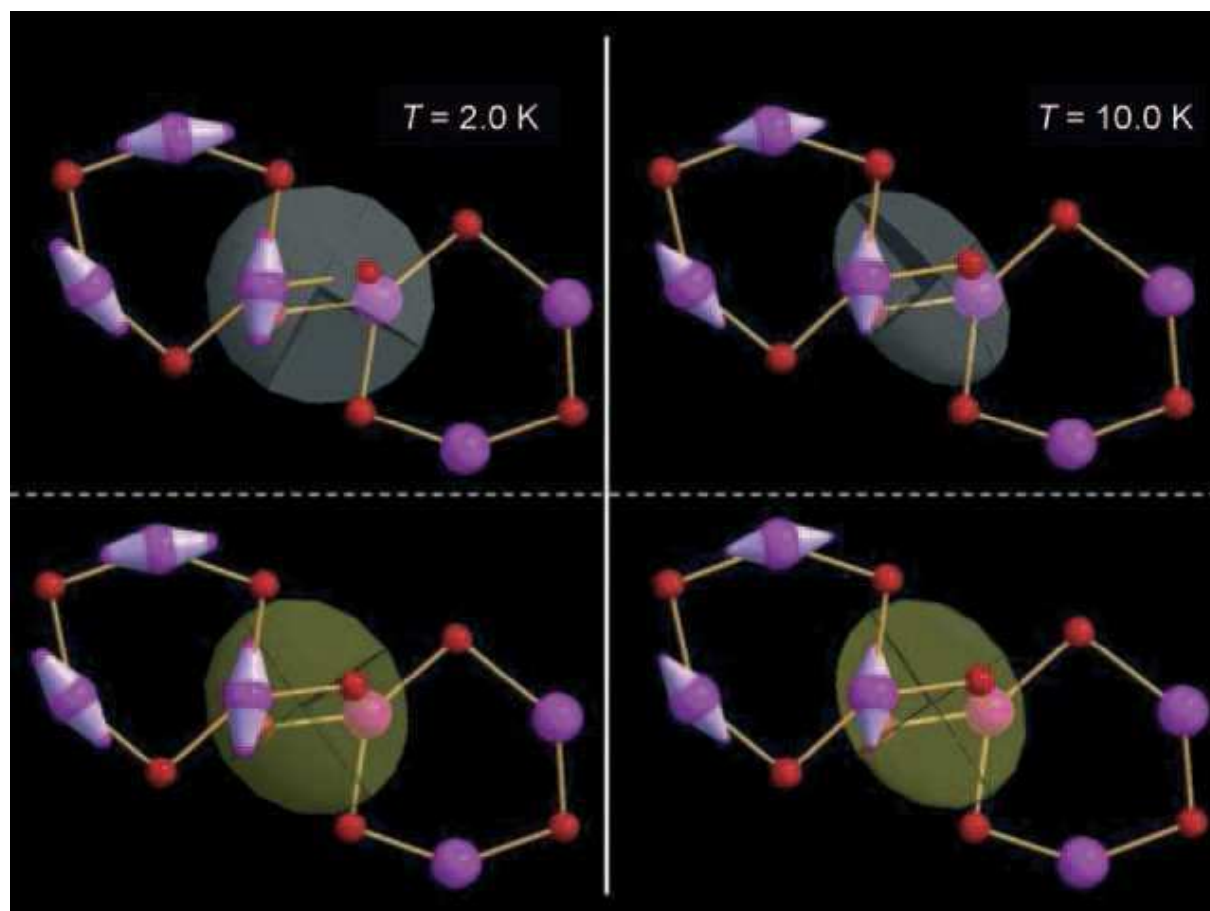


Figure 3.10: Ellipsoidal representation of the experimental (top) and calculated (bottom) susceptibility tensors of Dy_6 at two different temperatures. The tensors are superimposed onto the molecular structure of the magnetic core (Dy violet, O red); the orientation of the Dy easy axes estimated from *ab-initio* calculations are also shown.

	χ_1	χ_2	χ_3
$T=2.0$ K	2.35	2.13	0.511
$T=4.0$ K	3.04	1.89	0.568
$T=10$ K	2.05	1.12	0.360
$T=25$ K	1.00	0.552	0.233

Table 3.1: Principal values of the susceptibility tensor extracted from the data of Figure 3.9.

3.6 Energy spectrum for Dy₆

The complete simulation of all the rotations is shown in the Figure 3.9 and the calculated powder data in Figure 3.3. Only a partial agreement is expected at this level of approximation, as all transverse components of the dysprosium ions have been neglected in our models and the easy axes directions have been fixed to those resulting from the ab initio calculation. The out-of-plane components are therefore significantly smaller in the calculated tensors but the trend in the change of the magnetic anisotropy is however reproduced as shown in Figure 3.10 where the calculated susceptibility tensors are also indicated. The calculated energies as a function of the magnetic field applied in the plane (Figure 3.11) show that the ground state of Dy₆ is a non-magnetic doublet as in the case of Dy₃.⁶ This results from the weak AF interaction between the triangles. However, due to the breaking of the trigonal symmetry and a larger deviation of the easy axis of Dy₃ from the plane of the triangle, a weakly magnetic state is found at only 0.6 K above the ground state (compared with about 10 K in Dy₃). The disappearance of a step in the M versus H curve is therefore not surprising. The first excited state corresponds to the violation of J_{inter} , this being the weakest interaction, and does not affect the clockwise or anticlockwise arrangement of the magnetic moments in each triangle.

We can try to rationalize the dynamics of the magnetization of Dy₆ in the frame of the model we have developed. The main feature of Dy₆ is the presence of two different relaxation processes, one with rates comparable to those found for Dy₃, and a second one with much higher blocking temperatures. It would be tempting to associate the high temperature slow relaxation to the Dy₃ site, which has a different coordination environment compared with the original Dy₃ molecule, but this disagrees with the finding that this site has a smaller calculated energy gap between the ground and the first excited doublet (Table 3.2). Moreover, similar differences in the energy gaps were also calculated for Dy₃ but not observed in the dynamic behavior. An alternative explanation could be that it arises from the peculiar change in magnetic anisotropy from easy plane to easy axis on populating the excited states. It is intuitive that the more anisotropic character of the excited states can result in a slower relaxation process observed at higher temperature when these states have strong contributions to the ac susceptibility. The absence of faster relaxation in zero static field, which on the contrary was clearly evident in Dy₃, can also be associated to the linking of the two triangles. Relaxation through quantum tunneling is strongly suppressed when it involves simultaneous

magnetic flipping of more than one site, as has already been observed in weakly coupled dimers of Mn_4 SMM.¹¹

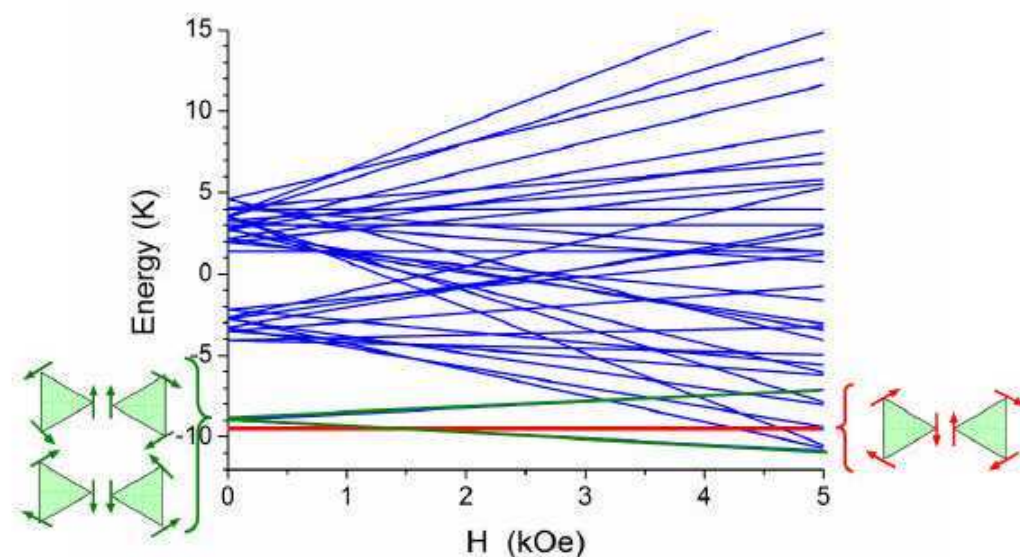


Figure 3.11: Energy levels diagram for Dy_6 calculated in the Ising approximation (see text). The orientation of the Dy spins in the low lying states is also schematized.

	Dy(1)	Dy(2)	Dy(3)
Easy axis direction(°)			
ϕ	82.4	82.1	64.8
θ	2.9	2.3	9.7
g_z gyromagnetic factor			
g_z	19.78	19.66	19.32
${}^6H_{15/2}$ Energy levels(cm^{-1})			
E0	0	0	0
E1	187	119	80
E2	259	185	163
E3	312	222	239
E4	348	242	307
E5	395	292	362
E6	466	342	403
E7	647	444	445

Table 3.2: CASSCF/RASSI-SO orientation of the single-ion easy anisotropy axis for the three Dy^{3+} ions in one of the triangular moieties of the Dy_6 system. θ is the angle subtended by an easy axis with respect to the plane of the triangle and ϕ the angle between the projection of each easy axis on to the plane of the triangle and the corresponding bisector of the triangle. The computed gyromagnetic factors along the single-ion easy anisotropy axes, g_z , and the energy of the eight ${}^6H_{15/2}$ Kramer's doublets are also included.

3.7 Conclusion

In conclusion, the linking of two Dy_3 to form Dy_6 has been found to give a spectacular increase in the temperature at which slowing down of the magnetization is observed from 8 to 25 K. This occurs in spite of the fact that the linking promotes an antiferromagnetic interaction, in contrast to what was recently observed for a similar arrangement of Dy_3 triangles,^{3h} where a ferromagnetic interaction was suggested. The observation of two relaxation regimes is apparently associated to an unprecedented change in the nature of the magnetic anisotropy from an easy plane to easy axis type on increasing the temperature. This change can be explained by breaking of the symmetry induced by linking the triangles. We can further note that this behavior contrasts to what is normally encountered in anisotropic systems on reducing temperature, where they are expected to become more, rather than less, anisotropic at low temperature. Although this needs verification with reference to other systems, it is a very exciting finding that a relatively long relaxation time, useful for instance in molecular spintronics devices, can be observed at high temperatures thanks to the properties of the excited states. More information on the temperature dependence of the magnetic anisotropy of complex molecules containing lanthanide ions is needed, in particular from oriented single crystal studies, in order to establish magnetostructural correlations. Fortunately, the straightforward single-crystal sample handling procedure developed herein can easily be applied to angle-resolved magnetometry on a wide range of compounds and should lead to the desired insights being gained rapidly.

Bibliography

- (1) D. Gatteschi, R. Sessoli, J. Villain *Molecular Nanomagnets*, Oxford University Press, Oxford, **2006**.
- (2) (a) C. M. Zaleski, E. C. Depperman, J. W. Kampf, M. L. Kirk, V. L. Pecoraro, *Angew. Chem., Int. Ed.* **2004**, *43*, 3912; (b) S. Osa, T. Kido, N. Matsumoto, N. Re, A. Pochaba, J. Mrozinski, *J. Am. Chem. Soc.* **2004**, *126*, 420; (c) A. Mishra, W. Wernsdorfer, K. A. Abboud, G. Christou, *J. Am. Chem. Soc.* **2004**, *126*, 15648; (d) F. He, M.-L. Tong, X.-M. Chen, *Inorg. Chem.* **2005**, *44*, 8285; (e) A. Mishra, W. Wernsdorfer, S. Parsons, G. Christou, E. K. Brechin, *Chem. Comm.* **2005**, 2086; (f) J.-P. Costes, M. Auchel, F. Dahan, V. Peyrou, M. Shova, W. Wernsdorfer, *Inorg. Chem.* **2006**, *45*, 1924; (g) F. Mori, T. Nyui, T. Ishida, T. Nogami, K.-Y. Choi, H. Nojiri, *J. Am. Chem. Soc.* **2006**, *128*, 1440; (h) C. Aronica, G. Pilet, G. Chastanet, W. Wernsdorfer, J.-F. Jacquot, D. Luneau, D. *Angew. Chem., Int. Ed.* **2006**, *45*, 4659; (i) M. Ferbinteanu, T. Kajiwara, K.-Y. Choi, H. Nojiri, A. Nakamoto, N. Kojima, F. Cimpoesu, Y. Fujimura, S. Takaishi, M. Yamashita, *J. Am. Chem. Soc.* **2006**, *128*, 9008; (j) V. M. Mereacre, A. M. Ako, R. Clérac, W. Wernsdorfer, G. Filoti, J. Bartolomé, C. E. Anson, A. K. Powell, *J. Am. Chem. Soc.* **2007**, *129*, 9248; (k) C. M. Zaleski, J. W. Kampf, T. Mallah, M. L. Kirk, V. L. Pecoraro, *Inorg. Chem.* **2007**, *46*, 1954; (l) V. Mereacre, A. M. Ako, R. Clérac, W. Wernsdorfer, I. J. Hewitt, C. E. Anson, A. K. Powell, *Chem. Eur. J.* **2008**, *14*, 3577; (m) T. C. Stamatatos, S. J. Teat, W. Wernsdorfer, G. Christou, *Angew. Chem. Int. Ed.* **2009**, *48*, 521; (n) V. Chandrasekhar, B. M. Pandian, R. Azhakar, J. J. Vittal, R. Clérac, *Inorg. Chem.* **2009**, *48*, 521; (o) G. Novitchi, W. Wernsdorfer, L. F. Chibotaru, J.-P. Costes, C. E. Anson, A. K. Powell, *Angew. Chem. Int. Ed.* **2009**, *48*, 1614; (p) A. M. Ako, V. Mereacre, R. Clérac, W. Wernsdorfer, I. J. Hewitt, C. E. Anson, A. K. Powell, *Chem. Commun.*, **2009**, 544.
- (3) (a) N. Ishikawa, M. Sugita, T. Ishikawa, S. Koshihara, Y. Kaizu, *J. Am. Chem. Soc.* **2003**, *125*, 8694; (b) L. G. Westin, M. Kritikos, A. Caneschi, *Chem. Commun.* **2003**, 1012-1013; (c) S. Takamatsu, T. Ishikawa, S. Koshihara, N. Ishikawa, *Inorg. Chem.* **2007**, *46*, 7250-7252; (d) J. K. Tang, I. Hewitt, N. T. Madhu, G. Chastanet, W. Wernsdorfer, C. E. Anson, C. Benelli, R. Sessoli, A. K. Powell, *Angew. Chem. Int. Ed.* **2006**, *45*, 1729; (e) M. A. Aldamen, J. M. Clemente-Juan, E. Coronado, C. Marti-Gastaldo, A. Gaita-Arino, *J. Am. Chem. Soc.* **2008**, *130*, 8874; (f) M. T. Gamer, Y. Lan, P. W. Roesky, A. K. Powell, A. K. R. Clérac, *Inorg. Chem.* **2008**, *47*, 6581; (g) Y.-Z. Zheng, Y. Lan, C. E. Anson, A. K. Powell, *Inorg. Chem.*, **2008**, *47*, 10813; (h) B. Hussain, D. Savard, T. J. Burchell, W. Wernsdorfer, M. Murugesu, *Chem. Commun.* **2009**, 1100.
- (4) J. Luzon, K. Bernot, I. J. Hewitt, C. E. Anson, A. K. Powell, R. Sessoli, *Phys. Rev. Lett.* **2008**, *100*, art.n°247205.
- (5) P. A. Malmqvist, B. O. Roos, B. Schimmelpfennig, *Chem. Phys. Lett.* **2002**, *357*, 230.
- (6) L. F. Chibotaru, L. Ungur, A. Soncini, *Angew. Chem. Int. Ed.* **2008**, *47*, 4126.
- (7) K. Bernot, J. Luzon, L. Bogani, A. Caneschi, D. Gatteschi, R. Sessoli, A. Vindigni, A. Rettori, M. G. Pini *Phys. Rev. B* **2009**, *79*, 134419

- (8) K. Bernot, J. Luzon, L. Bogani, M. Etienne, A. Caneschi, C. Sangregorio, M. Shanmugam, R. Sessoli, D. Gatteschi *J. Am. Chem. Soc.* **2009**, *131*, 5573.
- (9) A. Abragam, B. Bleaney, *Electron Paramagnetic Resonance of Transition Ions*, Dover, New York **1986**.
- (10) (a) S. Mitra, *Prog. Inorg. Chem.* **1977**, *22*, 309; (b) M. Gerloch, D. J. Mackey, *J. Chem. Soc., Dalton Trans.* **1972**, *3*, 415.
- (11) (a) W. Wernsdorfer, N. Aliaga-Alcalde, D. N. Hendrickson, G. Christou, *Nature* **2002**, *416*, 406; (b) S. Hill, R. S. Edwards, N. Aliaga-Alcalde, G. Christou, *Science* **2003**, *302*, 1015.
- (12) G. Karlstrom, R. Lindh, P. A. Malmqvist, B. O. Roos, U. Ryde, V. Veryazov, P. O. Widmark, M. Cossi B. Schimmelpfennig, P. Neogrady, L. Seijo, *Comput. Mater. Sci.* **2003**, *28*, 222-239.

Chapter 4

Dimers and chains of {3d-4f} single molecule magnets constructed from heterobimetallic tectons

<u>4.1 INTRODUCTION</u>	59
<u>4.2 CRYSTAL STRUCTURES</u>	60
<u>4.3 MAGNETIC MEASUREMENTS</u>	65
<u>4.4 CONCLUSION</u>	72

4.1 Introduction

The investigation of the magnetic anisotropy is of paramount importance for the investigation of all molecular systems that can act as nanomagnets, with a hysteresis that is observed in the absence of long-range magnetic order.¹ While in the previous chapters we have focused our attention on clusters of various nuclearities (Single Molecule Magnets, SMMs), equally interesting are one-dimensional coordination polymers (Single Chain Magnets, SCMs).^{2,3} Most SMMs and SCMs are however based on the combination of different spin carriers, where at least one of them must exhibit a strong uniaxial magnetic anisotropy. Let us take the case of heterospin Single Molecule Magnets. Various combinations of spin carriers (2p-3d; 2p-4f, 3d-4f, 3d-4d, etc.) have been employed in order to fulfill the required conditions for the observation of SMM behavior: a high spin ground state and a large easy-axis anisotropy. The first condition is accomplished employing pairs of spin carriers that interact ferromagnetically: $\text{Cu}^{\text{II}}-\text{Ln}^{\text{III}}$, $\text{Ni}^{\text{II}}-\text{Ln}^{\text{III}}$, $\text{rad}^{\bullet}-\text{Ln}^{\text{III}}$.⁴ The second one is fulfilled by employing strongly anisotropic metal ions: Mn^{III} , Co^{II} , Tb^{III} , Dy^{III} , Ho^{III} . Numerous 3d-4f SMMs have been constructed from Cu^{II} and Tb^{III} , Dy^{III} , or Ho^{III} .⁵ Other SMMs consist of high spin species obtained from nickel(II) ions interacting ferromagnetically with anisotropic lanthanides.⁶ The combination of paramagnetic ligands (rad^{\bullet}) with lanthanides that bring magnetic anisotropy was also successful in designing SMMs.⁷ Conversely, when the lanthanide is the isotropic Gd^{III} ion, the second metal ion has to be anisotropic. A nice example was recently reported by Chandrasekhar, Clérac *et al.*, and contains Gd^{III} and Co^{II} .⁸ Heterometallic SMMs based on Gd^{III} and Mn^{III} are also known.⁹ Finally, SMMs can be obtained by gathering two different anisotropic metal ions within the same molecular entity, *e. g.* $\text{Mn}^{\text{III}}-\text{Ln}^{\text{III}}$ ($\text{Ln}^{\text{III}} = \text{Tb}^{\text{III}}, \text{Dy}^{\text{III}}$).¹⁰

The anisotropic high-spin oligonuclear complexes can be connected through various spacers resulting in 1-D coordination polymers with very interesting magnetic properties: (1) if the spacers themselves are paramagnetic, Single Chain Magnets can be obtained, the magnetic interaction between the nodes and the spacers leading to either ferromagnetic or ferrimagnetic chains;¹¹ (2) if the spacers are diamagnetic, chains of SMMs are formed, provided that the intermolecular interactions are weak enough to prevent the transformation of the spin network into a classical antiferromagnet.¹² Recently, Wernsdorfer *et al.*¹³ and Clérac *et al.*¹⁴ have shown that the introduction of magnetic interactions between SMMs,

mediated by hydrogen bonds or bridging ligands, exert an influence on the quantum properties, shifting the quantum tunneling resonances with respect to the isolated SMMs.

The use of radicals to form 1-D structures with lanthanide ions have demonstrated to be a successful strategy towards the realization of SCM and the analysis of the magnetic anisotropy with angular resolved magnetometry has revealed a key tool to rationalize the magnetic behavior.¹⁵ We have therefore decided to extend the investigation to other type of 1-D systems, this time based on the interaction of 3d and 4f metal centers. We have therefore benefitted from the collaboration with the group of Prof. Marius Andruh of the University of Bucharest (RO). In a series of papers, Andruh and coworkers have shown that large heterometallic clusters or coordination polymers can be assembled using preformed heterometallic nodes and various spacers.¹⁶ The heterometallic nodes are easily obtained employing heterotopic compartmental ligands. Such ligands are, for example, Schiff bases derived from *o*-vanillin and diamines

Two novel 3d-4f heterometallic systems, which have been obtained following this synthetic approach, are here magnetically investigated: a tetranuclear complex, $[\text{Ni}_2(\text{valpn})_2\text{Dy}_2(\text{pdca})_2(\text{NO}_3)(\text{H}_2\text{O})_6](\text{NO}_3)\cdot 4\text{H}_2\text{O}$, and a ladder-like coordination polymer ${}^\infty[\text{Ni}_2(\text{H}_2\text{O})_2(\text{valpn})_2\text{Dy}_2(\text{tfa})_3]\cdot 4\text{CH}_3\text{CN}$ (H_2valpn is the Schiff-base resulted from the 2 : 1 condensation of 3-methoxy-salicylaldehyde with propylenediamine; $\text{pdca}^{2-} = 2,6\text{-pyridine-dicarboxylate}$; $\text{tfa}^{2-} = \text{terephthalate}$) (this two compounds are respectively abbreviated in **Ni₂Dy₂** and **[Ni₂Dy₂]_∞** for of the remaining of the chapter). The binuclear node, **[NiDy]**, has been chosen because of the magnetic anisotropy brought by the Dy^{III} ion. Moreover it has been shown that the exchange interaction between Dy^{III} and Ni^{II} in such compounds is ferromagnetic.^{6,17}

4.2 Crystal structures

Crystallographic investigation has been carried out in the University of Bucharest. We will describe here the results as these are fundamental for a rationalization of the magnetic properties.

The crystallographic investigation of **Ni₂Dy₂** reveals cationic tetranuclear species (See Table 4.1 for crystallographic data), uncoordinated nitrate ions and water molecules. The tetranuclear species can be described as resulting from the coordination of a $\{\text{Ni}(\text{NO}_3)(\text{H}_2\text{O})(\text{valpn})\text{Dy}(\text{H}_2\text{O})_2(\text{pdca})\}$ fragment, through an oxygen atom arising from one

carboxylato group, to the dysprosium ion from the second fragment, $\{\text{Ni}(\text{H}_2\text{O})_2(\text{valpn})\text{Dy}(\text{H}_2\text{O})(\text{pdca})\}$ (Figure 4.1).

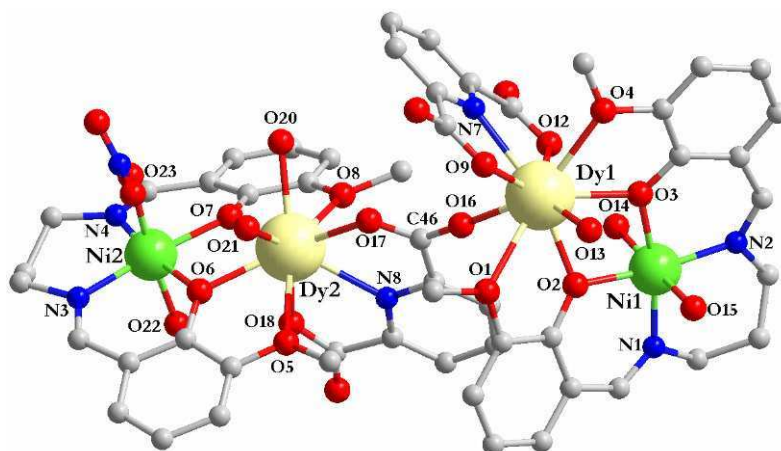


Figure 4.1: Perspective view of the tetranuclear complex Ni_2Dy_2 , along with the atom numbering scheme.

In both fragments the nickel ions are hexacoordinated, with a slightly distorted octahedral geometry. The coordination positions around the Ni1 ion are occupied by the two nitrogen atoms [Ni1 – N1 = 2.013(5); Ni1 – N2 = 2.030(4) Å] and the two phenoxo oxygen atoms arising from the valpn ligand [Ni1 – O2 = 2.024(3), Ni1 – O3 = 2.020(3) Å], with two aqua ligands in the apical positions [Ni1 – O14 = 2.107(3); Ni1 – O15 = 2.121(4) Å]. The coordination sphere around the Ni2 ion is a little different. The equatorial plane is formed by the two nitrogen atoms [Ni2 – N3 = 2.021(5); Ni2 – N4 = 2.040(5) Å] and the two phenoxo oxygen atoms of the Schiff-base ligand [Ni2 – O6 = 2.024(4), Ni2 – O7 = 2.024(3) Å], and the apical positions are occupied by one aqua ligand [Ni2 – O22 = 2.105(4) Å] and by one oxygen atom from a nitrate ion [Ni2 – O23 = 2.160(5) Å]. Both dysprosium ions are nine-coordinated by eight oxygens and one nitrogen. The Dy1 atom is coordinated by four oxygen atoms arising from the Schiff-base [Dy1 – O1 = 2.645(4); Dy1 – O2 = 2.329(3); Dy1 – O3 = 2.344(3); Dy1 – O4 = 2.579(3) Å], one aqua ligand [Dy1 – O13 = 2.408(3) Å], one nitrogen and two oxygen atoms from a pdca^{2-} ligand [Dy1 – O9 = 2.367(3) Å; Dy1 – N7 = 2.520(4) Å; Dy1 – O12 = 2.429(3) Å], as well as by a carboxylato bridging oxygen [Dy1 – O16 = 2.339(3) Å]. The second dysprosium atom, Dy2, is coordinated by the four oxygen atoms of the Schiff base [Dy2 – O5 = 2.579(4); Dy2 – O6 = 2.303(3); Dy2 – O7 = 2.307(3); Dy2 – O8 = 2.540(4) Å], two aqua ligands [Dy2 – O20 = 2.435(5) Å; Dy2 – O21 = 2.438(5) Å] and three donor atoms from a 2,6-pyridine-dicarboxylato ligand [Dy2 – O17 = 2.387(4); Dy2 – N8 = 2.500(4); Dy2 – O18 = 2.429(4) Å]. The Ni...Dy distances are around 3.5 Å (Ni1...Dy1

= 3.498; Ni2...Dy2 = 3.464 Å), while the two Dy ions are placed approximately twice as far (Dy1...Dy2 = 6.788 Å). Selected bond distances are collected in Table 4.2.

$[\text{Ni}_2\text{Dy}_2]_\infty$ (See Table 4.1 for crystallographic data) is a 1-D coordination polymer with a ladder-like topology (Figure 4.2). A step of the ladder is made by a $[\text{Ni}_2(\text{H}_2\text{O})_2(\text{valpn})_2\text{Dy}_2(\text{tfa})]^{2+}$ moiety, which results by connecting two $[\text{Ni}(\text{valpn})\text{Dy}(\text{H}_2\text{O})]^{3+}$ nodes by a terephthalato spacer. The neighbouring steps of the ladder are connected through other terephthalato anions, two for each $[\text{Ni}_2(\text{H}_2\text{O})_2(\text{valpn})_2\text{Dy}_2(\text{tfa})]^{2+}$ unit. Two types of terephthalato spacers are observed within the structure of $[\text{Ni}_2\text{Dy}_2]_\infty$. The first type is a symmetrical one, the terephthalato anion connecting two dysprosium ions from two heterodinuclear nodes within one step of the ladder, and each carboxylato group chelates a dysprosium ion. The second coordination mode consists of an asymmetrical bridge formed between two adjacent ladder steps: one carboxylato group is chelating a dysprosium ion, while the second one coordinates to the dysprosium and nickel ions from a binuclear node.

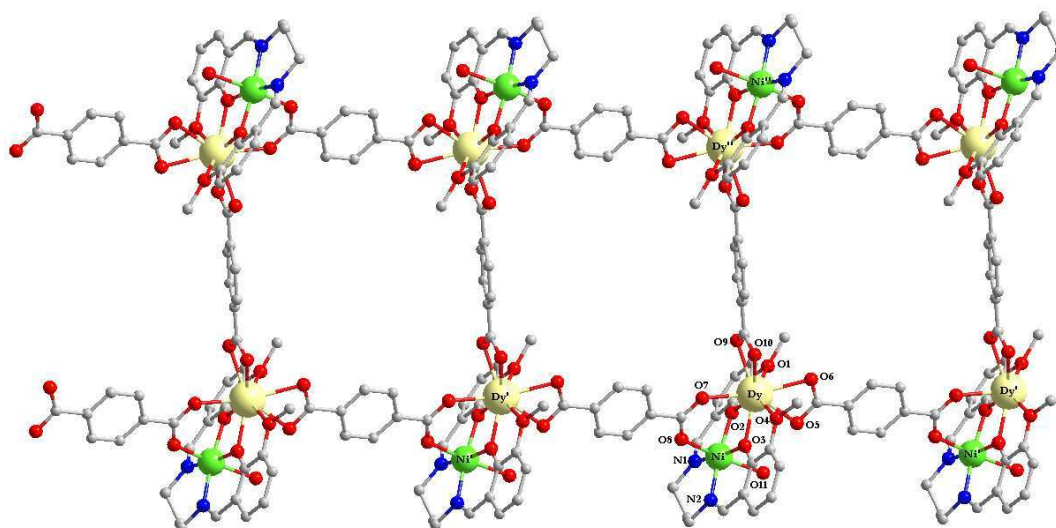


Figure 4.2: Perspective view of the ladder-like coordination polymer $[\text{Ni}_2\text{Dy}_2]_\infty$, and labeling scheme ($\square = -1 + x, y, z$; $\square\square = 2 - x, 1 - y, -z$).

The nickel ions display a slightly elongated octahedral geometry, with the equatorial positions occupied by two nitrogen atoms and two phenoxo oxygen atoms of the Schiff-base ligand [$\text{Ni1} - \text{O2} = 2.038(3)$, $\text{Ni1} - \text{O3} = 2.007(3)$, $\text{Ni1} - \text{N1} = 2.026(4)$, $\text{Ni1} - \text{N2} = 2.048(4)$ Å], while the axial positions are filled by one aqua ligand [$\text{Ni1} - \text{O11} = 2.203(3)$ Å], and one oxygen atom from a bridging carboxylato group [$\text{Ni1} - \text{O8} = 2.038(3)$ Å]. The dysprosium ions are surrounded by nine oxygen atoms: four oxygen atoms arise from the valpn²⁻ ligand [$\text{Dy1} - \text{O1} = 2.644(3)$ Å; $\text{Dy1} - \text{O2} = 2.282(3)$ Å; $\text{Dy1} - \text{O3} = 2.295(3)$ Å; $\text{Dy1} - \text{O4} =$

2.532(3) Å] and five others form three terephthalato spacers, i. e. two chelating carboxylato groups and one carboxylato group that bridges one nickel and one dysprosium ion [Dy1 – O5 = 2.427(3) Å; Dy1 – O6 = 2.493(3) Å; Dy1 – O7 = 2.381(3) Å; Dy1 – O9 = 2.427(3) Å; Dy1 – O10 = 2.438(3) Å]. The Ni...Dy distance within a node is 3.383 Å, while the shortest internode Dy...Dy distances are Dy...Dy'' = 11.334 Å and Dy...Dy' = 11.643 Å. Selected bond distances are gathered in Table 4.3.

Compound	Ni₂Dy₂	[Ni₂Dy₂]_∞
Chemical formula	C ₅₂ H ₆₆ N ₈ O ₃₂ Ni ₂ Dy ₂	C ₇₀ H ₆₈ N ₈ O ₂₂ Ni ₂ Dy ₂
<i>M</i> (g mol ⁻¹)	1757.51	1815.73
Temperature, (K)	293(2)	293(2)
Wavelength, (Å)	0.71073	0.71073
Crystal system	Monoclinic	Monoclinic
Space group	<i>P21/n</i>	<i>P21/n</i>
<i>a</i> (Å)	19.3054(6)	11.6443(4)
<i>b</i> (Å)	15.4938(3)	16.3722(4)
<i>c</i> (Å)	21.6876(7)	19.2871(8)
α (°)	90.00	90.00
β (°)	98.176(2)	97.641(3)
γ (°)	90.00	90.00
<i>V</i> (Å ³)	6421.1(3)	3644.3(2)
<i>Z</i>	4	2
<i>D_c</i> (g cm ⁻³)	1.797	1.651
μ (mm ⁻¹)	2.975	2.615
<i>F</i> (000)	3432	1808
Goodness-of-fit on <i>F</i> ²	1.033	1.114
Final <i>R</i> 1, <i>wR</i> ₂ [<i>I</i> >2σ(<i>I</i>)]	0.0507, 0.0977	0.0585, 0.0919
<i>R</i> 1, <i>wR</i> ₂ (all data)	0.0846, 0.1068	0.0902, 0.0996
Largest diff. peak and hole (eÅ ⁻³)	1.609, -1.261	0.844, -2.286

Table 4.1: Crystallographic data, details of data collection and structure refinement parameters for **Ni₂Dy₂** and **[Ni₂Dy₂]_∞**.

Ni1 - N1	2.013(5)	Dy1 - O1	2.645(4)
Ni1 - N2	2.030(4)	Dy1 - O2	2.329(3)
Ni1 - O2	2.024(3)	Dy1 - O3	2.344(3)
Ni1 - O3	2.020(3)	Dy1 - O4	2.579(3)
Ni1 - O14	2.107(3)	Dy1 - O9	2.367(3)
Ni1 - O15	2.121(4)	Dy1 - O12	2.429(3)
Ni2 - N3	2.021(5)	Dy1 - O13	2.408(3)
Ni2 - N4	2.040(5)	Dy1 - O16	2.339(4)
Ni2 - O6	2.024(4)	Dy1 - N7	2.520(4)
Ni2 - O7	2.024(3)	Dy2 - O5	2.579(4)
Ni2 - O22	2.105(4)	Dy2 - O6	2.303(3)
Ni2 - O23	2.160(5)	Dy2 - O7	2.307(3)
		Dy2 - O8	2.540(4)
		Dy2 - O17	2.387(4)
		Dy2 - O18	2.429(4)
		Dy2 - O20	2.435(5)
		Dy2 - O21	2.438(5)
		Dy2 - N8	2.500(4)

Table 4.2: Selected bond distances (Å) for $[Ni_2(valpn)_2Dy_2^{III}(pdca)_2(NO_3)(H_2O)_6](NO_3) \cdot 4H_2O$, Ni_2Dy_2

Ni1 – N1	2.026(4) Å	Dy1 – O1	2.644(3) Å
Ni1 – N2	2.048(4) Å	Dy1 – O2	2.282(3) Å
Ni1 – O2	2.038(3) Å	Dy1 – O3	2.295(3) Å
Ni1 – O3	2.007(3) Å	Dy1 – O4	2.532(3) Å
Ni1 – O8	2.038(3) Å	Dy1 – O5	2.427(3) Å
Ni1 – O11	2.203(3) Å	Dy1 – O6	2.493(3) Å
		Dy1 – O7	2.381(3) Å
		Dy1 – O9	2.427(3) Å
		Dy1 – O10	2.438(3) Å

Table 4.3: Selected bond distances for ${}_{\infty}[Ni_2(H_2O)_2(valpn)_2Dy_2(tfa)_3] \cdot 4CH_3CN$, $[Ni_2Dy_2]_{\infty}$

4.3 Magnetic Measurements

Our study started with a characterization of the magnetic behavior of polycrystalline samples. The static and dynamic magnetic properties of Ni_2Dy_2 and $[\text{Ni}_2\text{Dy}_2]_\infty$ have been investigated. Let us start with the tetranuclear compound, Ni_2Dy_2 . The temperature variation of the $\chi_M T$ product per tetranuclear unit is represented in Figure 4.3. At room temperature the value of $\chi_M T$ is 29.94 emu mol⁻¹K, which well corresponds to the four uncoupled paramagnetic centers: two Ni^{II} ions ($S = 1$, $g = 2$) and two Dy^{III} ions ($J = 15/2$, $S = 5/2$, $L = 5$, ${}^6\text{H}_{15/2}$; $g_{15/2} = 4/3$), the expected value being 30.34 emu mol⁻¹K. By lowering the temperature, $\chi_M T$ decreases continuously down to 12 K due to the depopulation of the Stark levels of the Dy^{III} ions. Below this temperature it remains almost flat, only slightly increasing, then to decrease below 6 K, reaching 24.96 emu mol⁻¹K at 2 K. The field dependence of the magnetization has been measured at $T = 2$ K and the results are reported in Figure 4.4. The magnetization rapidly increases up to 10 kOe to reach ca. 11 μ_B with a weak but linear increase for higher field.

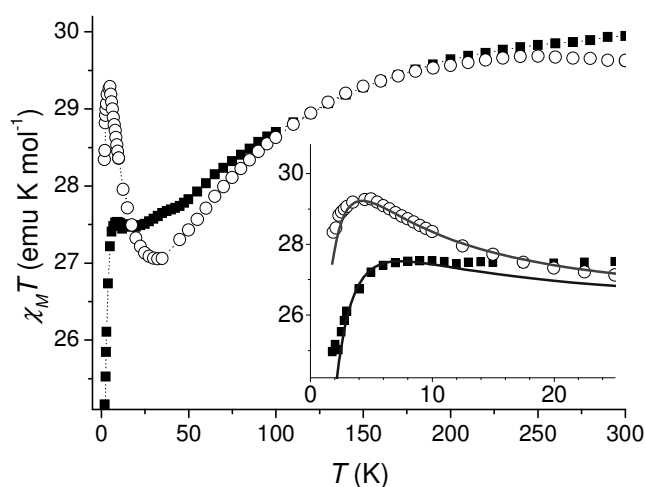


Figure 4.3: Plot of $\chi_M T$ versus T curves recorded for Ni_2Dy_2 (solid squares) and for $[\text{Ni}_2\text{Dy}_2]_\infty$ (open circles). In the inset the low temperature region is enlarged and the calculated $\chi_M T$ values are reported as solid grey lines (see text for the parameters)

A slightly different $\chi_M T$ behaviour has been observed for $[\text{Ni}_2\text{Dy}_2]_\infty$, as shown in Figure 4.3. The typical decrease of the $\chi_M T$ starts around 250 K but a more evident upturn is observed below 30 K, with $\chi_M T$ going from 27.06 to 29.29 emu K mol⁻¹. Also in this case a decrease is observed below 5 K. The magnetization versus field curve is very similar to that

of Ni_2Dy_2 , showing however a weaker increase at high field. The temperature dependence of the magnetization is very typical of anisotropic materials, and rescaling the data by plotting M . vs H/T gives superimposable curves only for lower fields (see inset of Figure 4.4).

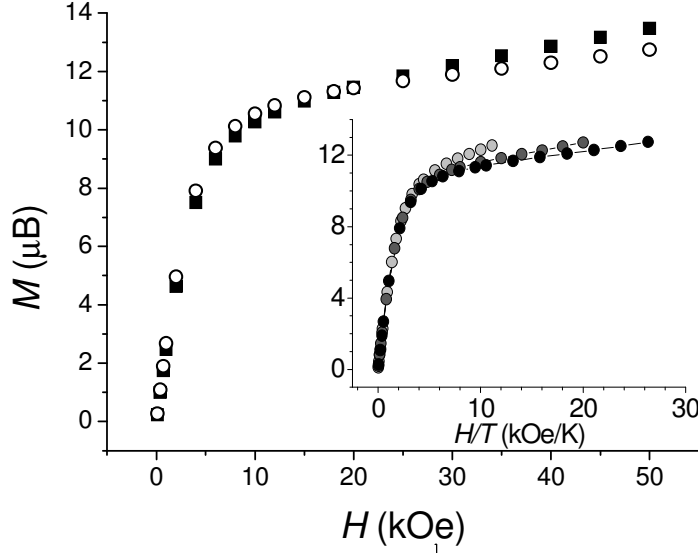


Figure 4.4: Field dependence of the magnetization for Ni_2Dy_2 (solid squares) and for $[\text{Ni}_2\text{Dy}_2]_\infty$ (open circles) measured at $T = 2$ K. In the inset the data for $\mathbf{2}$ measured at $T = 1.8$ K (black), 2.4 K (dark grey) and 4.4 K (grey) are plotted vs the scaled variable H/T to evidence deviations from superposition at high fields.

In order to get some qualitative information on the magnetic exchange involving the dysprosium and nickel pairs we have tried to simulate the low temperature behaviour assuming for the Dy(III) ions an effective spin $S_{\text{eff}} = 1/2$ with Ising type anisotropy.¹⁸ We have first analyzed the behaviour of $[\text{Ni}_2\text{Dy}_2]_\infty$ by assuming that the exchange interactions mediated by the tfa^{2-} ligands are negligible, thus reducing the Spin Hamiltonian to:

$$H_{\text{pair}} = -J_{\text{Dy-Ni}}^z S_{\text{Ni}}^z S_{\text{Dy}}^z + D_{\text{Ni}} \left[S_{\text{Ni}}^{z2} - \frac{1}{3} S_{\text{Ni}} (S_{\text{Ni}} + 1) \right] + g_{\text{Dy}}^z \mu_B H^z S_{\text{Dy}}^z + g_{\text{Ni}} \mu_B \mathbf{H} \mathbf{S}_{\text{Ni}} \quad (4.1)$$

The data in the inset of Figure 4.3 are satisfactorily reproduced assuming $g_{\text{Dy}}^z = 19.4$, $g_{\text{Dy}}^{x,y} = 1$, $g_{\text{Ni}} = 2.2$, $D_{\text{Ni}} = 4 \text{ cm}^{-1}$, and $J_{\text{Ni-Dy}}^z = 6 \text{ cm}^{-1}$. The large value estimated for g_{Dy}^z is typical of this ion and confirms the validity of the Ising model we have employed.^{18a, 19} The increase of $\chi_{\text{M}}T$ below 30 K is therefore attributed to the ferromagnetic exchange interaction between Ni-Dy, in agreement with what observed in phenoxo-bridged Ni-Gd pairs.^{6d,17} The exchange energy appears however smaller for Dy^{III} than for Gd^{III} despite the larger J value, as here an $S_{\text{eff}} = 1/2$ is employed. No magneto-structural correlations are available for Dy-M

pairs as in most cases the analysis of the magnetic data is only performed at a qualitative level. The decrease of $\chi_M T$ below 5 K is well accounted for by the single ion anisotropy of Ni^{II} , therefore hampering any estimation of the interactions mediated by the terephthalate ligand.

The Spin Hamiltonian parameters obtained for $[\text{Ni}_2\text{Dy}_2]_\infty$ have been employed for Ni_2Dy_2 , where we have added the Dy-Dy interaction mediated by the carboxylato bridge. The Spin Hamiltonian becomes:

$$H_{\text{tetra}} = H_{\text{pair}}^A + H_{\text{pair}}^B - J_{\text{Dy-Dy}}^z S_{\text{Dy}^A}^z S_{\text{Dy}^B}^z \quad (4.2)$$

where A and B refers to the two Ni-Dy pairs here assumed identical despite the significant structural differences. The very low temperature decrease is well reproduced by adding an antiferromagnetic Dy...Dy interaction $J_{\text{Dy-Dy}}^z = -1 \text{ cm}^{-1}$. According to literature data,²⁰ the exchange interaction between 4f metal ions bridged by the carboxylato group is supposed to be very weak. This value is however just indicative, as the single ion anisotropy of the Ni ion can be different from what estimated in $[\text{Ni}_2\text{Dy}_2]_\infty$. Moreover dipolar interactions are of the same order of magnitude but hard to estimate without a precise knowledge of the orientation of the easy axes of the Dy ions.^{19c} It must be noticed that the experimental $\chi_M T$ continues to decrease down to ca. 12 K in Ni_2Dy_2 . As a constant $\chi_M T$ would implies that only the ground doublet is populated we deduce that the the first excited doublet of the $J = 15/2$ multiplet is much closer in energy for Ni_2Dy_2 than for $[\text{Ni}_2\text{Dy}_2]_\infty$. This is in agreement with the higher slope in the M vs H curve at high fields observed for Ni_2Dy_2 . The assumption of our simplified Ising Spin Hamiltonian seems therefore less appropriate for this system than for $[\text{Ni}_2\text{Dy}_2]_\infty$. Moreover, in the absence of additional information from single crystal data all anisotropy axes have been assumed to be collinear. Non-collinearity of easy axes in molecular systems comprising Dy^{III} has been recently shown to affect substantially the magnetic behaviour.²¹

The dynamic magnetic behavior of Ni_2Dy_2 was investigated in the 0.2 - 25 kHz range by using alternating current (*ac*) susceptometry. In zero static field both in-phase (χ') and out-of-phase (χ'') components of the magnetic susceptibility show frequency dependence (Figure 4.5). The shape of the signals is broad, without maxima, suggesting multiple relaxation processes, as well as fast quantum tunneling of the magnetization.

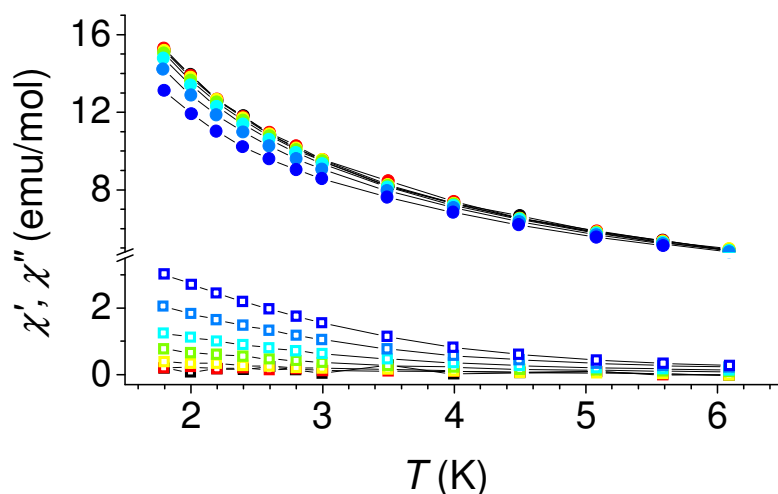


Figure 4.5: Real (solid circles) and imaginary (open squares) components of the ac susceptibility of Ni_2Dy_2 measured in zero static field and in the frequency range 0.2 -25 kHz (colour scale from red to blue)

This effect is even more evident in the zero field ac data of $[\text{Ni}_2\text{Dy}_2]_\infty$, which reveal the typical levelling of χ'' (Figure 4.6). Peaks in χ'' vs. T are observed when the variation of the relaxation time, τ , with temperature allows to go through the condition for maximum χ'' signal, *i.e.* $\omega\tau = 1$ with ω the angular frequency of the ac field.

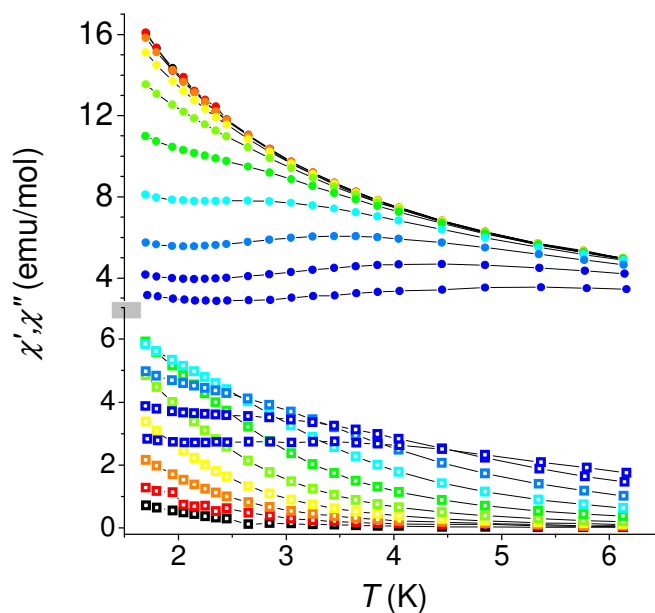


Figure 4.6: Real (solid circles) and imaginary (open squares) components of the ac susceptibility of $[\text{Ni}_2\text{Dy}_2]_\infty$ measured in zero static field and in the frequency range 0.2 -25 kHz (colour scale from red to blue)

When the relaxation time depends weakly on temperature, *i.e.* in the presence of tunneling, these peaks become severely distorted and an accurate estimation of the relaxation time can only be done by plotting χ'' as a function of the frequency of the oscillating field as done in Figure 4.7. While Ni_2Dy_2 does not show maxima, these are well defined for **2** but they become almost temperature independent below 2 K. The tunneling rate is therefore estimated to be of the order of 2 kHz, while the extracted relaxation times are reported in the Arrheniu plot of Figure 4.8. The data strongly deviate from a linear behaviour with the relaxation time approaching saturation at low temperature. By only fitting the high temperature data and assuming $\tau = \tau_0 \exp(\Delta/kT)$ a very small energy barrier $\Delta = 2$ K is estimated, associated to a very large pre-exponential factor $\tau_0 = 1.3 \times 10^{-5}$ s, confirming that we are observing a smooth transition between a thermally activated regime and a quantum tunneling one.

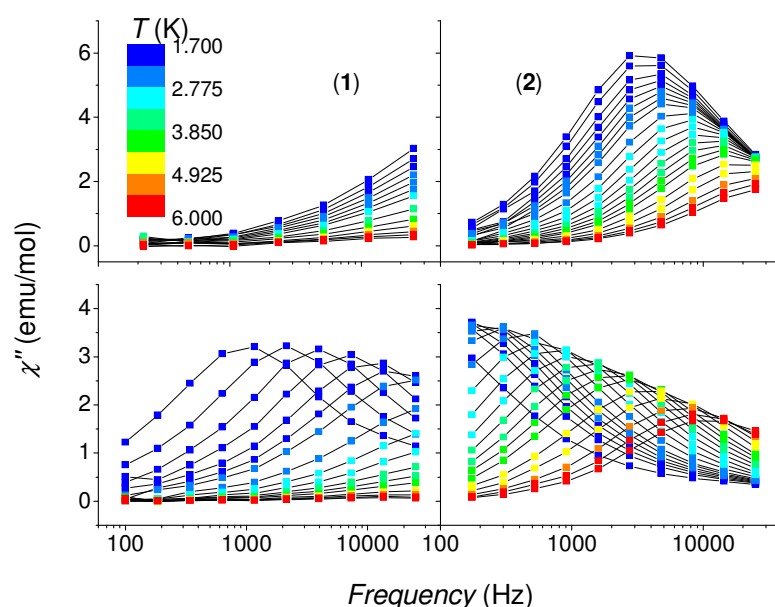


Figure 4.7: Frequency dependence of the imaginary components of the ac susceptibility of Ni_2Dy_2 (left) and of $[\text{Ni}_2\text{Dy}_2]_\infty$ (right) measured in zero static field upper panels and in a static magnetic field of 750 and 1000 Oe for Ni_2Dy_2 and $[\text{Ni}_2\text{Dy}_2]_\infty$, respectively (lower panels). Temperature color scheme in the legend

The analysis of the magnetization dynamics in lanthanide-based SMMs is much more complex than in the case of metal ions with quenched orbital momentum, for which the Spin Hamiltonian approach is able to rationalize most observations.² It is generally assumed that relaxation at intermediate temperatures, *i. e.* lower than the Debye temperature of the system, occurs through a thermally activated process that involves the first excited Stark levels.²² However, especially for low symmetric environments, the transverse components of the

crystal fields efficiently admix the states on opposite sides of the barrier generated by the Ising anisotropy. It is thus rather common to observe below 4 K an efficient underbarrier mechanism of relaxation.^{4b,7} This is indeed what observed in Ni_2Dy_2 and $[\text{Ni}_2\text{Dy}_2]_\infty$.

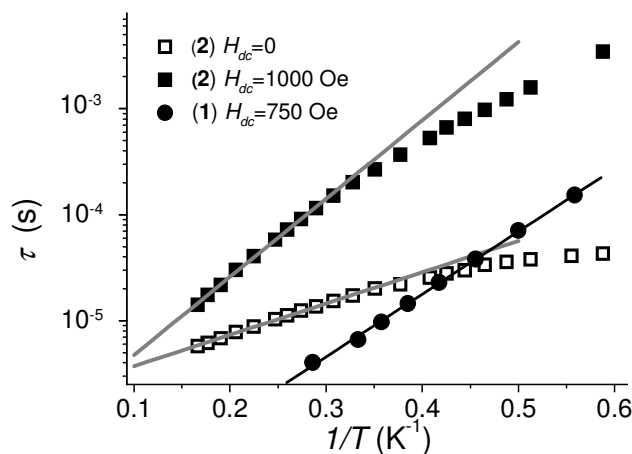


Figure 4.8: Temperature dependence of the relaxation time reported as an Arrhenius plot for Ni_2Dy_2 in 750 Oe static field and for $[\text{Ni}_2\text{Dy}_2]_\infty$ in both zero and 1000 Oe static field. The solid lines represent the linear fit as described in the text.

The mechanism of quantum tunneling can be reduced by applying a static field that removes the degeneracy of the levels on the opposite sides of the barrier.² For this reason the *ac* measurements were carried also in the presence of a static field, which was selected to be 750 Oe and 1000 Oe for Ni_2Dy_2 and $[\text{Ni}_2\text{Dy}_2]_\infty$, respectively, by scanning the field at $T = 2$ K and selecting the one that shift the peak in χ'' to the lowest frequency. χ'' exhibits now frequency maxima for both compounds (lower part of Figure 4.7), allowing an estimation of the Arrhenius parameters also for Ni_2Dy_2 , i. e. $\Delta = 13.6$ K and $\tau_0 = 7.7 \cdot 10^{-8}$ s, the last value being typical of SMM behaviour. The same analysis performed on $[\text{Ni}_2\text{Dy}_2]_\infty$ provides $\Delta = 17.4$ K and $\tau_0 = 8.0 \cdot 10^{-7}$ s. These parameters are extracted from the high temperature data to exclude from the fitting the curvature observed at low temperature but are anyhow only indicative of the energy gap between the ground and the first excited doublets. Interestingly a smaller Δ value is observed for Ni_2Dy_2 , in agreement with the trend observed for both $\chi_M T$ vs T and M vs H curves. The application of a static field, despite its strong effect, does not seem to be able to totally suppress tunnelling in $[\text{Ni}_2\text{Dy}_2]_\infty$, in contrast with what observed in Ni_2Dy_2 . This is not surprising, because in $[\text{Ni}_2\text{Dy}_2]_\infty$ tunneling has shown to be very efficient.

Another important parameter is the width of the distribution of the relaxation time, which has been investigated by plotting χ'' vs. χ' in the so called Argand plot. The deviations

from the ideal behaviour of a single relaxation time that results in a semicircle are taken into account by an empirical parameter α .²³ For Ni_2Dy_2 this parameter has been found to oscillate between 0.16 and 0.24, without any distinct trend (See Figure 4.9). Such values are rather common in SMM.^{2, 24}

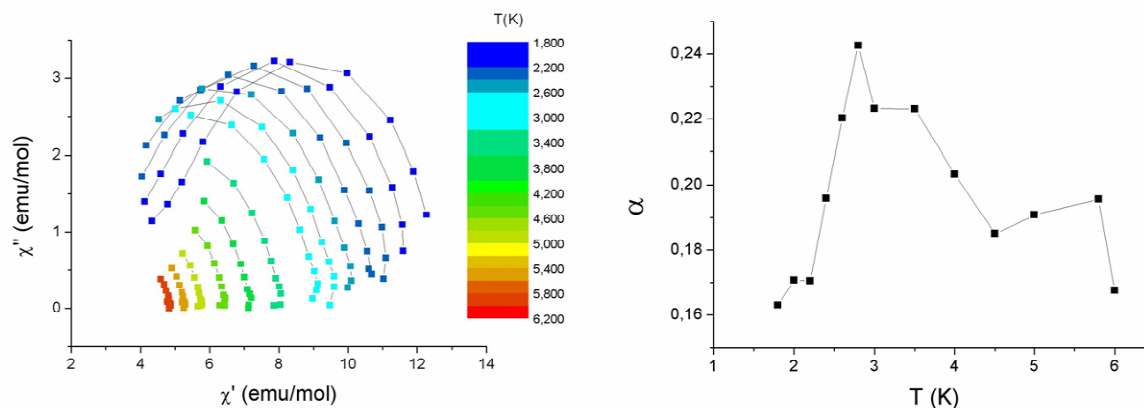


Figure 4.9: On the left the Argand plot of Ni_2Dy_2 at different temperatures (see colour scale) is reported. The extracted temperature dependence of the width of the distribution of the relaxation times (α parameter) is reported on the right.

In the case of $[\text{Ni}_2\text{Dy}_2]_\infty$ a constant increase from $\alpha=0.10$ to 0.30 on decreasing the temperature is observed (see Figure 4.10). This trend is usually encountered when at low temperature quantum tunneling becomes efficient,^{24c-e} and suggests that disorder or defects more strongly affect the admixing of the states, and thus the tunneling rate, than the height of the barrier.

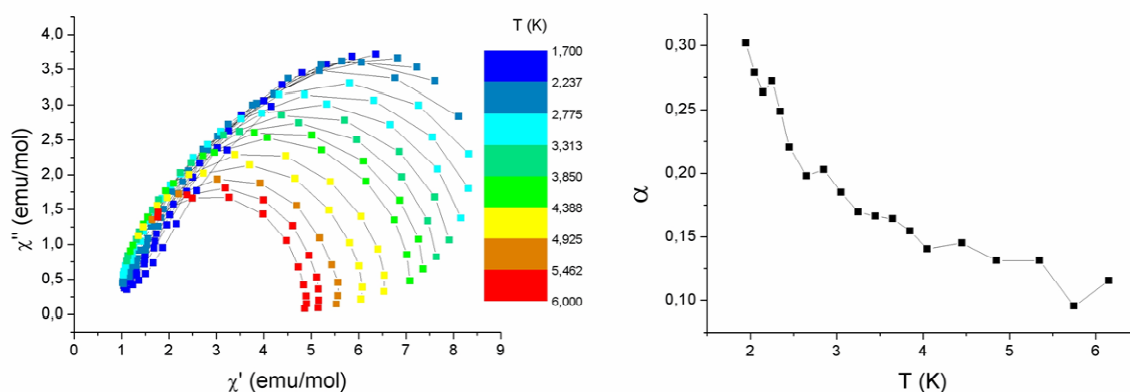


Figure 4.10: On the left the Argand plot of compound $[\text{Ni}_2\text{Dy}_2]_\infty$ at different temperatures (see colour scale) is reported. The extracted temperature dependence of the width of the distribution of the relaxation times (α parameter) is reported on the right.

4.4 Conclusion

The new systems described here illustrate that anisotropic high spin 3d-4f binuclear complexes can be organized in either high-nuclearity clusters or in coordination polymers, preserving their SMM behavior. Both compounds exhibit a strong tunnelling, despite the chain character of $[\text{Ni}_2\text{Dy}_2]_\infty$. This is not surprising as we have no evidence of a sizeable interaction mediated by the tfa^{2-} diamagnetic ligands. On the other hand, as shown in a previous paper,¹¹ a chain of SMMs can be transformed into a SCM by connecting the heterometallic nodes through paramagnetic spacers, *e.g.* metalloligands. The barrier observed for $[\text{Ni}_2\text{Dy}_2]_\infty$ is however higher than that of Ni_2Dy_2 , in agreement with the static properties that suggests a larger separation between the ground and the first excited doublet of the Dy^{III} Stark levels. Surprisingly tunnelling survives also in a static field for $[\text{Ni}_2\text{Dy}_2]_\infty$, while is more efficiently suppressed in Ni_2Dy_2 . We can tentatively attribute this observation to the weak Dy-Dy interaction present in Ni_2Dy_2 in analogy with what observed in a Dy-Radical tetramer.⁷ Further investigations performed for instance by diluting the Dy-Ni pairs in diamagnetic analogues containing yttrium are necessary to confirm this hypothesis.

Given the very low energy barriers observed for the two compounds, and the fact that the organization in 1-D structure of 3d-4f building blocks fails to provide any improvement in the blocking temperature, we have decided not to apply time consuming angle resolved magnetometry to these two compounds.

Bibliography

- (1) R. Sessoli, D. Gatteschi, A. Caneschi, M. A. Novak, *Nature*, **1993**, 365, 141.
- (2) (a) D. Gatteschi, R. Sessoli, J. Villain, *Molecular Nanomagnets*, Oxford University Press, **2006**;
(b) D. Gatteschi, R. Sessoli, *Angew. Chem., Int. Ed.*, **2003**, 42, 268.
- (3) (a) C. Coulon, H. Miyasaka, R. Clérac, *Struct. Bond.*, **2006**, 122, 163; (b) L. Bogani, A. Vindigni, R. Sessoli and D. Gatteschi, *J. Mater. Chem.*, **2008**, 18, 4750.
- (4) Recent reviews: (a) M. Andruh; J.-P. Costes, C. Diaz, S. Gao, *Inorg. Chem.*, **2009**, 48, 3342; (b) R. Sessoli, A. K. Powell, *Coord. Chem. Rev.*, **2009**, 253, 2328.
- (5) See, for example: (a) J. P. Costes, F. Dahan and W. Wernsdorfer, *Inorg. Chem.* **2006**, 45, 5; (b) C. Aronica, G. Pilet, G. Chastanet, W. Wernsdorfer, J. F. Jacquot, D. Luneau, *Angew., Chem. Int. Ed.* **2006**, 45, 4659; (c) J.-P. Costes, M. Auchel, F. Dahan, V. Peyron, S. Shova, W. Wernsdorfer, *Inorg. Chem.*, **2006**, 45, 1924; (d) T. Hamamatsu, K. Yabe, M. Towatari, S. Osa, N. Matsumoto, N. Re, A. Pochaba, J. Mrozinski, J.-L. Gallani, A. Barla, P. Imperia, C. Paulsen, J.-P. Kappler, *Inorg. Chem.*, **2007**, 46, 4458; (e) T. Kajiwara, M. Nakano, S. Takaishi, M. Yamashita, *Inorg. Chem.*, **2008**, 47, 8604; (f) G. Novitchi, W. Wernsdorfer, L. F. Chibotaru, J.-P. Costes, C. E. Anson, A. K. Powell, *Angew. Chem., Int. Ed.*, **2009**, 48, 1614.
- (6) (a) F. Pointillart, K. Bernot, R. Sessoli and D. Gatteschi, *Chem.-Eur. J.* **2007**, 13, 1602; (b) V. Chandrasekhar, B. M. Pandian, R. Boomishankar, A. Steiner, J. J. Vittal, A. Hourri, R. Clérac, *Inorg. Chem.*, **2008**, 47, 4918; (c) F. Mori, T. Ishida, T. Nogami, *Polyhedron*, **2005**, 24, 2588; (d) T. Yamaguchi, Y. Sunatsuki, H. Ishida, M. Kojima, H. Akashi, N. Re, N. Matsumoto, A. Pochaba, J. Mrozinski, *Inorg. Chem.*, **2008**, 47, 5736.
- (7) G. Poneti, K. Bernot, L. Bogani, A. Caneschi, R. Sessoli, W. Wernsdorfer, D. Gatteschi, *Chem. Commun.*, **2007**, 1807.
- (8) V. Chandrasekhar, B. M. Pandian, R. Azhakar, J. J. Vittal, R. Clérac, *Inorg. Chem.*, **2007**, 46, 5140.
- (9) (a) V. Mereacre, A. M. Ako, R. Clérac, W. Wernsdorfer, I. J. Hewitt, C. E. Anson, A. K. Powell, *Chem.-Eur. J.* **2008**, 14, 3577; (b) C. M. Zaleski, E. C. Depperman, J. W. Kampf, M. L. Kirk, V. L. Pecoraro, *Angew. Chem. Int. Ed.*, **2004**, 43, 3912; (c) T. C. Stamatou, S. J. Teat, W. Wernsdorfer, G. Christou, *Angew. Chem., Int. Ed.*, **2009**, 48, 521.
- (10) (a) V. Mereacre, A. M. Ako, R. Clerac, W. Wernsdorfer, I. J. Hewitt, C. E. Anson, A. K. Powell, *Chem.-Eur. J.*, **2008**, 14, 3577; (b) C. M. Zaleski, E. C. Depperman, J.W. Kampf, M. L. Kirk, V. L. Pecoraro, *Angew. Chem. Int. Ed.* **2004**, 43, 3912.
- (11) D. Visinescu, A. M. Madalan, M. Andruh, C. Duhayon, J.-P. Sutter, L. Ungur, W. Van den Heuvel, L. F. Chibotaru, *Chem.-Eur. J.*, **2009**, 15, 11808.
- (12) R. Inglis, L. F. Jones, K. Mason, A. Collins, S. A. Moggach, S. Parson, S. P. Perlepes, W. Wernsdorfer, E. K. Brechin, *Chem.-Eur. J.*, **2008**, 14, 9117.
- (13) W. Wernsdorfer, N. Aliaga-Alcalde, D. N. Hendrickson, G. Christou, *Nature*, **2002**, 416, 406.

- (14) (a) L. Lecren, O. Roubeau, Y.-G. Li, X. F. Le Goff, H. Miyasaka, F. Richard, W. Wernsdorfer, C. Coulon, R. Clérac, *Dalton Trans.*, **2008**, 755; (b) O. Roubeau, R. Clérac, *Eur. J. Inorg. Chem.*, **2008**, 4315; (c) L. Lecren, W. Wernsdorfer, Y.-G. Li, A. Vindigni, H. Miyasaka, R. Clérac, *J. Am. Chem. Soc.*, **2007**, 129, 5045.
- (15) K. Bernot, J. Luzon, A. Caneschi, D. Gatteschi, R. Sessoli, L. Bogani, A. Vindigni, A. Rettori, and M. G. Pini, *Phys. Rev. B* **2009**, 79, 134419.
- (16) (a) M. Andruh, *Pure Appl. Chem.*, **2005**, 77, 1685. (b) M. Andruh, *Chem. Commun.*, **2007**, 2565; (c) R. Gheorghe, P. Cucos, M. Andruh, J. P. Costes, B. Donnadieu, S. Shova, *Chem.-Eur. J.*, **2006**, 12, 187; (d) M. Andruh, D. G. Branzea, R. Gheorghe, A. M. Madalan, *CrystEngComm.*, **2009**, 11, 2571.
- (17) (a) T. Shiga, N. Ito, A. Hidaka, H. Ohkawa, S. Kitagawa, M. Ohba, *Inorg. Chem.*, **2007**, 46, 3492; (b) C. A. Barta, S. R. Bayly, P. W. Read, B. O. Patrick, R. C. Thompson, C. Orvig, *Inorg. Chem.*, **2008**, 47, 2280; (c) S. Dhers, S. Sahoo, J.-P. Costes, C. Duhayon, S. Ramasesha, J.-P. Costes, *CrystEngComm.*, **2009**, 11, 2078; (d) J.-P. Sutter, S. Dhers, R. Rajamani, S. Ramasesha, J.-P. Costes, C. Duhayon, L. Vendier, *Inorg. Chem.*, **2009**, 48, 5820; (e) J.-P. Costes, T. Yamaguchi, M. Kojima, L. Vendier, *Inorg. Chem.*, **2009**, 48, 5555.; (f) J.-P. Costes, F. Dahan, A. Dupuis, J.-P. Laurent, *Inorg. Chem.*, **1997**, 36, 4284.
- (18) (a) R. D. L. Carlin, *Magnetochemistry*, Springer-Verlag, Berlin, **1986**; (b) W. P. Wolf, *Braz. J. Phys.*, **2000**, 30, 794.
- (19) (a) L. F. Chibotaru, L. Ungur, A. Soncini, *Angew. Chem., Int. Ed.*, **2008**, 47, 4126.; (b) K. Bernot, J. Luzon, L. Bogani, M. Etienne, C. Sangregorio, M. Shanmugam, A. Caneschi, R. Sessoli, D. Gatteschi, *J. Am. Chem. Soc.*, **2009**, 131, 5573. (c) I. J. Hewitt, Y. Lan, C. E. Anson, J. Luzon, R. Sessoli, A. K. Powell, *Chem. Commun.*, **2009**, 6765.
- (20) See, for example: (a) L. Canadillas-Delgado, J. Pasán, O. Fabelo, M. Hernández-Molina, F. Lloret, M. Julve, C. Ruiz-Pérez, *Inorg. Chem.*, **2006**, 45, 10585, and references therein.
- (21) (a) L. F. Chibotaru, L. Ungur, A. Soncini, *Angew. Chem., Int. Ed.*, **2008**, 47, 4126. (b) J. Luzon, K. Bernot, I. J. Hewitt, C. E. Anson, A. K. Powell, R. Sessoli, *Phys. Rev. Lett.*, **2008**, 100, 247205. (c) K. Bernot, J. Luzon, R. Sessoli, A. Vindigni, J. Thion, S. Richeter, D. Leclercq, J. Larionova, A. Van Der Lee, *J. Am. Chem. Soc.*, **2008**, 130, 1619.
- (22) (a) A. Abragam, B. Bleaney, *Electron Paramagnetic Resonance of Transition Ions*, Dover, New York, **1986**. (b) N. Ishikawa, *Polyhedron*, **2007**, 26, 2147.
- (23) K. S. Cole, Cole R. H., *J. Chem. Phys.*, **1941**, 9, 341.
- (24) (a) M.-H. Zeng, M.-X. Yao, H. Liang, W.-X. Zhang, X.-M. Chen, *Angew. Chem. Int. Ed.* **2007**, 46, 1832.; b) D. Wu, D. Guo, Y. Song, W. Huang, C.-Y. Duan, Q.-J. Meng, O. Sato, *Inorg. Chem.* **2009**, 48, 854. c) A. Cornia, L. Gregoli, C. Danieli, A. Caneschi, R. Sessoli, L. Sorace, A. L. Barra, W. Wernsdorfer, *Inorg. Chim. Acta*, **2008**, 361, 3481. d) L. Gregoli, C. Danieli, A. L. Barra, P. Neugebauer, G. Pellegrino, G. Poneti, R. Sessoli, A. Cornia, *Chem.-Eur. J.*, **2009**, 15, 6456. e) T. Kajiwara, K. Takahashi, T. Hiraizumi, S. Takaishi, M. Yamashita, *Polyherdron*, **2009**, 28, 1860.

Chapter 5

Single molecule magnet behaviour in robust Dysprosium-biradical complexes

<u>5.1 INTRODUCTION</u>	77
<u>5.2 SYNTHESIS AND CRYSTAL STRUCTURE ANALYSIS</u>	77
<u>5.3 SOLUBILITY STUDY</u>	81
<u>5.4 MAGNETIC MEASUREMENTS</u>	83
<u>5.5 CONCLUSION</u>	88

5.1 Introduction

In the previous chapter we have seen that the design of complex architectures based on 4f metal ions does not necessarily leads to the desired results. The major drawback in the use of lanthanide ions is in fact represented by the weak exchange interactions that they experience in the three-positive oxidation state. The use of mono-atomic linkers, like the alkoxides discussed in chapters 2 and 3 is a solution. In these respects the combination of lanthanide with organic radicals like Nitronyl-nitroxides^{1,2} remains a valid alternative for the synthesis of 2p-4f Single Molecule³ and Single Chain Magnets⁴ as already discussed in chapter 1.

In this last chapter we will go back to 2p-4f systems previously discussed but looking at them from a different perspective. In fact, an emerging trend in molecular magnetism is their organization on surfaces.⁵ To allow a reliable grafting of molecules on surfaces, through dip-coating for example, the objects have to be soluble. However the polymeric nature of the lanthanide-radical one-dimensional chains, makes them highly insoluble. The corresponding monomers are not suitable either as the weak Ln-O_{rad} bonds do not provide the necessary stability in solution.

In order to overcome these problems we decided to use a bidentate ligand⁶ named NITmbis(1,3-bis-(1'-oxyl-3'-oxido-4',4',5',5'-tetramethyl-4,5-hydro-1*H*-imidazol-2-yl)benzene)⁷ where an unpaired electron is delocalized on each imidazole ring. These two electrons are expected to be ferromagnetically coupled. Moreover the N-O distances observed in the free radical and in its copper complex⁸ are suitable to chelate big cations such as lanthanides. Indeed, reaction of the radical with Dy(hfac)₃·2H₂O⁹ yields the [Dy(hfac)₃(NITmbis)]₂ complex, noted **DyNITmbis** hereafter, where each Dy^{III} cation is bound to one bidentate biradical.

5.2 Synthesis and Crystal Structure analysis

The radical NITmbis = (1,3-bis-(1'-oxyl-3'-oxido-4',4',5',5'-tetramethyl-4,5-hydro-1*H*-imidazol-2-yl)benzene) was prepared following the reported procedure.⁷

To obtain the complex on one hand 0.05 mmol (19.4 mg) of NITmbis were dissolved in 5 ml of CHCl₃. On the other hand, 0.05 mmol (41 mg) of Dy(hfac)₃·2H₂O (hfac⁻ = 1,1,1,5,5,5-hexafluoroacetylacetonate)¹⁰ were dissolved in 5 ml of CHCl₃. Both solutions were poured simultaneously in a 15 ml hot heptane solution. After some days of slow evaporation, deep-blue

prismatic crystals of $[\text{Dy}(\text{hfac})_3(\text{NITmbis})]_2$ (noted **DyNITmbis**) appeared and found suitable for X-Ray diffraction.

Crystals were selected and then frozen at $T = 150 \text{ K}$ under a stream of dry N_2 on a APEXII Bruker-AXS diffractometer for data collection ($\text{Mo-K}\alpha$ radiation, $\lambda = 0.71073 \text{ \AA}$). The compound was found to crystallize in the triclinic P-1 ($N^{\circ}2$) space group with $a = 12.1870(4) \text{ \AA}$, $b = 13.1630(4) \text{ \AA}$, $c = 31.5810(11) \text{ \AA}$, $\alpha = 90.0010(14)^\circ$, $\beta = 79.8310(15)^\circ$, $\gamma = 76.7410(14)^\circ$, $V = 4849(3) \text{ \AA}^3$, $Z = 4$.¹¹ Data reduction was accomplished using SADABS program. Absorption correction were applied. Structure was solved by direct methods (SIR97)¹² and refined (SHELXL 97)¹³ by full-matrix least-squares methods as implemented in the WinGX software package.¹⁴

The asymmetric unit is composed of two crystallographically independent $[\text{Dy}(\text{hfac})_3(\text{NITmbis})]$ moieties (Figure 5.1), and two chloroform molecules (Figure 5.2). Each Dy^{III} ions is surrounded by eight oxygen atoms that belong to three hfac^- ligands and one NITmbis biradical ligand. The average $\text{Dy-O}_{\text{NITmbis}}$ distances are slightly longer ($2.385(4) \text{ \AA}$) than the average $\text{Dy-O}_{\text{hfac}}$ distances ($2.353(4) \text{ \AA}$) (Table 5.1). The arrangement of these ligands leads to a 4,4-bicapped trigonal prism as coordination polyhedron of the lanthanide ions (C_{2v} symmetry). A regular bicapped trigonal prism is characterized by the four ideal dihedral angles taking the following values: 0, 21.8, 48.2 and 48.2° .¹⁵

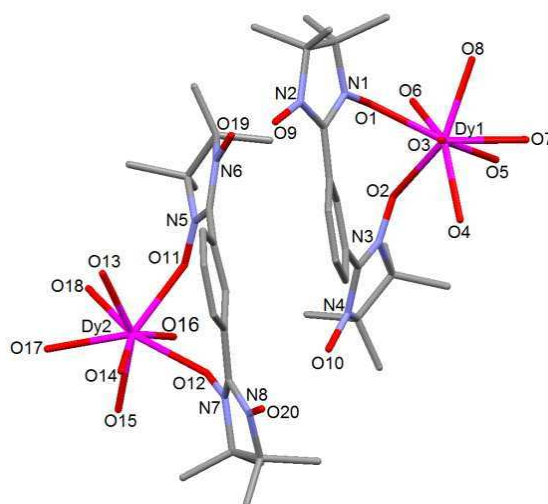


Figure 5.1: Simplified view of the asymmetric unit of DyNITmbis.

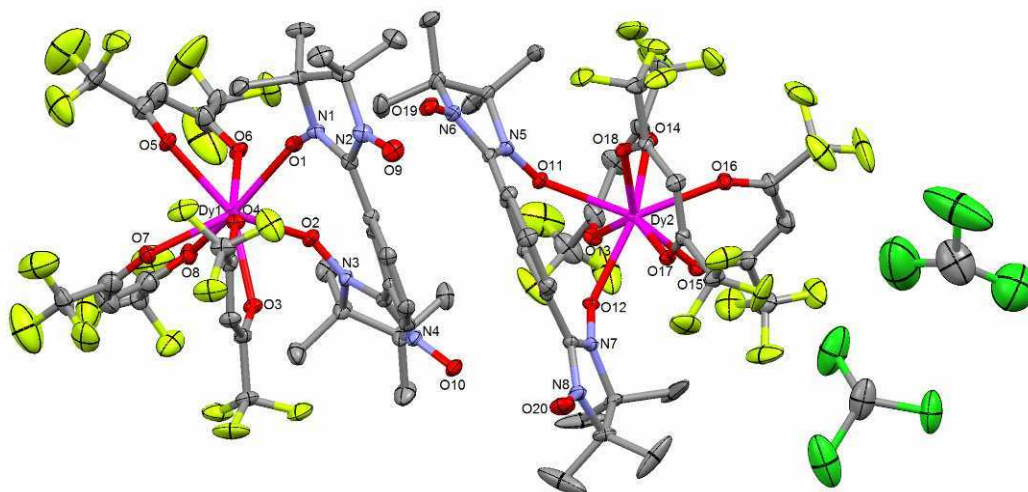


Figure 5.2: ORTEP view of the asymmetric unit of **DyNITmbis** with thermal ellipsoids at 30% probability. Hydrogen atoms are omitted for clarity.

	DyNITmbis
Dy(1)-O(1)	2.392(4)
Dy(1)-O(2)	2.380(4)
Dy(1)-O(3)	2.332(4)
Dy(1)-O(4)	2.377(4)
Dy(1)-O(5)	2.336(4)
Dy(1)-O(6)	2.384(4)
Dy(1)-O(7)	2.373(4)
Dy(1)-O(8)	2.356(4)
Dy(2)-O(11)	2.418(4)
Dy(2)-O(12)	2.350(4)
Dy(2)-O(13)	2.359(4)
Dy(2)-O(14)	2.330(4)
Dy(2)-O(15)	2.324(4)
Dy(2)-O(16)	2.366(4)
Dy(2)-O(17)	2.369(4)
Dy(2)-O(18)	2.327(4)

Table 5.1: Selected bond lengths for **DyNITmbis**

In the case of **DyNITmbis**, these values are equal to 2.46(17) [1.49(15)], 22.33(16) [22.33(15)], 41.51(16) [41.51(16)] and 41.51(16) [48.97(15)]° for Dy1 and Dy2 respectively. In a previous work, the NITmbis radical was reacted with the Cu(hfac)₂ precursor and crystallize with all the Cu(II) centers linked to the radical in a monodentate mode.⁸ When using Dy(hfac)₃, which is bigger than the 3d precursor, the two imidazole rings rotate and favour the bidentate chelating mode. Consequently the biradicals are coordinated by two of their four N-O groups. The rotation mechanism is then driven by the bond lengths difference between Cu-O (1.91-1.97 Å) and Dy-O (2.32-2.42 Å). Here the two five-membered heterocyclic rings and the benzene ring show average twist angles of 26.2(2)° compared to 33° for the uncoordinated free

biradical.⁸ A pseudo dinuclear compound of formula $[\text{Dy}(\text{hfac})_3(\text{NITmbis})]_2$ is formed due to π - π interactions between the two benzene groups of the two biradicals (Figure 5.1 and 5.3). The distances between the N-O systems are in the 3.088(5)-4.391(6) Å range (Figure 5.4). Hence the two sub-units are closely stacked and many magnetic interaction pathways between them are possible. This justifies why the pseudo dinuclear moiety is considered for the magnetic analysis.

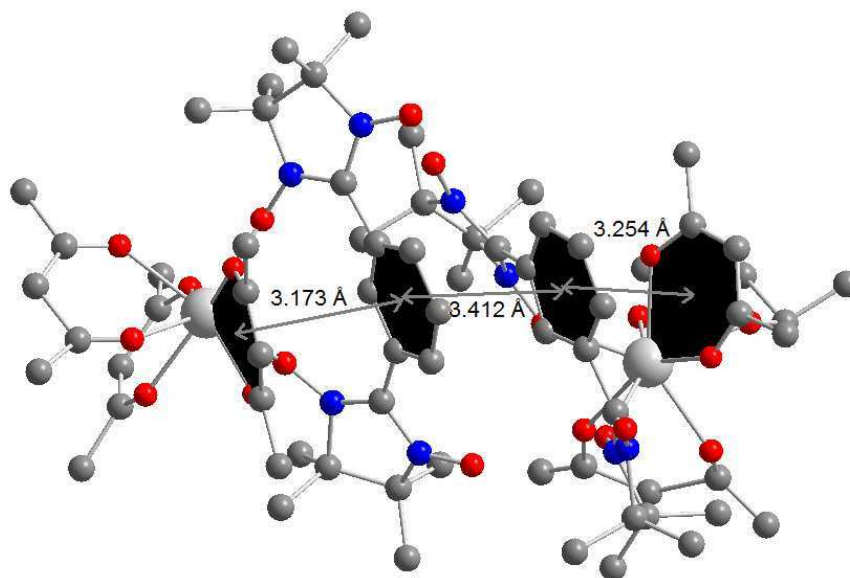


Figure 5.3: Schematic view of the packing of two *DyNITmbis* units highlighting the π - π interactions between the aromatic systems of the *hfac*⁻ ligands and phenyl groups. The distances which are given correspond to the shortest distances between two atoms.

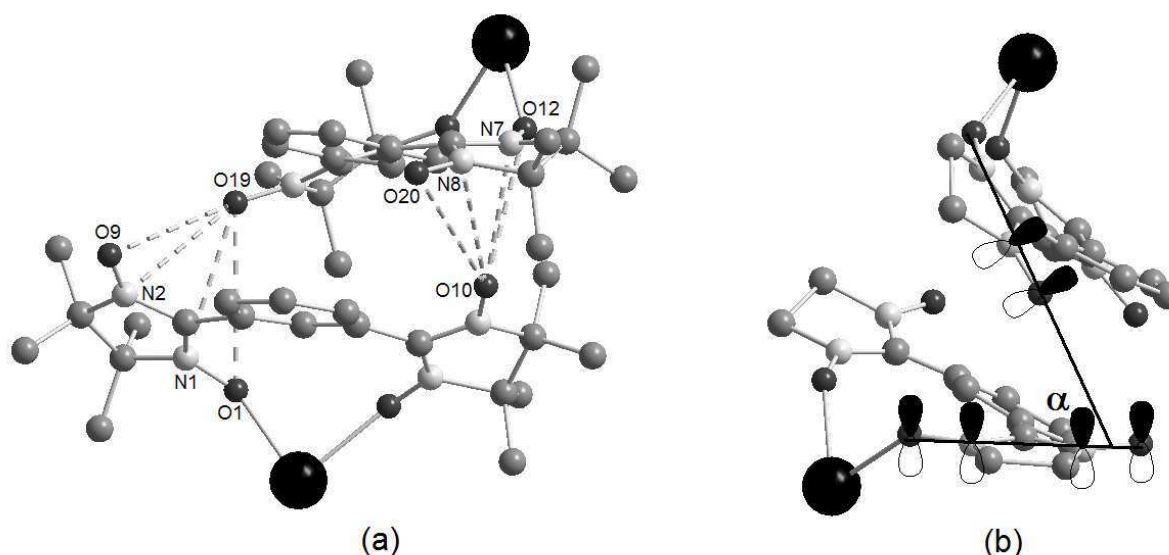


Figure 5.4: (a) Schematic view of the interactions between the free N_i -O19 and N_i -O10 groups with the O9-N2-C-N1-O1 and O20-N8-C-N7-O12 systems. The O19-O9, O19-N2, O19-N1, O19-O1, O10-O20, O10-N8, O10-N7 and O10-O12 distances are equal to 4.391(6), 3.648(6), 3.088(5), 3.365(5), 4.706(7), 3.289(6), 3.374(5) and 3.897(5) Å respectively. (b) Highlight of the α angle (79.4°) between the two planes containing the π radical orbitals.

5.3 Solubility study

UV-visible absorption spectroscopy has been performed on NITmbis and DyNITmbis in solid state, using the KBr disk method, and in solutions of both species in CH₂Cl₂ ($c = 5.10^{-5}$ mol L⁻¹) on a varian Cary 5000 UV-visible-NIR spectrometer equipped with an integration sphere.

As expected, a blue shift of the charge transfer band is visible when comparing free and coordinated radical (Figure 5.5 and 5.6) in solid state or solution. This is due to the electron-withdrawing effect of the coordinated Dy(hfac)₃ fragment. The blue shift is visible for several days in solution.

As radicals are characterized by a narrow and intense EPR signal the EPR solution spectra of DyNITmbis have been recorded on a Bruker Elexsys E500 spectrometer.

The DyNITmbis spectra compared with those of an equimolar NITmbis solution evidences in the first case a much weaker signal. This suggests that only a very small amount of free radical is released into the solution after two days (Figure 5.7). These two types of investigations evidence that DyNITmbis is particularly stable in dichloromethane solution.

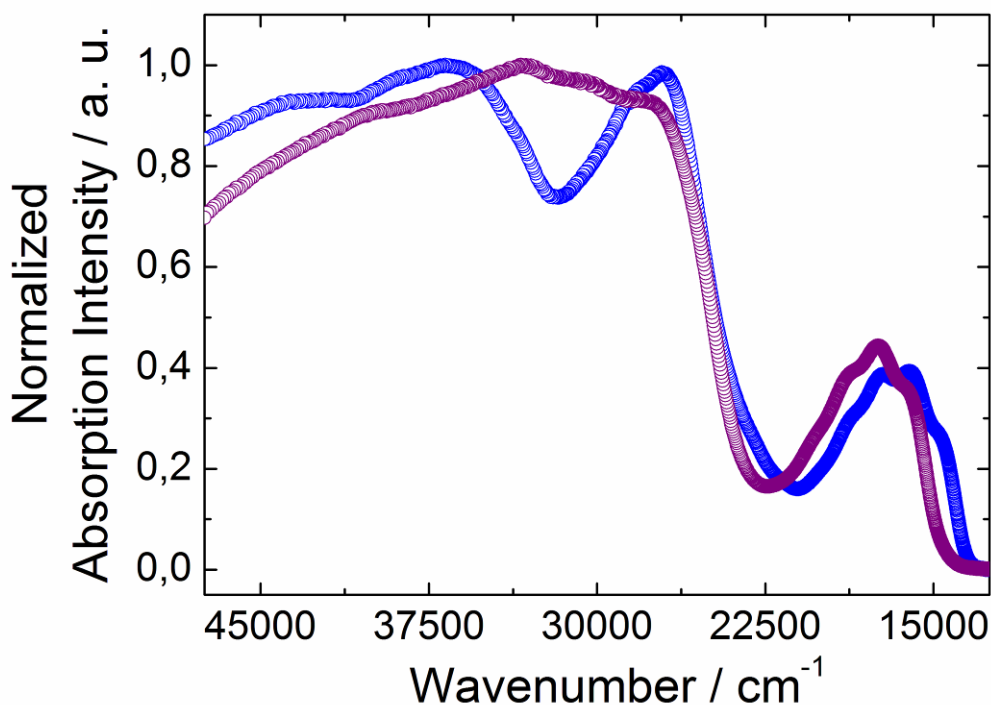


Figure 5.5: Experimental solid-state UV-visible absorption spectra of NITmbis (blue open circles) and DyNITmbis (purple open circles).

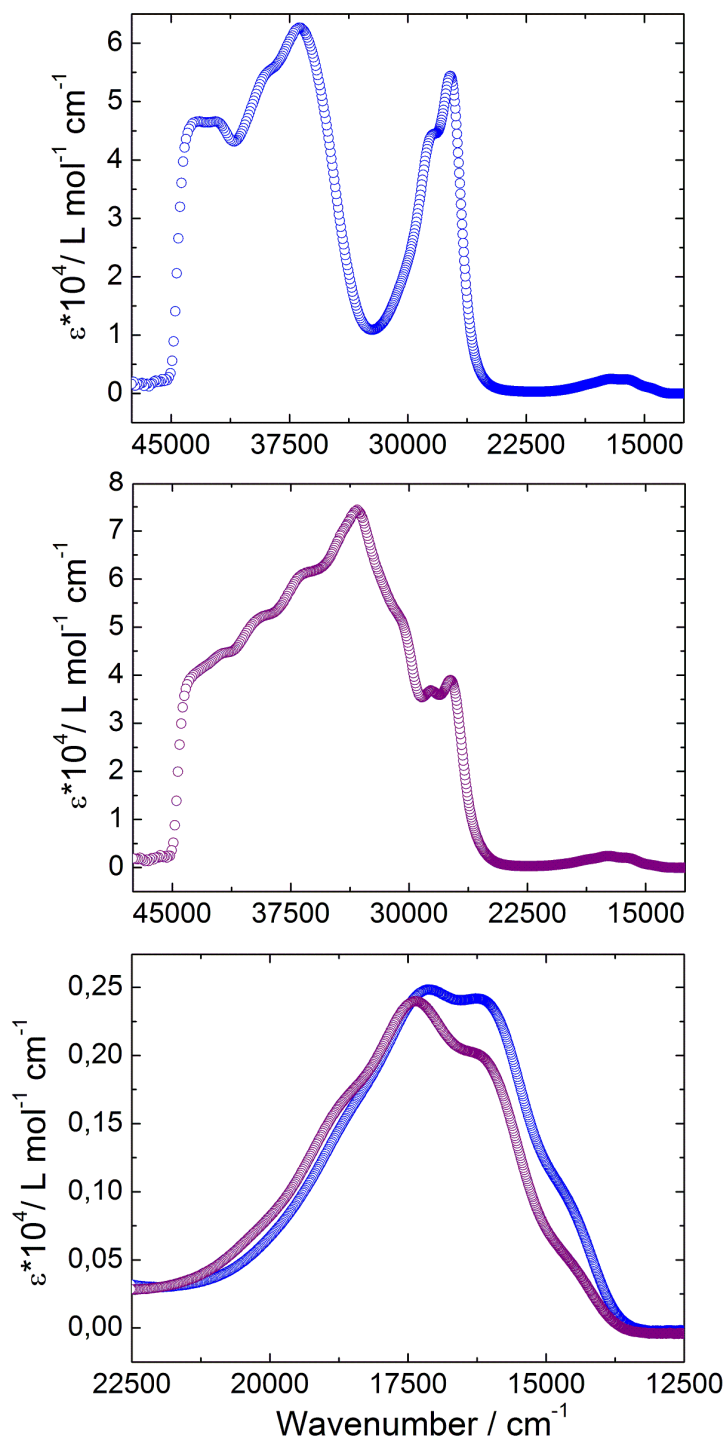


Figure 5.6: Experimental UV-visible absorption spectra of NITmbis (top) and DyNITmbis (center) in CH_2Cl_2 ($c = 5 \cdot 10^{-5} \text{ mol} \cdot \text{L}^{-1}$) at room temperature. Zoom of the charge transfer region for both species highlighting the change of shape of the curves and the blue shift (bottom).

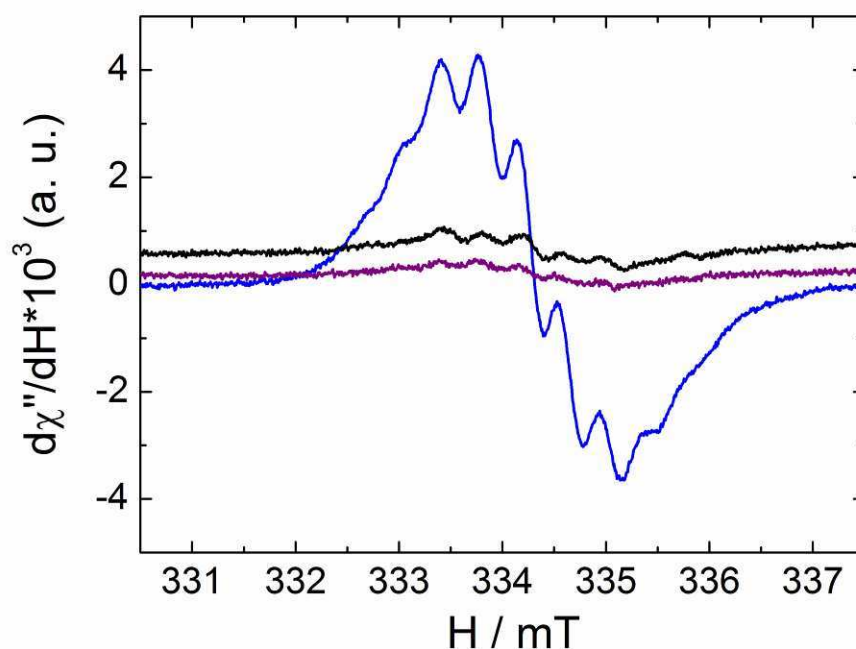


Figure 5.7: X-Band (9.364 GHz) EPR spectra of NITmbis (blue line), DyNITmbis (purple line) and two days aged DyNITmbis CH_2Cl_2 solution (black line). All solutions are equimolar.

5.4 Magnetic Measurements

5.4.1 dc Measurements

The *dc* magnetic measurements were carried out on slightly crushed single crystals of DyNITmbis embedded in grease to hamper orientation of the microcrystals by magnetic torque. The room temperature value of the $\chi_M T$ product is $30.00 \text{ cm}^3 \text{ K mol}^{-1}$ (Figure 5.8), slightly higher than expected for four radicals ($S = \frac{1}{2}$ and $g = 2.00$) and two ${}^6\text{H}_{15/2}$ states of two magnetically independent Dy^{III} ($29.84 \text{ cm}^3 \text{ K mol}^{-1}$) ions.¹ The curve decreases slowly to reach a minimum at 30 K with $\chi_M T$ of $27.80 \text{ cm}^3 \text{ K mol}^{-1}$. Below this temperature, the $\chi_M T$ products increase quickly to reach $34.38 \text{ cm}^3 \text{ K mol}^{-1}$ at 3 K. The crystal field effect of the anisotropic Dy^{III} ions has an influence on the thermal variation of $\chi_M T$ but for low temperatures only the ground states of the lanthanides are populated. The marked increase of $\chi_M T$ at low temperature suggests that ferromagnetic interactions dominate the magnetic behaviour. Previous works on substituted xylylene,¹⁶ phenylene bisoxamates¹⁷ and radicals¹⁸ has shown that the intraligand interaction is ferromagnetic since the coordinating moieties are coordinated in *meta* mode on the phenyl group. Moreover the packing of the complex in pairs suggests that intermolecular magnetic interactions through the non-coordinating NO groups are possible.¹⁹ The observed low

temperature increase in the $\chi_M T$ product is too large to be attributed only to ferromagnetic interactions between the radicals it implies a ferromagnetic interaction of the Dy^{III} ions with the coordinated radicals and eventually ferromagnetic intermolecular interactions as already observed in lanthanide-NIT radical systems.^{1,3a}

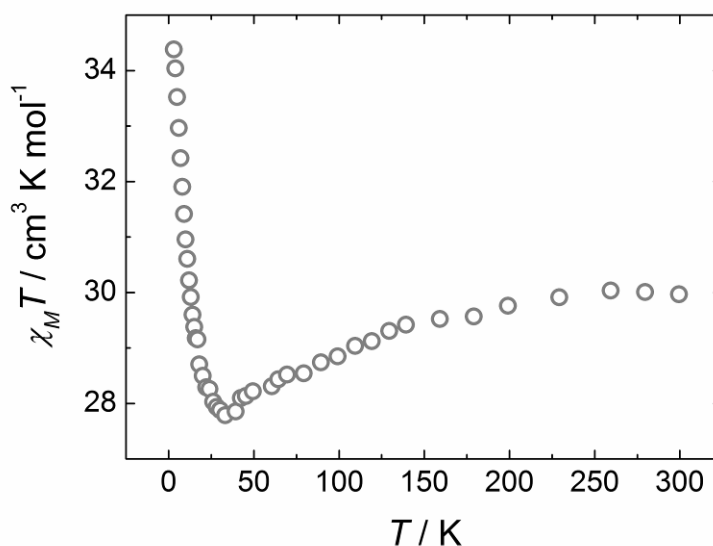


Figure 5.8: Temperature dependence of the $\chi_M T$ product from dc magnetic measurements for **DyNITmbis** (open gray circles).

5.4.2 ac Measurements

Studies on similar compounds have shown that some of them can present slow relaxation of the magnetization and pure quantum tunnelling of the magnetization at relatively high temperature.^{3a} That is why the dynamic magnetic behaviour of **DyNITmbis** has been investigated in a wide range of temperature: between 3.6K and 1.55K with a standard ^4He -cooled cryostat and between 1.72K and 0.52K with a ^3He -cooled one. In-phase (χ_M') and out-of-phase (χ_M'') contributions to the susceptibility were first measured in the absence of dc field. The two sets of measurements are plotted against the temperature (Figure 5.9) or frequency (Figure 5.10).

DyNITmbis shows clear frequency dependence of the susceptibility below 2.5 K typical of Single Molecule Magnet behaviour. Both components of the ac susceptibility go through a frequency dependent maximum on lowering the temperature but start to increase again below 0.8 K. This behaviour is typical of the onset of pure quantum tunnelling regime. We have extracted the relaxation time, τ , from the frequency dependence of χ_M'' (Figure 5.10) assuming $\tau=(2\pi\nu)^{-1}$ at the frequency of the maximum.

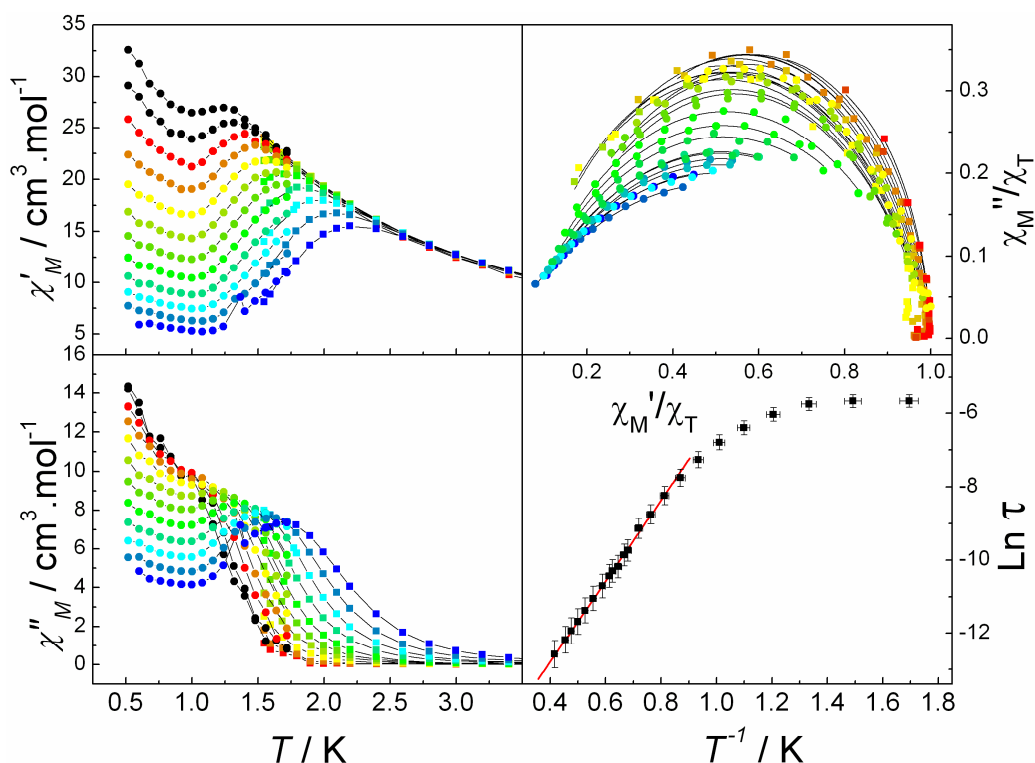


Figure 5.9: Temperature dependence of χ'_M (left top) and χ''_M (left bottom) measured in zero static field. Argand diagram in the temperature range 0.52-3.60 K (right top). The lines represent the best-fit calculated values for each temperature with an extended Debye model. Arrhenius plot with best fit of the high temperature region (right bottom).

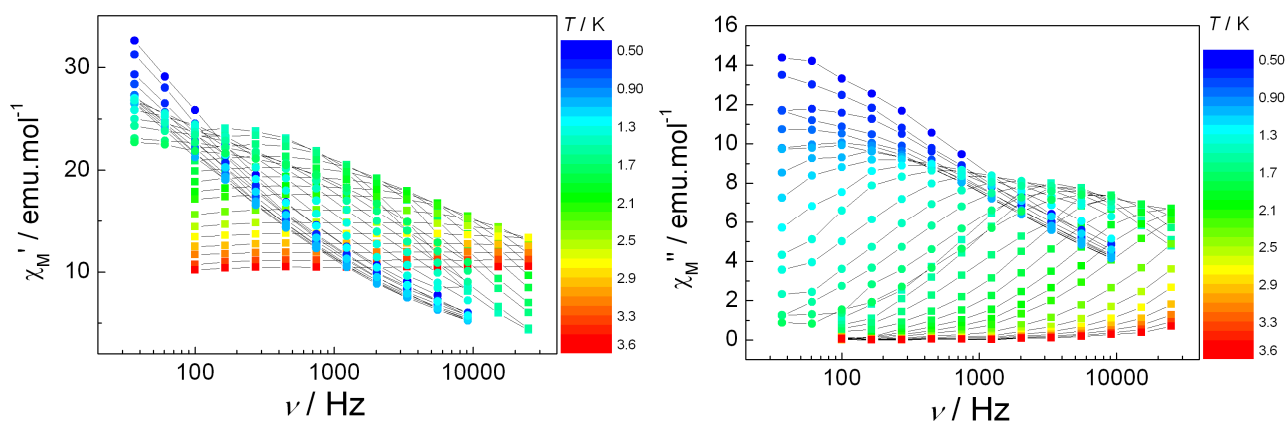


Figure 5.10: Frequency dependence of the in-phase and out-of-phase susceptibility measured in the 0.5-3.7 K temperature range on 15 logarithmic-spaced frequencies. From 0.5K to 1.72 K a ^3He -cooled cryostat was used, 36-9161Hz (circles). From 1.55K to 3.6K a ^4He -cooled cryostat was used, 100-25000Hz (squares).

The results, reported in Figure 5.9, show down to 1.2 K a thermally activated regime described by the Arrhenius law,¹⁹ $\tau = \tau_0 \exp(\Delta/k_B T)$, with $\tau_0 = 2.3 \pm 0.3 \cdot 10^{-8}$ s and an activation barrier of 11.6 ± 0.3 K, $R = 0.99954$. Below 1.2 K a progressive saturation of the relaxation time is observed that becomes practically temperature independent below 0.80 K and equal to 4.0

ms. A tunneling rate of ca. 40 Hz is therefore estimated for this system. To confirm the SMM behaviour the Argand plots have been derived and shown (Figure 5.9). The curves were normalized by the isothermal susceptibility (χ_T) to facilitate comparison. These plots allow characterizing the distribution of the relaxation times in the molecule using an extended Debye model for fitting.²⁰ Values of χ_T and α are shown in Table 5.2. They confirm that the frequency dependence above 1.16 K corresponds to a SMM behaviour since α is in the range 0.2 – 0.3. In the tunnelling regime α increases to ca. 0.5. Such behaviour has been already observed²¹ and suggests that the tunnelling mechanism is more sensitive to local strain or disorder than the thermally activated one.

To evidence if tunnelling also affects the magnetization dynamics at higher temperature the ac susceptibility is measured in 1 kOe external field (Figure 5.11) to remove the degeneracy of the levels on opposite sides of the anisotropy barrier. The height of the signal is reduced by 10% in $\chi_M T$ but a similar frequency dependence is observed. Arrhenius plot analysis gives $\tau_0 = 3.7 \pm 0.4 \cdot 10^{-8}$ s and $\Delta = 10.7 \pm 1$ K, $R = 0.99914$ (Figure 5.12), that are within error coincident with those extracted from zero field measurements. Thus, the quantum tunneling in zero field is negligible.

T(K)	χ_T	α	R^2	T(K)	χ_T	α	R^2
0.52	72.73	0.50	0.99943	1.32	29.71	0.27	0.97887
0.6	73.76	0.54	0.99947	1.40	28.08	0.26	0.99369
0.68	54.41	0.48	0.99911	1.48	25.96	0.22	0.99043
0.76	57.50	0.51	0.99842	1.50	25.14	0.24	0.97046
0.84	51.13	0.48	0.99960	1.56	24.75	0.20	0.99850
0.92	44.63	0.48	0.99947	1.60	24.67	0.25	0.9617
1	44.35	0.45	0.99936	1.64	23.25	0.16	0.99653
1.08	39.00	0.40	0.99785	1.70	23.50	0.26	0.95233
1.16	35.72	0.37	0.99640	1.72	22.72	0.23	0.99501
1.24	32.43	0.34	0.98960				

Table 5.2: Main fitting parameters for the Argand plot.

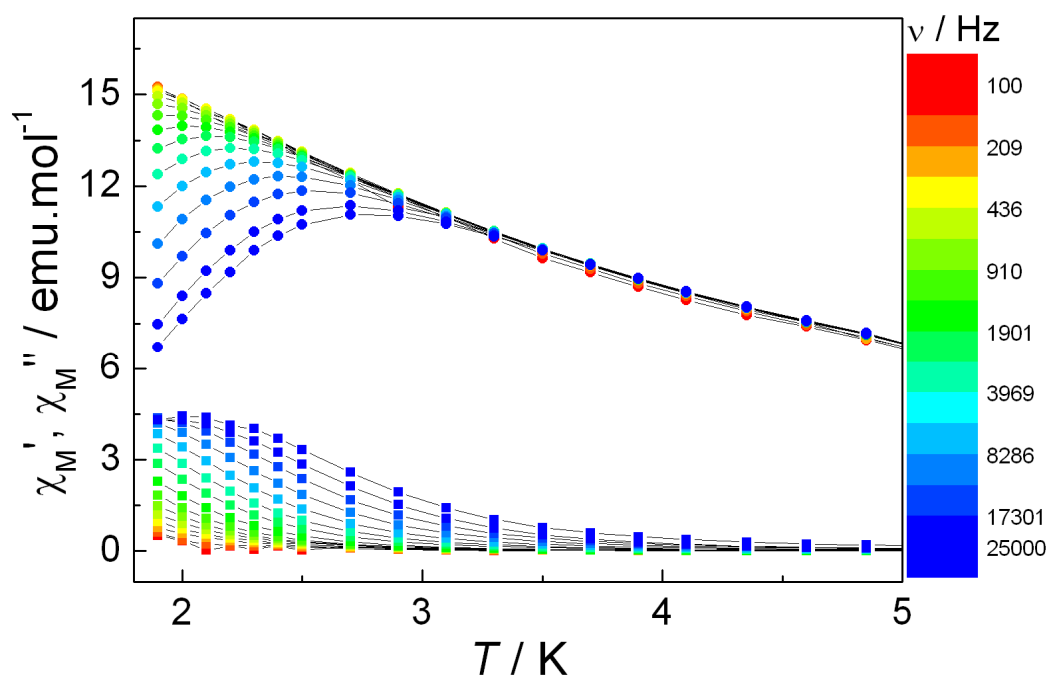


Figure 5.11: Temperature dependence of the in-phase (circles) and out-of-phase (squares) susceptibility measured in the 1.5-5K temperature range with 15 logarithmic-spaced frequencies (100-25000Hz) in a 1 kOe external field.

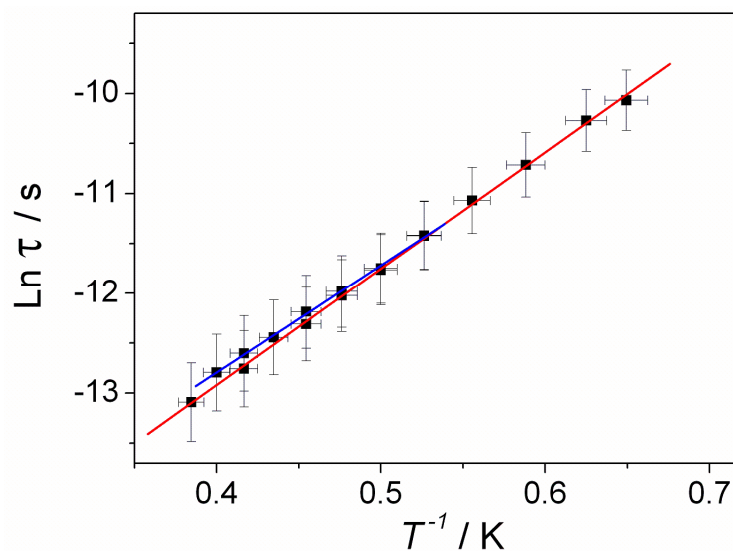


Figure 5.12: Temperature dependence of the relaxation time (logarithmic) as extracted from the out-of-phase susceptibility measured without (square, red line as best fit) or with a 0.1 kOe external field (circles, blue line as best fit). Data are fitted with an Arrhenius law, parameters can be found in the text.

The magnetization dynamics of **DyNITmbis** shows a rather sharp transition from a thermally activated regime with no evidence of zero field quantum tunnelling, to a pure quantum tunnelling regime. This observation is quite uncommon.²² In fact, many examples of pure, or heteronuclear (3d-4f, 3d-5f) Dy-based complexes²³ display slow relaxation of the magnetization only if zero-field fast-tunneling is suppressed by a small external field,²⁴ while in

other cases a strong slowing down of the relaxation is observed also in the thermally activated regime. For instance the application of the external field drastically modified the dynamic properties of the $[\text{Dy}(\text{hfac})_3(\text{NITpPy})]$ complex,³ suggesting that the additional interactions between the two unpaired electrons of the biradical could have some role in damping the quantum tunneling of the magnetization. Indeed the quantum regime is here attained at a temperature that is reduced by a factor larger than two.

5.5 Conclusion

In conclusion, we designed a Dy-nitronyl-nitroxide biradical complex soluble and stable in solution thanks to the chelating coordination mode of the radical. Crystal packing shows that two complexes are paired through π - π interactions. The combination of intra- and intermolecular interaction could be responsible of the sharp transition from a thermally activated to a quantum tunnelling regime. Theoretical investigations on the **DyNITmbis** are underway in order to understand the behaviour of this SMM together with doping in isotropic and diamagnetic analogues in order to better characterize the role of intermolecular magnetic interactions.

Finally, the stability in solution of this Dy-NIT adduct makes it a good candidate to deposit it onto surface in films or monolayers. Nitronyl- nitroxides radicals can be functionalized with sulfur-containing groups,²⁵ and have been shown to retain their paramagnetic nature also when chemically grafted to noble metals.²⁶ Indeed, the $\text{CH}_2\text{-S-CH}_3$ substitution on the aromatic ring of the radical is under progress in order to make these complexes anchorable on gold.

Bibliography

- (1) C. Benelli and D. Gatteschi, *Chem. Rev.* **2002**, 102, 2369.
- (2) A. Caneschi, D. Gatteschi, R. Sessoli and P. Rey, *Acc. Chem. Res.*, **1989**, 22, 392.
- (3) (a) G. Poneti, K. Bernot, L. Bogani, A. Caneschi, R. Sessoli, W. Wernsdorfer and D. Gatteschi, *Chem. Commun.* **2007**, 1807. (b) D. Yoshihara, S. Karasawa and N. Koga, *J. Am. Chem. Soc.* **2008**, 130, 10460 and references therein.
- (4) (a) A. Caneschi, D. Gatteschi, N. Lalioti, C. Sangregorio, R. Sessoli, G. Venturi, A. Vindigni, A. Rettori, M. G. Pini and M. A. Novak, *Angew. Chem.* **2001**, 113, 1810; *Angew. Chem. Int. Ed.* **2001**, 40, 1760. (b) L. Bogani, C. Sangregorio, R. Sessoli and D. Gatteschi, *Angew. Chem. Int. Ed.* **2005**, 44, 5817. (c) K. Bernot, L. Bogani, A. Caneschi, D. Gatteschi and R. Sessoli, *J. Am. Chem. Soc.* **2006**, 128, 7947. (d) H. Miyasaka, T. Madanbashi, K. Sugimoto, Y. Nakazawa, W. Wernsdorfer, K. Sugiura, M. Yamashita, C. Coulon and R. Clérac, *Eur. J. Chem* **2006**, 12, 7028.
- (5) (a) J. Gomez-Segura, I. Diez-Perez, N. Ishikawa, M. Nakano, J. Veciana and D. Ruiz-Molina, *Chem. Commun.* **2006**, 2866. (b) L. Vitali, S. Fabris, A. Mosca Conte, S. Brink, M. Ruben, S. Baroni and K. Kern, *Nano Lett.* **2008**, 8, 3364. (c) K. Katoh, Y. Yoshida, M. Yamashita, H. Miyasaka, B. K. Breedlove, T. Kajiwara, S. Takaishi, N. Ishikawa, H. Isshiki, Y. F. Zhang, T. Komeda, M. Yamagishi, J. Takeya, *J. Am. Chem. Soc.* **2009**, 131, 9967.
- (6) (a) C. Lescop, E. Belorizky, D. Luneau and P. Rey, *Inorg. Chem.* **2002**, 41, 3375, and references therein. (b) X-L. Wang, L-C. Li and D-Z. Liao, *Inorg. Chem.* **2010**, 49, 4735.
- (7) F. E. Ullman, J. H. Osiecky, D. G. B. Boocock and R. Darcy, *J. Am. Chem. Soc.* **1972**, 94, 7049.
- (8) A. Caneschi, P. Chiesi, L. David, D. Gatteschi and R. Sessoli, *Inorg. Chem.*, **1993**, 32, 1445.
- (9) M. F. Richardson, W. F. Wagner and D. E. Sands, *J. Inorg. Nucl. Chem.* **1968**, 30, 1275.
- (10) Richardson, M. F.; Wagner, W. F.; Sands, D. E. *J. Inorg. Nucl. Chem.* **1968**, 30, 1275.
- (11) (a) E. L. Muetterties and L. J. Guggenberger, *J. Am. Chem. Soc.* **1974**, 96, 1748. (b) M. G. B. Drew, *Coord. Chem. Rev.* **1977**, 24, 179.
- (12) Altomare, A.; Cascarano, G.; Giacovazzo, C.; Guagliardi, A.; Burla, M. C.; Polidori, G.; Camalli, M. *J. Appl. Crystallogr.* **1994**, 27, 435.
- (13) G. M. Sheldrick, SHELXL-97, Program for refinement of crystal structures, University of Göttingen, Germany, **1997**.
- (14) Farrugia, L. J. *J. appl. Crystallogr.* **1999**, 32, 837.
- (15) D.A. Dougherty, *Acc. Chem. Res.* **1991**, 24, 88.
- (16) (a) R. Ruiz, J. Faus, F. Lloret, M. Julve and Y. Journaux, *Coord. Chem. Rev.* **1999**, 193-195, 1069. (b) I. Fernández, R. Ruiz, J. Faus, M. Julve, F. Lloret, J. Cano, X. Ottenwaelder, Y. Journaux and M. C. Muñoz, *Angew. Chem. Int. Ed.*, **2001**, 40, 3039. (c) A. R. Paital, T. Mitra, D. Ray, W. T. Wong, J. Ribas-Ariño, J.J. Novoa, J. Ribas and G. Aromí, *Chem. Commun.*, **2005**, 5172. (d) T. Glaser, M. Gerenkamp and R. Fröhlich, *Angew. Chem. Int. Ed.*, **2002**, 41, 3823.
- (17) (a) K. Inoue and H. Iwamura, *J. Am. Chem. Soc.* **1994**, 116, 3173. (b) K. Inoue, T. Hayamizu, H. Iwamura, D. Hashizume and Y. Ohashi, *J. Am. Chem. Soc.* **1996**, 118, 1803. (c) K. Tanaka, K. Furuichi, M. Kozaki, S. Suzuki, D. Shiomi, K. Sato, T. Takui and K. Okada, *Polyhedron* **2007**, 26, 2021.
- (18) F. Pointillart, K. Bernot, L. Sorace, R. Sessoli and D. Gatteschi, *Dalton Trans.* **2007**, 2689.

- (19) K. S. Cole and R. H. Cole, *J. Chem. Phys.* **1941**, 9, 341.
- (20) D. Gatteschi, R. Sessoli and J. Villain, *Molecular Nanomagnets*, Oxford University Press, Oxford, **2006**.
- (21) (a) L. Gregoli, C. Danieli, A. L. Barra, P. Neugebauer, G. Pellegrino, G. Poneti, R. Sessoli and A. Cornia, *Chemistry Eur. J.*, **2009**, 15, 6456. (b) T. Kajiwara, K. Takahashi, T. Hiraizumi, S. Takaishi and M. Yamashita, *Polyhedron* **2009**, 28, 1860.
- (22) (a) P. H. Lin, T. J. Burchell, R. Clérac and M. Murugesu, *Angew. Chem. Int. Ed.* **2008**, 47, 8848. (b) G-F. Xu, Q-L. Wang, P. Gamez, Y. Ma, R. Clérac, J. Tang, S-P. Yan, P. Cheng and D-Z. Liao, *Chem. Commun.*, **2010**, 46, 1506
- (23) R. Sessoli and A. K. Powell, *Coord. Chem. Review*, **2009**, 253, 2328.
- (24) W. Wernsdorfer, N. Allaga-Alcalde, D. N. Hendrickson and G. Christou, *Nature*, **2002**, 416, 406.
- (25) M. Matsushita, N. Ozaki, T. Sugawara, F. Nakamura and M. Hara, *Chem. Lett.* **2002**, 596.
- (26) M. Mannini, L. Sorace, L. Gorini, F. M. Piras, A. Caneschi, A. Magnani, S. Menichetti and D. Gatteschi *Langmuir* **2007**, 23, 2389.

Conclusions and perspective

In this thesis work we have focused our attention on different types of molecular magnetic materials, all of them comprising dysprosium(III), selected because of its strong uniaxial magnetic anisotropy. This gives rise to a ground Kramer doublet that can be handled as an effective classical spin $\frac{1}{2}$, whose effective g tensor can be estimated from *ab-initio* calculation.

The investigation of molecular materials based on anisotropic 4f ions is complicated by the fact that the metal environment is in most cases of low symmetry. The direction of easy magnetization is thus difficult to predict, and in most cases the easy axes of interacting 4f ions are not collinear one to each other.

Angular resolved magnetometry, employed in this thesis first on a mononuclear system and at a later stage on a more complex polynuclear complex, has revealed to be a precious tool. This technique is indeed rather old, but its combination with high sensitivity SQUID magnetometry, and its integration in automatic measurement sequences make its use accessible to the chemical community working in molecular magnetism.

An important result of this work is represented also by the development of a protocol to orient and handle single crystals for angular resolved magnetometry, which is expected to extend significantly the use of the technique to unstable crystals as well as to those growing in complex morphologies.

Despite these significant advances the technique remains rather time consuming and its use should always be evaluated at the light of the properties exhibited by the investigated material. While we have decided not to apply it to the investigation of the 3d-4f systems described in this thesis we can foresee its use in the characterization of other lanthanide-radical systems. These last ones have been widely investigated but we want to highlight here a different use of this materials.

In the previous chapter we have already mentioned the novel trend in molecular magnetism, showing increasing interest on the organization of magnetic molecules on surfaces. In fact the magnetic bistability of SMMs and SCMs could represent a significant advance in density of data storage but this requires that the addressing of a single molecule is achieved. The recent observation that the “memory” effect is present in tetranuclear iron(III) SMMs grafted on gold¹ and that also quantum effects² can be observed have opened interesting perspectives. Scanning Probe Microscopies³ have the necessary resolution but require that the molecules are organized on flat surfaces. Moreover, the rich quantum behavior of SMMs could be exploited in molecular spintronics, the emerging field of electronics where also the spin degree of freedom of the conduction electrons is exploited.⁴

At the moment investigations of lanthanide-based SMMs on surface are restricted to the double-decker compounds with phthalocyanine ligands.⁵ These are in fact very stable molecules and

recently have been successfully deposited through thermal evaporation.⁶ Being flat molecules, they can be well characterized by Scanning Tunnel Microscopy. However, their magnetic investigation through X-ray Magnetic circular dichroism has revealed that the dynamics of the magnetization is strongly influenced by the organization in a monolayer on a noble metal⁷.

These results suggest that a better control between the molecule and the substrate is achieved by ligand design associated to self assembling of monolayer of pre-functionalized molecules with anchoring groups suited for specific surfaces.

One of the major difficulties encountered in the investigation of SMMs organized on surface is the vanishingly small amounts of magnetic centers present on the surface that makes the use of traditional magnetometry not suited for their investigation. XMCD is well suited for this purpose but its use is restricted by the limited access to synchrotron facilities.

An alternative method, suited to investigate strongly anisotropic molecules like SMM based on Dy³⁺, Tb³⁺, and Ho³⁺, is the use of torque magnetometry with high sensitivity cantilevers and capacitance bridges. The technique is commonly used on crystalline sample⁸, but the deposition of a gold layer on an ultra-thin Cu-Be cantilever and the subsequent grafting of SMM can increase the sensitivity, especially if high magnetic fields are employed. If this approach is going to be developed, it is mandatory that the direction of the easy axis of magnetization is known with great accuracy, and angle resolved magnetometry is expected to become more and more employed.

With this purpose in mind the research described in this thesis has been concluded with some preliminary experiments of deposition of Ln-based SMMs on gold surface.

Thanks to the efforts of Dr. Lapo Gorini, an organic chemist, the analogue of the NITmbis radical described in chapter 5, see Figure C.1, with a sulphur containing anchoring group, has been synthesized following the procedure schematized in Figure C.2

Previous investigations, carried out in the Florence laboratory, have shown that the radical nature of these molecules is preserved once grafted to a gold substrates. The stability induced by the chelating properties of this bi-radicals toward lanthanide ions, described in chapter 5, makes it the anchoring of intact Dy-NITmbis molecules on gold and efforts are actually devoted to reach this goal.

The chemical fragility of complexes comprising nitronyl-nitroxide radicals is expected to be anyhow much larger than other complexes comprising much more robust ligands, i.e. the functionalized DOTA-like ligands that are currently investigated in the laboratory (H₄DOTA = 1,4,7,10-tetraazacyclododecane-N,N',N'',N'''-tetraacetic acid). We want however to conclude this thesis by underlining a potential advantage in the use of radical ligands.

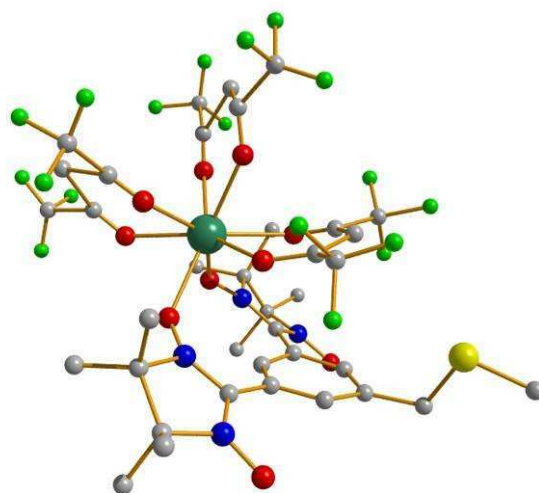


Figure C.1: Representation of $[Dy(hfac)_3\text{-DiNitSMe}]$ cluster (where: DiNitSMe = 1 (Methylthio)-Methyl-Phenyl-3,5-DiNitronyl-Nitroxide and hfac = 1,1,1,5,5,5 hexafluoroacetylacetonate).

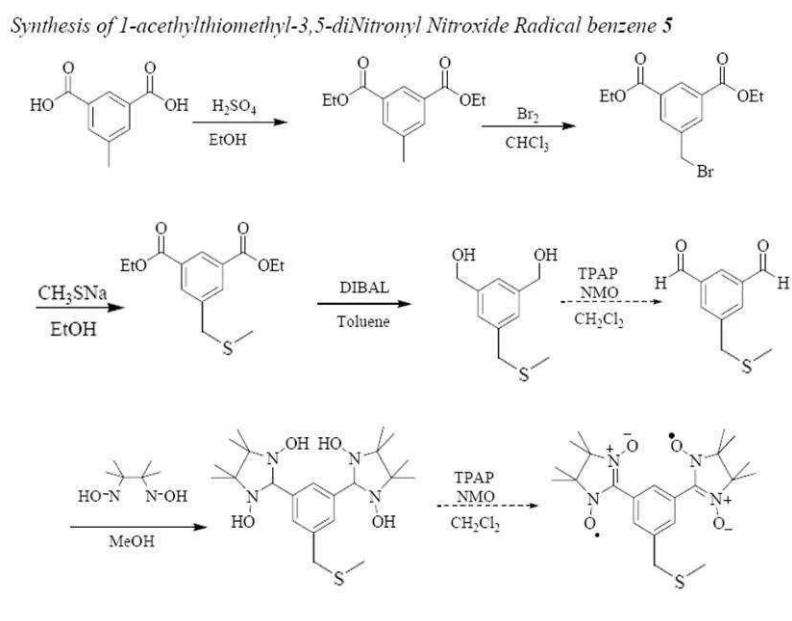


Figure C.2: Synthetic route of the functionalized radical DiNitSMe ((Methylthio)-Methyl-Phenyl-3,5-DiNitronyl-Nitroxide)

With the goal of magnetic addressing of single molecules on surfaces the use of Magnetic Force Microscopy appears inadequate because the lateral resolution is far from the molecular scale, relying on the sensing of long-range magnetostatic forces. Moreover its application to investigate paramagnetic systems is still controversial, even if already extended to super-paramagnets.

Recently its use has been however extended to probe the antiferromagnetic ordering of Nickel oxide,⁹ thus reaching atomic resolution, thanks to the exchange interaction between the

atoms at the tip apex and the atoms on the surface. The extension of Magnetic Exchange Force Microscopy (MExFM) from inorganic structures to molecules on surfaces seems at a first glance hampered by the presence of the non-magnetic ligands around the magnetic core. However, if the metal ion is coordinated to a nitronyl-nitroxide organic radical the spin density is strongly localized on the outer part of the molecule. For instance we show in Figure 6.3 a system currently under investigation. Such a system, where to a sulphur functionalized radical an additional donor atom (a pyridine nitrogen atom) has been inserted to increase the stability of the complex thanks to the chelating effect, is potentially suited for investigations with MExFM. At variance with most molecular systems, the spins of the radical and of the metal ion are strongly coupled via direct exchange rather than via super-exchange. Using a magnetic tip, we can thus envisage to probe the spin density delocalized on the outer oxygen atom in order to reveal the magnetic state of the metal ion(s) in an indirect fashion.

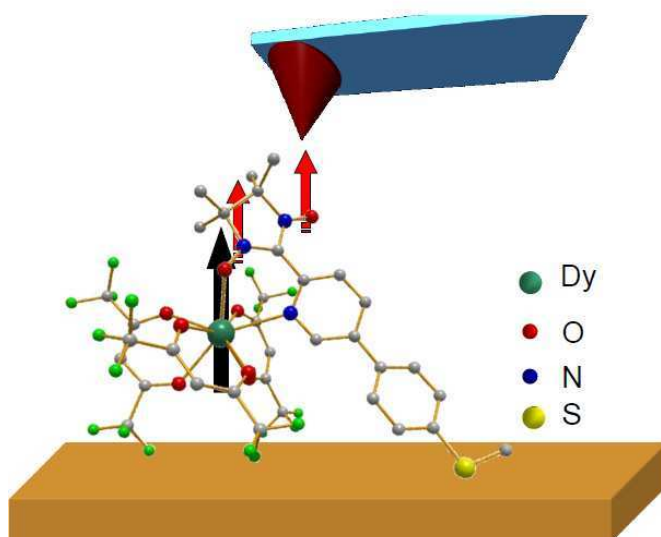


Figure C.3: Schematic view of a perspective application of robust dysprosium(III) nitronyl-nitroxide systems to investigate the magnetism of single molecules on surface. A Dy-NITR system, known to give slow relaxation of the magnetization, has been modified to allow its grafting on gold. A magnetic tip can probe the accessible non-coordinating oxygen atoms, whose unpaired electron's spin is however coupled to the magnetic moment of the metal ion.

Bibliography

- (1) M. Mannini, F. Pineider, Ph. Saintavit, C. Danieli, E. Otero, C. Sciancalepore, A. M. Talarico, M. A. Arrio, A. Cornia, D. Gatteschi, R. Sessoli, *Nature Mater.*, **2009**, 8, 194.
- (2) M. Mannini, F. Pineider, C. Danieli, F. Totti, L. Sorace, Ph. Saintavit, M.-A. Arrio, E. Otero, L. Joly, J. C. Cezar, A. Cornia & R. Sessoli, *Nature* advance online publication, **2010**, doi:10.1038/nature09478.
- (3) R. Wiesendanger, *Scanning Probe Microscopy and Spectroscopy*, Cambridge University Press, Cambridge (UK), **1994**.
- (4) Sanvito, S. *J. Mater. Chem.* **2007**, 17, 4455. b) Bogani, L.; Wernsdorfer, W. *Nature Mater.* **2008**, 7, 179.
- (5) (a) L. Vitali, S. Fabris, A. M. Conte, S. Brink, M. Ruben, S. Baroni, K. Kern, *Nano Letters*, **2008**, 8, 3364. (b) K. Katoh, Y. Yoshida, M. Yamashita, H. Miyasaka, B. K. Breedlove, T. Kajiwara, S. Takaishi, N. Ishikawa, H. Isshiki, Y. F. Zhang, T. Komeda, M. Yamagishi, J. Takeya, *J. Am. Chem. Soc.*, **2009**, 131, 9967.
- (6) S. Stepanow, J. Honolka, P. Gambardella, L. Vitali, N. Abdurakhmanova, T.-C. Tseng, S. Rauschenbach, S- L. Tait, V. Sessi, S. Klyatskaya, M. Ruben, K. Kern, *J. Am. Chem. Soc.* **2010**, 132, 11900.
- (7) L. Margheriti, D. Chiappe, M. Mannin, P. E. Car, P. Saintavit, M. A. Arrio, F. Buatier de Mongeot, J. C. Cezar, F. M. Piras, A. Magnani, E. Otero, A. Caneschi, R. Sessoli, *Adv. Mater.*, **2010**, On line, DOI: 10.1002/adma.201003275.
- (8) (a) A. Cornia et al., *J. Magn. Magn. Mater.*, **2001**, 226, 2012. (b) O. Waldmann et al., *Phys. Rev. Lett.*, **2004**, 92, 096403.
- (9) U. Kaiser et al., *Nature* **2007**, 446, 522.

Appendix

<u>A.1 DC-MAGNETOMETER</u>	101
<u>A.2 VSM MAGNETOMETER</u>	103
<u>A.3 AC-MAGNETOMETER</u>	104
<u>A.4 HORIZONTAL ROTATOR</u>	111

A.1 *dc*-magnetometer

The basic magnetic technique used in molecular magnetism is the *dc* magnetometry. Before the 70's torque force-based measurements, such as the Faraday balance were used. This latter method, where a crystal is suspended in a field on a thin fiber, was also used to characterize the magnetic anisotropy of single crystals.

These “mechanical methods” were then replaced by “flux sensing methods” where the movement of a magnetic moment induces an electromotive force (efm) in a detection coil. This inductive detection of the magnetic moment is performed by devices sensitive only to the gradient of the magnetic field. They are thus named gradiometers. There are different types of gradiometers but the most used ones are second order gradiometers. Such coils allows for suppressing the effect of the external field and of the drift of the flux on the measurement. Such gradiometers are measuring only the contribution to the efm generated by the sample. This also permits a simpler extraction and fitting of the signal (see Figure A.1).

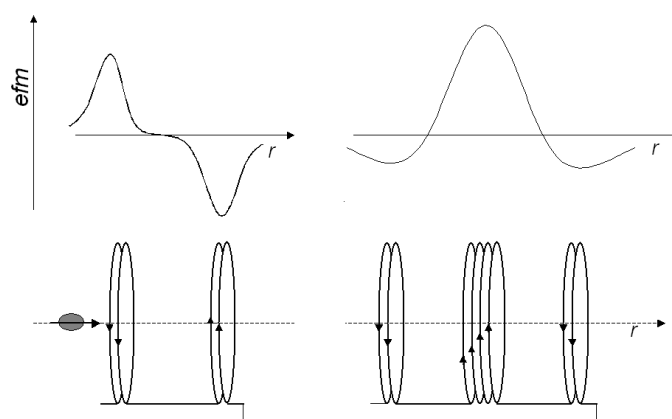


Figure A.1: First (left) and second order gradiometers (right) and the dependence of the induced efm on the position on the sample

To provide a better sensitivity to the magnetometers, advanced flux-sensing techniques were employed at the beginning of the 70's and were based on devices named SQUID. SQUID is an acronym for “Super-conducting QUantum Interference Device”, and the magnetometers using these devices have been named by analogy “SQUID-magnetometers”.

The SQUIDs are made of one superconducting ring, in which the flux is “quantized”, and two Josephson junctions (for a *dc*-SQUID), where Josephson tunneling of the Cooper pairs occurs. The SQUID is taken in a ^4He bath to ensure the good superconductivity of its ring.

The sample is then moved in the gradiometer and induces an electromotive force reported in the upper part Figure A.1.

The *dc*-SQUID then uses the quantum interferences that occur between the two pathways that enclose the area where the magnetic flux is modified by the sample (see Figure A.2). The current of the SQUID is thus modulated by the flux induced in the ring by an external magnetic field.

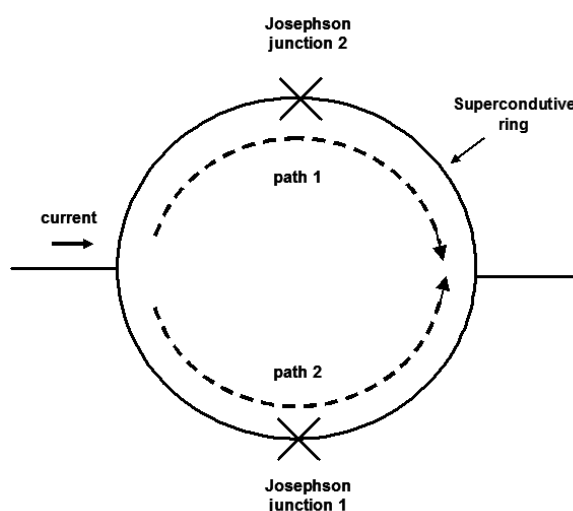


Figure A.2: Scheme of a *dc*-SQUID. The current goes through a superconducting ring with two Josephson junctions.

The sample is then moved through the coils and a feed-back coil is used to compensate the effect of the sample when it comes into the coils. The voltage that is needed to compensate the flux generated by the sample is proportional to its magnetization. After calibration with a known sample (generally paramagnetic gadolinium salts), one can accurately estimate the magnetization of the sample. Nowadays SQUID magnetometers can detect signals as low as 10^{-9} emu.

We will not go deeper in the description of this apparatus but useful information can be found in reference. User's manuals provided by the SQUID suppliers are also a good source of information.

A.2 VSM magnetometer

The Vibrating Sample Magnetometer is another flux sensing method. This technique is based on a first order gradiometer inside of which a sample is oscillating at a frequency around 50 Hz. This is a quite old technique but still used because the utilization of modern phase sensitive detector (lock-in) has considerably increased its sensitivity.

Consequently the apparatus is sensitive enough and do not require the use of a SQUID. This is an advantage since SQUID cannot work over 80 kOe because of their sensitivity to the field. With a VSM, measurements can be performed until very high field and high sweep rates (120 kOe at 12 kOe/min in Florence).

The sweep rate problem

We want here to put in light a problem of the VSM measurement rarely taken in consideration. It concerns the influence of the sweep rate of the magnetic field. In fact, in order to detect magnetic phenomena having a short lifetime compared to the one of a SQUID hysteresis measurement, some experiment requires a fast sweeping of the magnetic field. Usually, the acquisition of the magnetic moment is made while sweeping.

However, this creates some measurement artifacts and artificial hysteresis. In fact, each point of the curve is recorded thanks to an average of 30 measurements performed by the lock-in amplifier. The whole measure takes about 0.5 s. The problem is that between the beginning and the end of the measure the field change (of about 100 Oe when sweeping at 12 kOe min⁻¹). Hence on a full loop the error is of about 200 Oe on the opening of the hysteresis. This has to be corrected when measuring samples with very low values of the coercitive field, or displaying complicated behavior at low field (zero field step,...). The phenomenon became negligible for sweep rate below 0.4 kOe min⁻¹.

In the following all the curves recorded with a sweep rate above 0.4 kOe min⁻¹ were thus corrected to take into account this artifact.

A.3 *ac*-magnetometer

ac susceptometry is a useful technique that allows for the study of the dynamic behavior of magnetic materials. It has provided the first evidences of slow relaxation of the magnetization in low dimensional materials in the beginning of the 90's and his nowadays widely used.

An *ac* susceptometer is made of a primary coil where the sample is inserted. In this coil a small *ac* field (about 3 Oe) is generated by an *ac* current provided by a lock-in. The magnetic moment of the sample oscillates as a response of the applied *ac* field. This oscillation is detected by a secondary coil, fixed inside of the primary one. This coil is made in two parts winded in opposite direction to compensate the contribution to the signal of the primary coil (see Figure A.3). A first order gradiometer is thus employed and absolute values for the susceptibility are obtained by measuring the induced voltage by the sample in the minimum and maximum of the gradiometer. The signal is then detected by the lock-in, in amplitude and phase.

The *ac* insert used in Florence is a courtesy of Patrick Rosa, and is able to operate in a 100-25000 Hz frequency range.

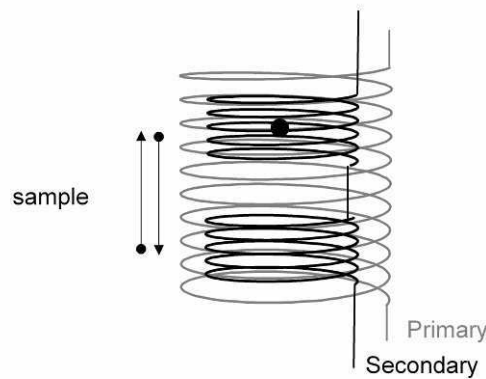


Figure A.3: Scheme of the coil used in an *ac* susceptometer (rep. from 2)

In an *ac*-susceptometer the applied field is thus:

$$H = h \cos \omega t \quad (\text{I.1})$$

where ω is the frequency of the *ac* current in the primary coil. Since the whole system is inserted in a ^4He -cooled cryostat provided with a superconducting magnet, an external field H_0 can be applied. The field is thus:

$$H = H_0 + h \cos \omega t \quad (\text{I.2})$$

The difference between the *dc* and *ac* susceptibility is explained on Figure A.4. While in conventional *dc* technique the magnetic susceptibility is estimated through a low field approximation and gives:

$$\chi = M/H \quad (\text{I.3})$$

using *ac* susceptometry we can measure the slope of the magnetization curve and have access to the true susceptibility of the sample through:

$$\chi = \partial M / \partial H \quad (\text{I.4})$$

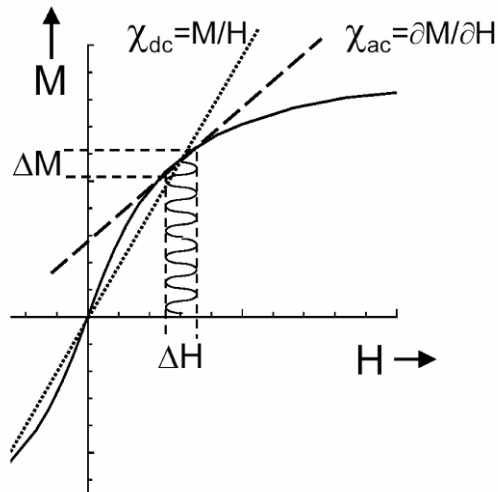


Figure A.4: Scheme of a magnetization curve evidencing the differences between the *dc* and *ac* susceptibility. (reproduced from 2).

Consequently, the accuracy of an *ac* measurement does not depend of the static applied field and investigations can be done in zero field, avoiding thus any saturation effects.

From the dynamic point of view, if the magnetization of the sample is not in phase anymore with the oscillating field the susceptibility becomes:

$$\chi(\omega) = \chi'(\omega) - i\chi''(\omega) \quad (\text{I.5})$$

where χ' and χ'' are the real and imaginary part of the susceptibility. On the thermodynamic point of view we can define two limiting cases:

- when ω , the frequency of the *ac* field, is slow compared to the relaxation rate of the system, there is no phase lag of the magnetization and the susceptibility is called *isotherm* and noted χ_T .
- on the contrary, when the system is not able to follow the *ac* field because it oscillate too fast compared to the relaxation rate, the measured susceptibility is called *adiabatic*, and noted χ_S .

Casimir and Du Pré have proposed to insert these parameters in the equation I.5, and the susceptibility becomes:

$$\chi(\omega) = \chi_S + \frac{\chi_T - \chi_S}{1 + i\omega\tau} \quad (\text{I.6})$$

where τ is the time needed by the system to come back to a thermodynamical equilibrium. This relaxation is mainly governed by mechanism involving phonons. Consequently, the *isothermal* susceptibility $\chi_T(\omega)$ corresponds to an equilibrium with phonons. In the second limiting case, the system has no time to exchange energy with the external world and the *adiabatic* susceptibility can be interpreted has the susceptibility of the magnetic system isolated from the thermal bath.

The two components of the susceptibility can be written as:

$$\chi' = \frac{\chi_T - \chi_S}{1 + \omega^2\tau^2} + \chi_S \quad \text{and} \quad \chi'' = \frac{(\chi_T - \chi_S)\omega\tau}{1 + \omega^2\tau^2} \quad (\text{I.7})$$

these relations are similar to the ones determined for the dielectrics by Debye. The frequency dependence of these two quantities is depicted in Figure A.5

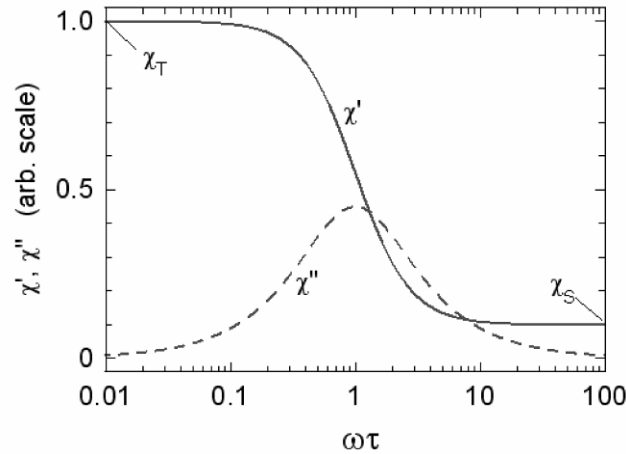


Figure A.5: Scheme of the theoretical frequency dependence of the real and imaginary component of the susceptibility in a semi-log scale. (rep. from 2)

By plotting $\chi''(\omega)$ against $\chi'(\omega)$ we obtain a so-called Argand plot that allows for an estimation of the distribution of the relaxation times in the sample. The equation I.6 is modified to take into account the distribution (dispersion) of the relaxation times through a parameter α :

$$\chi(\omega) = \chi_s + \frac{\chi_T - \chi_s}{1 + (i\omega\tau)^{1-\alpha}} \quad (\text{I.8})$$

When $\alpha=0$, the whole system relaxes with the same characteristic time. On the contrary the larger is α the wider is the dispersion of the relaxation times in the system. We report in Figure A.6 a normalized Argand. We can see a remarkably low α in both powder and single crystal sample. That means that, when the sample relaxes slowly, almost only one relaxation time is present.

However we can notice that the value of χ_s value is significantly larger than in the powder experiment suggesting that part of the sample relaxes very rapidly. Further investigations have shown that this large χ_s value is due to the random distribution of the crystallites orientation in the powder sample. The components of the magnetization perpendicular to the easy axis relax much faster and thus also at high frequency can follow the oscillating field.

We see here that the Argand plot is very useful since it permits not only a determination of the relaxation time, but it also shows if a part of the sample is fast relaxing or not.

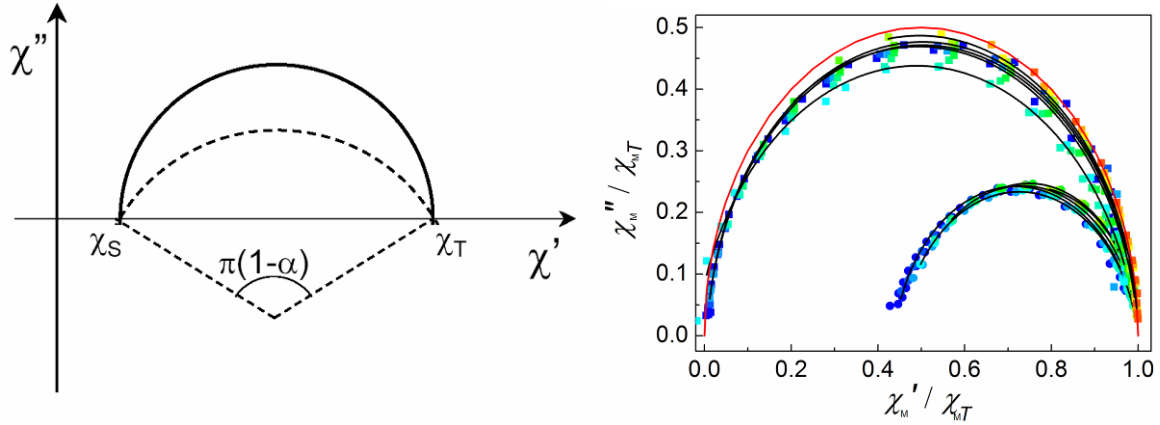


Figure A.6: (left) Theoretical Argand plot with (dotted line) or without (full line) distribution of the relaxation time. (right) Argand plot for **16**, for crystal (squares) and powder (circles). Black lines are the corresponding fits. In red, the curve corresponding to one relaxation time ($\alpha=0$).

When the relaxation becomes very slow it can be monitored by directly following the decay of the magnetization. That is to say that the magnetization can be written as:

$$M(t) = M_{\text{equ}}(H) + \delta M_0 \exp(-t/\tau) \quad (\text{I.9})$$

where M_{equ} is the equilibrium magnetization and τ the relaxation time. If τ is measured at different temperature in the superparamagnetic temperature range an increase of the relaxation time on cooling is observed. This can be expressed by an Arrhenius formula:

$$\tau = \tau_0 \exp\left(\frac{T_0}{T}\right) \quad (\text{I.10})$$

By plotting the logarithm of τ against T^{-1} we have a straight line, which make a first analysis of the results much easier. The pre-exponential factor τ_0 is called characteristic relaxation time. The relaxation of the magnetization supposes the presence of an energy barrier that can be introduced in I.10 to afford:

$$\tau = \tau_0 \exp(\Delta E/k_B T) \quad (\text{I.11})$$

The slope of the Arrhenius plot provides thus the activation energy that is needed by the system to relax. We report in Figure A.7 the Arrhenius plot extracted from an *ac*

measurements. This kind of treatment of the data also allows for an easy visualization of different dynamic regimes in a sample. For instance, two different regimes have been evidenced here, each of one with its own characteristic relaxation time (τ_0) and energy barrier (Δ).

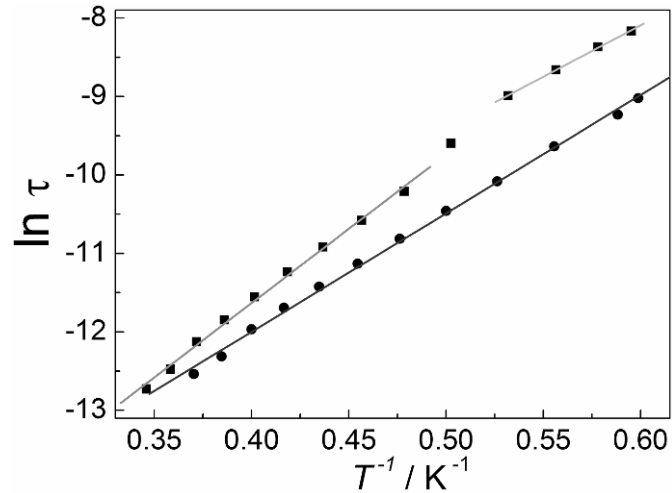


Figure A.8: Arrhenius plot for the powder (circles) and the oriented single crystal (squares) and the respective linear fits.

To draw this kind of graph τ can be extracted by considering the situations in which $\omega\tau=1$. It can be done by plotting the temperature at which χ'' display a maximum following:

$$\tau(T_{\max}) = \frac{1}{2\pi\nu} \quad (\text{I.12})$$

or better by fitting the χ'' vs ω curves with the equation I.6.

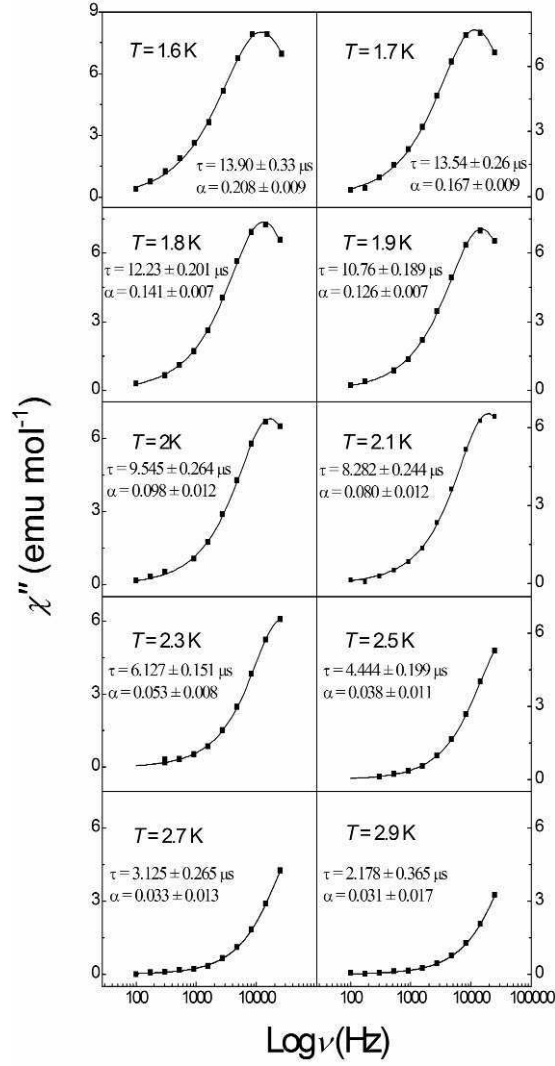


Figure A.8: χ_M'' vs $\log \nu$ diagrams extracted from ac susceptibility measurement taken in zero external magnetic field for ten different temperatures ranging from 1.6 to 2.9 K. Solid lines: fits obtained with the expression A6.

A more explicit form of I.6 is $\chi''(2\pi\nu) = (\chi_T - \chi_S) \frac{(2\pi\nu\tau)^{1-\alpha} \cos(\pi\alpha/2)}{1 + 2(2\pi\nu\tau)^{1-\alpha} \sin(\pi\alpha/2) + (2\pi\nu\tau)^{2-2\alpha}}$ (I.13)

A.4 Horizontal Rotator

The measurement of the angular dependence of the magnetization on single crystals has been widely used during this thesis. Directly transposed from an EPR procedure, this experimental technique has been progressively optimized in our laboratory. This provides a further improvement of the torque methods used in the 60's and allows for measuring small crystals. But even if it seems quite a simple procedure, the complete characterization of a sample is not an obvious task at all.

In fact, from the operative point of view, it is easier to work with an EPR (Electron Paramagnetic Resonance) setup where a single crystal sample holder connected to a goniometer can be used and rotated along an axis which is orthogonal to the magnetic field. But in the case of EPR silent compounds as the Dy-based ones studied during this work, one has to find another way to get access to this data, and the horizontal SQUID rotator has to be employed.

There are two main drawbacks for performing a rotating single crystal measurement on a SQUID magnetometer. i) The magnetic measurement cannot be done simply by rotating the straw that holds the sample along its vertical axis. In fact, the field that is generated by the magnet is vertical as well and therefore the crystal has to be rotated perpendicularly to the field. ii) As we use a built-in He-cooled cryostat there is no easy access to the crystal and simple goniometer, as the one used for EPR measurements, cannot be employed here.

In Florence, we have customized a Cryogenic S600 magnetometer with a Quantum Design Horizontal Rotator insert. The wiper seal of the commercial insert has been modified to fit in the Cryogenic S600 gate and a plastic double screw was designed to ensure a good inserting of the sample in the cryostat. Special rings were also designed to ensure the air tightness of the setup but also to allow the rotation, without vacuum loss, of the internal rod.

The sample holder is made of a small brass plate which is fixed into an half cut brass tube that perfectly fits in the sample room. A small copper-beryllium wire is linked to the plate and transmits to the sample holder the rotation of the internal rod. This rod is rotated by the motor, which is computer controlled and also ensures independently the vertical extraction of the signal (see Figure A.9).

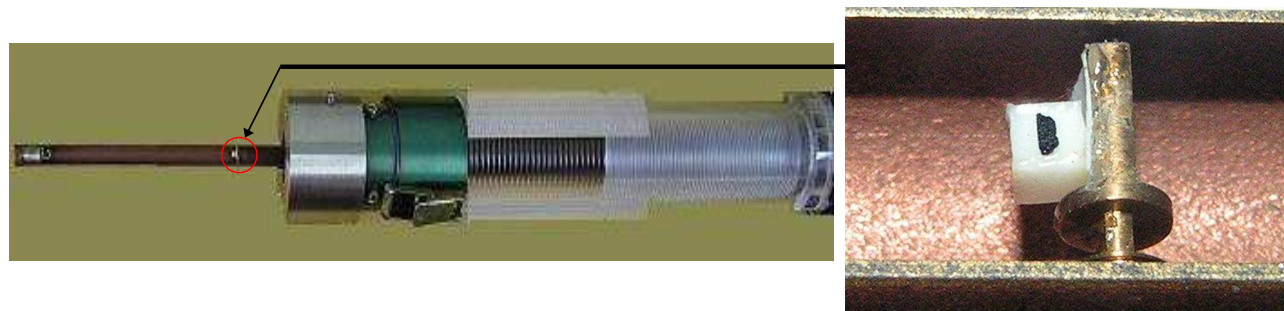


Figure A.9: Pictures of the horizontal sample rotator, (left) the half cut brass tube and the modified wiper seal to work on a Cryogenic SQUID magnetometer; (right) in white the Teflon cube support.

To fully characterize the anisotropy tensor of a crystalline material the most accurate way is to proceed to collect the data from three strictly orthogonal rotations. In order to change the rotation axis the investigated crystal has to be taken out of the cryostat. This is a very critical step for different reasons: i) the shape of the crystal in most cases does not allow to align it along a known reference frame in all rotations (e.g. it can be hard to correctly align a slab-like crystals standing on one of the little faces), b) crystals of molecular materials are often quite fragile and often do not resist to the thermal shock. As a result they easy break when moving them to change the orientation on the sample rotator. A Teflon cube of 2 mm height is used to limit the manipulation of the crystal and to ensure the good orthogonality of the three rotations (see Figure A.9).

Experimental path

During this thesis (see chapter 3), an experimental procedure has been developed and optimized. In previous works using the horizontal rotator, the Teflon cube was used in order to avoid the excessive manipulation of samples and to make easier the orientation of the crystals in the three orthogonal rotations. However, the crystallographic information related to the used rotation axes still remained a main drawback of the procedure. In fact, the three rotation axes, corresponding to the edges of the cube, must be related to the molecular structure. The solution we have found consists in using the Teflon cube from the very first step, as a sample holder but especially as a referential.

Since crystals don't always grow in a specific habit, the visual identification of the faces can be an issue. Moreover, crystals could be mechanically fragile, and or deteriorate themselves in time during the time consuming manipulation to orient them on the cube, for instance for the loss of solvent molecules of crystallization. The first step was then to set the

crystal on a 2mm Teflon cube (where a Cartesian system has already been defined and marked) and to cover it with epoxy glue (or Apiezon N grease), which keep the crystal fixed, avoid solvent loss and contact with air and moisture.

The cube was then fixed on a goniometer and placed on a single-crystal diffractometer with the cube's X axis set parallel to a defined angle, in order to have a reference. The determination of the crystallographic cell and the orientation matrix is then effectuated. Using the diffractometer's CCD camera combined to the diffraction software, the X, Y, and Z faces of the cube are considered as crystal faces, and their corresponding Miller's indices are evaluated by the diffractometer software. Once the orientation of the external (cube) reference frame XYZ is known in the crystal reference frame thanks to the hkl indices, the transformation matrix linking our XYZ system and the orthogonal crystal's frame (in general $ab'c^*$ for a triclinic space group, that reduces to abc in the orthorhombic or higher symmetry ones) can be obtained.

The angular dependence of the M/H ratio was then measured in a static field. Special care should be placed to measure at sufficiently low fields to avoid excessive magnetic torque but also to assure that the magnetization is linear in H, so that the M/H ratio can be assumed to correspond to the susceptibility. Using the shape of the cube and changing the face on which the cube lies on the rotator, three sets of angular dependent data with rotation along three perpendicular directions are easily collected, giving us information on the magnetic susceptibility for the whole space.

The magnetization data were fitted assuming the tensorial relation $\mathbf{M}=\chi\mathbf{H}$. For \mathbf{H} rotating in the $\alpha\beta$ plane we can use the expression:

$$M(\theta)=\chi_{\alpha\alpha}H(\cos\theta)^2+\chi_{\beta\beta}H(\sin\theta)^2+2\chi_{\alpha\beta}H\sin\theta\cos\theta$$

where α and β stay for the vectors of \mathbf{X} , \mathbf{Y} , and \mathbf{Z} in a cyclic permutation and θ is the angle between \mathbf{H} and the α vector.

Using the transformation matrix defined previously, the susceptibility tensor can be expressed in the $ab'c^*$ system.

$$A \chi_{XYZ} A^{-1} = \chi_{ab'c^*}$$

The orientation of the principal axes of the anisotropy tensor is then easily evaluated in respect of molecular geometrical parameters, i.e. bonds, pseudo symmetry elements, etc., by expressing also the atomic coordinates in the orthogonalized crystallographic reference frame.

AVIS DU JURY SUR LA REPRODUCTION DE LA THESE SOUTENUE

Titre de la thèse : Magnetic anisotropy in dysprosium based compounds.

Nom Prénom de l'auteur : ETIENNE Mael

Membres du jury : Monsieur CORNIA
Monsieur MALLAH
Monsieur GUILLOU
Madame DAIGUEBONNE
Madame SESSOLI
Monsieur CANESCHI

Signature Cornia
T M A L L A H
Guillou
Daiguebonne
Sessoli
Caneschi


Président du jury : *Talal* MALLAH

Date de la soutenance : 14/12/2010

Reproduction de la thèse soutenue :

- Thèse pouvant être reproduite en l'état
 Thèse ne pouvant être reproduite
 Thèse pouvant être reproduite après corrections suggérées

Le Directeur,

Thamed Drissi


Rennes, le 14/12/2010

Signature du Président du jury

T M A L L A H